PACIFIC EARTHQUAKE ENGINEERING
RESEARCH CENTER

An Empirical Model for Fourier Amplitude Spectra using the NGA-West2 Database

Jeff Bayless

Norman A. Abrahamson

Department of Civil and Environmental Engineering
University of California, Davis

PEER Report No. 2018/07
Pacific Earthquake Engineering Research Center
Headquarters at the University of California, Berkeley

December 2018

PEER 2018/07
December 2018

An Empirical Model for Fourier Amplitude Spectra using the NGA-West2 Database

Jeff Bayless

Norman A. Abrahamson

Department of Civil and Environmental Engineering
University of California, Davis

PEER Report No. 2018/07
Pacific Earthquake Engineering Research Center
Headquarters at the University of California, Berkeley

December 2018

ABSTRACT

An empirical ground-motion model (GMM) for shallow crustal earthquakes in California and Nevada based on the NGA-West2 database [Ancheta et al. 2014] is presented. Rather than the traditional response spectrum GMM, this model is developed for the smoothed effective amplitude spectrum (EAS) as defined by PEER [Goulet et al. 2018]. The EAS is the orientation-independent horizontal component Fourier amplitude spectrum (FAS) of ground acceleration. The model is developed using a database dominated by California earthquakes, but takes advantage of crustal earthquake data worldwide to constrain the magnitude scaling and geometric spreading. The near-fault saturation is guided by finite-fault numerical simulations and non-linear site amplification is incorporated using a modified version of Hashash et al. [2018]. The model is applicable for rupture distances of 0–300 km, **M** 3.0 – 8.0, and over the frequency range 0.1–100 Hz. The model is considered applicable for Vs_{30} in the range 180–1500 m/sec, although it is not well constrained for Vs_{30} values greater than 1000 m/sec. Models for the median and the aleatory variability of the EAS are developed. Regional models for Japan and Taiwan will be developed in a future update of the model. A MATLAB program that implements the EAS GMM is provided as an electronic appendix.

ACKNOWLEDGMENTS

This study was funded by the Pacific Gas & Electric Company Geosciences. Any opinions, findings, and conclusions or recommendations expressed in this material are those of the authors and do not necessarily reflect those of the Pacific Earthquake Engineering Research Center (PEER).

CONTENTS

LIST OF TABLES

LIST OF FIGURES

1 Introduction

The traditional approach for developing ground-motion models (GMMs) for engineering applications is to use response spectral values for a range of spectral periods. The response spectra GMMs can be used in either deterministic or probabilistic seismic hazard analyses to develop design response spectra. The response spectral values represent the response of a simple structure to the input ground motion and does not directly represent the ground motion itself. As an alternative, Fourier spectral values can be used instead of response spectral values. There are several advantages to using Fourier spectra in place of response spectra: (1) the scaling of Fourier spectra in the GMM is easier to constrain using seismological theory, (2) linear site response remains linear at all frequencies and does not depend on the spectral content of the input motion, as is the case for response spectra [Bora et al. 2016], and (3) for calibrating input parameters and methods for finite-fault simulations based on comparisons with GMMs, Fourier spectra are more closely related to the physics in the simulations.

An empirical Fourier spectrum GMM for shallow crustal earthquakes in California and Nevada based on the Pacific Earthquake Engineering Research Center (PEER) Next Generation Attenuation-West 2 (NGA-West2) database [Ancheta et al. 2014] is developed. The ground-motion parameter used in the GMM is the smoothed effective amplitude spectrum (EAS), as defined by PEER [Goulet et al. 2018]. The effective amplitude spectrum EAS is the orientation-independent horizontal component Fourier amplitude spectrum (FAS) of ground acceleration that can be used with random vibration theory to estimate the response spectral values.

This paper describes the development of the empirical model using ground-motion data as the foundation, along with finite-fault simulations computed using the SCEC Broadband Platform [Maechling et al. 2015] to constrain the near-fault large-magnitude scaling, and the analytical site response modeling to capture the nonlinear site amplification [Hashash et al. 2018]. Rather than simply fitting the empirical data, emphasis is placed on building the model using both the empirical data and analytical results from these seismological and geotechnical models so that the GMM extrapolates in a reasonable manner. A MATLAB program that implements the EAS GMM is provided in an electronic appendix. A model for the inter-frequency correlation of residuals derived from this GMM is presented in Bayless and Abrahamson [2018].

1.1 EFFECTIVE AMPLITUDE SPECTRUM GROUND-MOTION INTENSITY MEASURE

The EAS, defined in Kottke et al. [2018] and used in the PEER NGA-East project [PEER 2015; Goulet et al. 2018], can be calculated from an orthogonal pair of FAS using Equation (1.1):

$$\mathrm{EAS}(f) = \sqrt{\frac{1}{2}\left[\mathrm{FAS}_{HC1}(f)^2 + \mathrm{FAS}_{HC2}(f)^2\right]} \tag{1.1}$$

where FAS_{HC1} and FAS_{HC2} are the FAS of the two orthogonal horizontal components of the ground motion and f is the frequency in Hz. The EAS is independent of the orientation of the instrument. Using the average power of the two horizontal components leads to an amplitude spectrum that is compatible with the use of random vibration theory (RVT) to convert Fourier spectra to response spectra. The EAS is smoothed using the Konno and Ohmachi [1998] smoothing window, which has weights and window parameter defined by Equations (1.2) and (1.3):

$$W(f) = \left\{\frac{\sin\left[b\log\left(f/f_c\right)\right]}{b\log\left(f/f_c\right)}\right\}^4 \tag{1.2}$$

$$b = \frac{2\pi}{b_w} \tag{1.3}$$

The smoothing parameters are described in Kottke et al. [2018]: "W is the weight defined at frequency f for a window centered at frequency f_c and defined by the window parameter b. The window parameter b can be defined in terms of the bandwidth, in $\log_{10}$ units, of the smoothing window, b_w." The Konno and Ohmachi smoothing window was selected by PEER NGA-East because it led to minimal bias on the amplitudes of the smoothed EAS when compared to the unsmoothed EAS. The bandwidth of the smoothing window, b = 1.88.5, was selected such that the RVT calibration properties before and after smoothing were minimally affected [Kottke et al. 2018]. For consistency with the PEER database used to develop empirical FAS models, the smoothed EAS is used with the same smoothing parameters as described in Kottke et al. [2018].

1.2 ON THE SELECTION OF FOURIER AMPLITUDES

In seismic hazard and earthquake engineering applications, the pseudo-spectral acceleration (PSA) of a 5% damped single degree of freedom (SFOF) oscillator is a commonly used intensity measure (IM). The PSA is useful for many applications; however it has drawbacks which are discussed here. The EAS component of the FAS is used as the IM for this study, because the FAS is a more direct representation of the frequency content of the ground motions than PSA and is better understood by seismologists. This leads to several advantages, both in the empirical modeling and in forward application. The reasoning behind these claims is explained in this section.

The PSA calculation involves solving the differential equation for the response of a SDOF oscillator (with given damping) due to a specified forcing function, selecting the peak response of the oscillator, and scaling the peak oscillator displacement by the square of the oscillator natural frequency, ω. This calculation can be repeated for a range of oscillators with different natural frequencies to develop a response spectrum. The elastic SDOF oscillator response is described by the following second order, linear, inhomogeneous differential equation:

$$m * a(t) + c * v(t) + k * u(t) = p(t) \tag{1.4}$$

where m is the SDOF lumped mass, $a(t)$ denotes the SDOF lateral acceleration, c denotes the viscous damping coefficient, $v(t)$ denotes the SDOF lateral velocity, k denotes the lateral stiffness, $u(t)$ denotes the SDOF lateral displacement relative to the ground, and $p(t)$ denotes the time-dependent forcing function due to the earthquake ground motion [Chopra 2007].

Duhamel's convolution integral, also known as the unit impulse response procedure, is one approach to solving a linear differential equation, such as the one given by Equation (1.4). With this method, the response of the system (initially at rest) to a unit impulse force is shown (e.g., in Chopra [2007] to be:

$$h(t-\tau) = \frac{1}{m\omega_d} e^{-\zeta\omega(t-\tau)} \sin\left[\omega_d (t-\tau)\right], \quad t \geq \tau \tag{1.5}$$

where τ is the time instance of the impulse, ω_d is the damped natural frequency, and ζ is the fraction of critical damping. The entire loading history (such as that due to ground acceleration) can then be represented as a succession of infinitesimally short impulses, each producing its own response of the form of Equation (1.5). Since the system is linearly elastic, the total response is the superposition of the responses to all impulses which make up the entire loading history. Taking the limit of the sum as the width of the impulse approaches zero leads to the general expression of Duhamel's integral for an arbitrary forcing function:

$$u(t) = \frac{1}{m\omega_d} \int_0^t p(\tau)\, e^{-\zeta\omega(t-\tau)} \sin\left[\omega_d (t-\tau)\right] d\tau = \int_0^t p(\tau)\, h(t-\tau) = h(t) \otimes p(t) \tag{1.6}$$

where $\otimes$ is the convolution operator. Equation (1.6) is called the convolution integral because convolution is performed in the time domain between the unit impulse response (h), and the force due to ground acceleration (p). Then, by the convolution property of the Fourier transform, the time-domain convolution of h and p can be expressed in the frequency domain as the point-wise multiplication of the Fourier transforms of h and p.

In Figure 1.1, these steps are shown using an example recorded acceleration time history. In the figure, the thin solid black line is the FAS of the recorded acceleration time history, or $\left|F\{p\}\right|$, where F denotes the Fourier transform operator. The solid heavy lines are the FAS of the SDOF oscillator impulse response, or $\left|F\{h\}\right|$. $\left|F\{h\}\right|$ is plotted for three different oscillator frequencies: 0.5, 2.0, and 10.0 Hz, as identified in the figure legend. The dashed lines are the

FAS of the SDOF response to the ground motion, $\left|F\{u\}\right|$, at the same three frequencies. By Equation 1.4, and the convolution property of the Fourier transform, for a given oscillator frequency, $\left|F\{u\}\right| = \left|F\{p\}\right| * \left|F\{h\}\right|$. This result can be confirmed qualitatively in Figure 1.1.

Figure 1.1 illustrates that oscillators with different natural frequencies are controlled by different frequency ranges of the ground motion. At relatively higher oscillator frequencies (e.g., 10 Hz; green lines in Figure 1.1), where there is little energy left to resonate the oscillator, the PSA ordinates are dominated by a wide frequency band of the ground motion that ultimately equals the integration over the entire spectrum of the input ground motion [Bora at al. 2016]. This can be observed in Figure 1.1, where the dashed green line traces the ground motion FAS for frequencies less than about 4 Hz. The short period PSA is then controlled by the dominant period of the input ground motion, rather than the natural period of the oscillator.

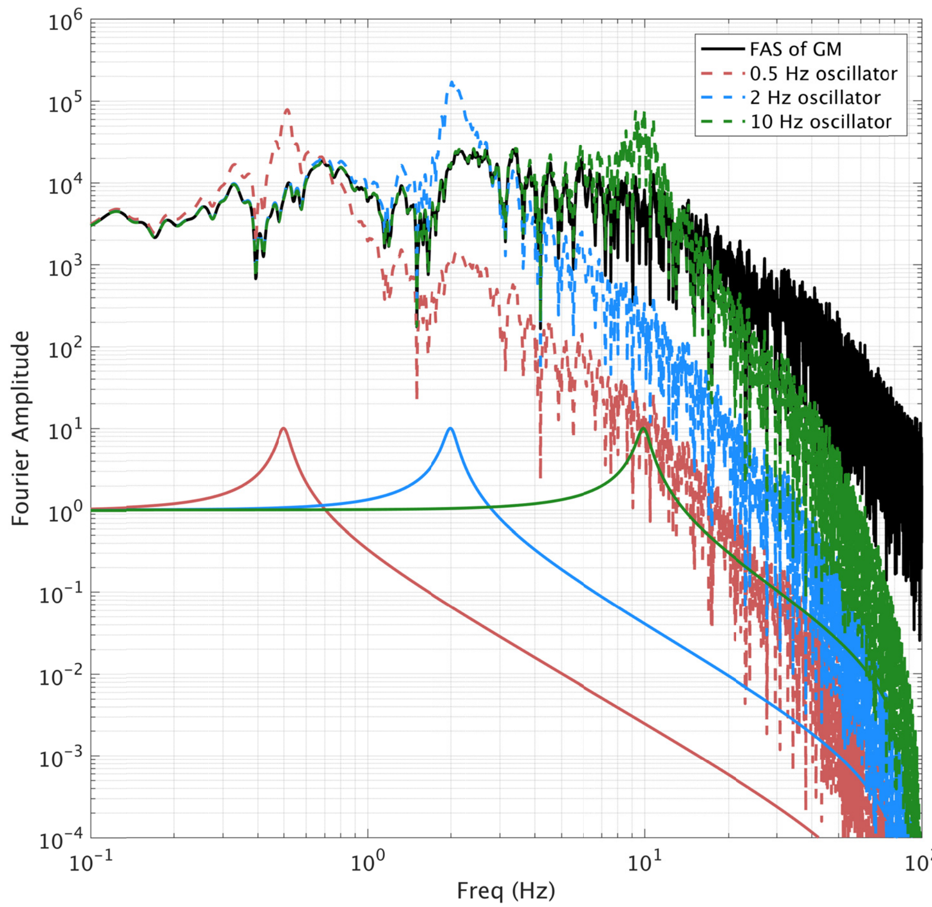

Figure 1.1 **Fourier amplitudes developed from an example ground motion recording and SDOF oscillator response, illustrating the range of frequencies contributing to the response spectrum calculation.**

In summary, PSA provides the spectrum of peak response from a SDOF system, which is influenced by a range of frequencies, and the breadth of that range is dependent on the oscillator period. The FAS provides a more direct representation of the frequency content of the ground motions, and since the Fourier transform is a linear operation, the FAS is a much more straightforward representation of the ground motion. As a result, recordings from small earthquakes can be used to constrain path and site effects without dependence on response spectral shape. Numerous seismological models of the FAS are available (e.g. Brune [1970] and Boore et al. [2014]) to provide a frame of reference during model development. Additionally, using FAS more easily facilitates future calibration of the inter-frequency correlation of ground-motion simulation methods because there is not a strong reversal of the correlation coefficients at high frequencies, as described in Bayless and Abrahamson [2018].

2 Ground-Motion Data

The PEER NGA-West2 strong-motion database includes over 21,000 three-component strong-motion records recorded worldwide from shallow crustal earthquakes, including aftershocks, in active tectonic regimes since 2003 [Ancheta et al. 2014]. Earthquake magnitudes in the full database range from 3 to 7.9 and rupture distances extend to over 1500 km. Earthquakes and recordings identified as questionable in quality or with undesirable properties are excluded; see Abrahamson et al. [2014] for a complete list of criteria for exclusions. At distances under 100 km, recordings from crustal earthquakes worldwide are retained to constrain the magnitude scaling and geometric spreading. At the larger distances (up to 300 km), region-specific anelastic attenuation and linear site effects due to the regional crustal structure are accounted for by including recordings only from California and Nevada. Only events with at least five recordings per earthquake are included.

The EAS has been calculated for each record in the database up to the Nyquist frequency by PEER [Kishida et al. 2016]. The usable frequency range limitations of each record are accounted for by applying the recommended lowest and highest usable frequencies for response spectra determined from Abrahamson and Silva [1997] as:

$$\text{Lowest usable frequency (LUF)} = 1.25 * \max\left(\text{HPF}_{HC1}, \text{HPF}_{HC2}\right) \tag{2.1}$$

$$\text{Highest usable frequency (HUF)} = \frac{1}{1.25} * \min\left(\text{LPF}_{HC1}, \text{LPF}_{HC2}\right) \tag{2.2}$$

where HPF is the record high-pass filter frequency, LPF is the record low-pass filter frequency, and $HC1$ and $HC2$ are the two horizontal components of a three-component time series. The factors of 1.25 in Equations (2.1) and (2.2) were originally used by Abrahamson and Silva [1997] to ensure that the filters did not have a significant effect on the response spectral values. By limiting the usable period range using these factors, the frequency interval of the impulse response of a 5% damped oscillator will not exceed the filter values. And retaining this usable frequency range maintains consistency with the response spectrum calculations. Based on inspection of the usable frequency range of the data, the LUF was restricted to a minimum value of 0.1 Hz, and the HUF was restricted to a maximum value of 24 Hz for all recordings. Therefore, the regressions were performed between 0.1–24 Hz.

After screening for record quality, recording distance, minimum station requirements, and frequency limitations, the final dataset consists of 13,346 unique records from 232 earthquakes, both of which vary as a function of frequency. Figure 2.1 shows the frequency dependence of the number of earthquakes and recordings used in regressions steps 1 and 3 (listed in Table 4.2 and explained in Section 4). Figure 2.2 shows a magnitude versus rupture distance scatterplot of the NGA-West2 database subsets used in regression step 1 at f = 0.2 and 10 Hz.

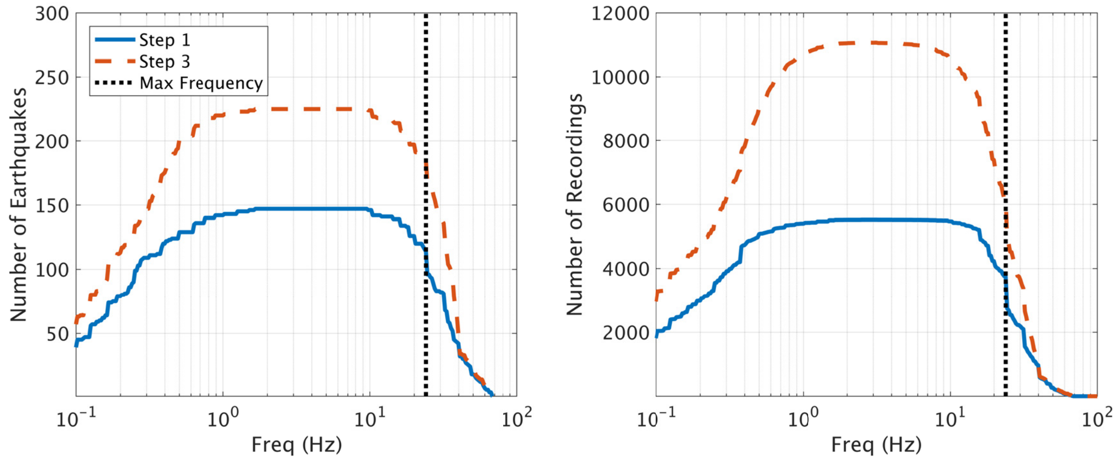

Figure 2.1 **Number of earthquakes and recordings from the NGA-West2 EAS database used in the regression steps 1 and 3, versus frequency. The regressions were performed between 0.1–24 Hz; higher frequencies are included in this figure only to display the rapid reduction of available data with increasing frequency.**

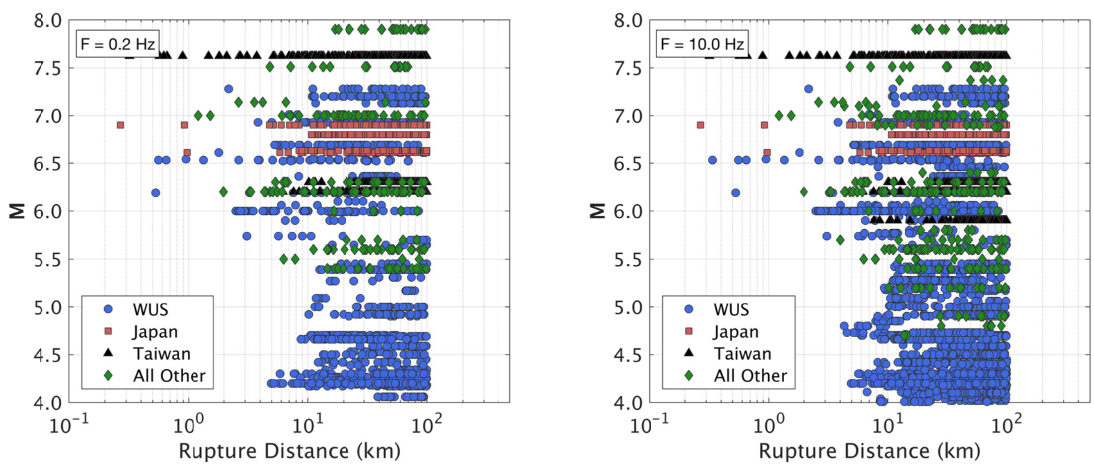

Figure 2.2 **Magnitude versus rupture distance pairs of the NGA-W2 EAS database subset used in regression step 1, at 0.2, and 10.0 Hz.**

3 Median Model Functional Form

The model parameters are defined in Table 3.1. The scaling of the source is primarily described by moment magnitude (**M)**. Source effects are also modeled using the depth to the top of the rupture plane (Z_{tor}), and a style-of-faulting flag for normal faults (F_{NML}). These source effects can be considered as proxies for stress drop scaling. The closest distance to the rupture plane, R_{RUP} is used as the distance measure for path scaling. The linear and nonlinear site effects are parameterized using V_{s30}, the time-averaged shear-wave velocity in the top 30 m of the soil column below the site. Use of V_{s30} does not imply that 30 m is the key depth range for the site response, but rather that V_{s30} is correlated with the entire soil profile [Abrahamson and Silva 2008]. The scaling with respect to soil depth is parameterized by the depth to the shear-wave velocity horizon of 1 km/sec, Z_1.

Table 3.1 Model parameter definitions.

Parameter	Definition
EAS	Effective amplitude spectrum (g-sec). The EAS is the orientation-independent horizontal component Fourier amplitude spectrum (FAS) of ground acceleration, defined in Goulet et al. [2018].
M	Moment magnitude
Z_{tor}	Depth from the surface to the top of the rupture plane (km)
F_{NM}	Style of faulting flag; 1 for Normal faulting earthquakes, 0 for all others.
R_{RUP}	Rupture distance (km)
V_{s30}	Time averaged shear wave velocity in the upper 30 meters (m/sec)
Z_1	Depth from the surface to shear wave velocity horizon of at least 1 km/sec (km)
I_r	Peak ground acceleration for the Vs30 = 760 m/sec condition (g)

The model prediction for the EAS (units g-sec) ground motion is given by Equation (3.1):

$$\ln \mathrm{EAS} = \ln \mathrm{EAS}_{\mathrm{med}} + \varepsilon\sigma \tag{3.1}$$

where σ is the total aleatory variability, and the standard-normal random variable ε is the number of standard deviations above or below the median. The median estimate of the EAS ($\mathrm{EAS}_{\mathrm{med}}$, with units g-sec) can be calculated from Equation (3.2), where each of the model components are described in the following sections.

$$\ln \mathrm{EAS}_{\mathrm{med}} = f_M + f_P + f_S + f_{Z_{tor}} + f_{NM} + f_{Z_1} \tag{3.2}$$

3.1 MAGNITUDE SCALING, f_M

To capture the effects of energy radiated at the source, the formulation of the magnitude scaling is adopted from the Chiou and Youngs [2008; 2014] GMMs for response spectra. A polynomial magnitude scaling formulation was tested (e.g., Abrahamson et al. [2014]), and after evaluating the data found that both formulations fit the data well, but the Chiou and Youngs [2014] formulation would extrapolate more reasonably. Additionally, the Chiou and Youngs [2014] formulation has undergone several years of testing and refinement and is based on seismological models for the source FAS [Chiou and Youngs 2008], which translates directly to this application. The expression for the magnitude scaling is given by Equation (3.3):

$$f_M = c_1 + c_2\left(\mathbf{M} - 6\right) + c_3 \ln\left(1 + e^{c_n\left(c_M - \mathbf{M}\right)}\right) \tag{3.3}$$

The components of f_M are described in Chiou and Youngs [2008]. To recap, the formulation captures approximately linear magnitude scaling at low frequencies (well below the source corner) and high frequencies (well above the source corner) with a nonlinear transition in between, where the transition shifts to lower frequencies for larger magnitudes. The coefficient c_1 works jointly with the c_2 and c_3 terms to approximately represent the mean spectral shape after correcting for all other adjustments. The coefficient c_2 is the frequency independent linear **M** scaling slope for frequencies well above the theoretical corner frequency. The term with coefficient c_3 captures both the approximately linear scaling of the FAS below the theoretical corner frequency, and the non-linear transition to that scaling. The coefficient c_n controls the width of the magnitude range over which the transition between low- and high-frequency linear scaling occurs, and the coefficient c_M is the magnitude at the midpoint of this transition. All of the magnitude scaling terms were determined in the regression.

3.2 PATH SCALING, f_P

Together with the magnitude scaling, the extensively-tested path scaling formulation of Chiou and Youngs [2014] is utilized:

$$f_P = c_4 \ln\left\{R_{\mathrm{RUP}} + c_5 \cosh\left[c_6 \max\left(\mathbf{M} - c_{hm}, 0\right)\right]\right\} + \left(-0.5 - c_4\right)\ln\left(\hat{R}\right) + c_7 R_{\mathrm{RUP}} \tag{3.4}$$

$$\hat{R} = \sqrt{R_{\mathrm{RUP}}^{2} + 50^{2}} \tag{3.5}$$

The components of Equation (3.4) are described in Chiou and Youngs [2008]. To recap, the term with coefficient c_4 captures near-source geometric spreading, which is magnitude and frequency dependent. The magnitude and frequency dependence on the geometric spreading is introduced by adding a term to the rupture distance inside the log-distance term, expressed by the term with coefficient c_5. This additive distance is designed to capture the near-source amplitude saturation effects of the finite-fault rupture dimension. This term is a frequency-dependent constant for small magnitudes, and transitions to be proportional to exp (**M**) for large magnitudes, with the largest additive distance at high frequencies. Since the hyperbolic cosine is a monotonically increasing function, the coefficient c_5 controls the scaling of this term, and coefficients c_6 and c_{hm} control the gradient.

Since the coefficients c_5, c_6, and c_{hm} are multiplied with c_4, there is potential for trade-off between them. The regression procedure is started with the values for coefficients c_5, c_6, and $c$hm from Chiou and Youngs [2014] to obtain c_4 from the data, ensuring the model did not over-saturate. Using Equations (3.3) and (3.4), the full saturation condition (no magnitude scaling at zero distance) leads to the following constraint on the coefficients: $c_2 = -c_4 c_6$. For c_2 values larger than the full saturation value, there will be a positive magnitude scaling at zero distance (i.e., not full saturation). It is reasonable for the EAS to have some scaling at zero distance even though the PSA is nearly fully saturated at high frequencies. The PSA saturates in part because the procedure involves selecting the peak response of the oscillator over all time, meaning it is not affected by duration. Conversely, the EAS is not a peak response operator, and so it will continue to scale for large magnitudes at short distance due to the longer source durations. This is the contribution of the lower amplitudes over the duration of the signal.

The near-source saturation of magnitude scaling is checked against the data and against finite–fault simulations (see Section 6 for more details) and the EAS saturation in this model does not disagree with those from the simulations. In later stages of the regression, the coefficients c_5, c_6, and c_{hm} are also determined empirically. The values from the regression do not change enough to impact the model, so coefficient values are fixed from Chiou and Youngs [2014] for c_5, c_6, and c_{hm} in the final model. Thus, the coefficients c_2 and c_4 control the saturation in the model development.

Following Chiou and Youngs [2014], at large distances, the distance scaling smoothly transitions to be proportional to $R^{-0.5}$ to model surface wave rather than body wave geometric spreading effects. This effect is introduced with the $\ln\left(\hat{R}\right)$ term, which controls at distances greater than 50 km by subtracting the c_4 coefficient and imposing a -0.5 slope. Effects of crustal anelastic attenuation (Q) are captured through the term with the frequency-dependent coefficient c_7. The Q scaling does not require magnitude dependence for the EAS.

3.3 SITE RESPONSE, f_S

The V_{S30} (m/sec) dependence of site amplification is modeled using Equation (3.6):

$$f_S = f_{SL} + f_{NL} \tag{3.6a}$$

$$f_{SL} = c_8 \ln\left[\frac{\min\left(V_{s30}, 1000\right)}{1000}\right] \tag{3.6b}$$

$$f_{NL} = f_2 \ln\left(\frac{I_R + f_3}{f_3}\right) \tag{3.6c}$$

$$f_2 = f_4\left\{e^{f_5\left[\min\left(V_{s30}, V_{\text{ref}}\right) - 360\right]} - e^{f_5\left(V_{\text{ref}} - 360\right)}\right\} \tag{3.6d}$$

$$\ln\left(I_R\right) = 1.238 + 0.846 \ln\left[\text{EAS}_{\text{ref}}\left(f = 5\text{ Hz}\right)\right] \tag{3.6e}$$

where the linear site amplification is given by f_{SL}, and the nonlinear site amplification is given by f_{NL}, which is the analytical site amplification function for FAS in the western United States (WUS) modified from Hashash et al. [2018].

The linear site term, f_{SL}, is formulated as a linear function of ln(V_{s30}) and is centered on the reference V_{s30} of 1000 m/sec. The f_{SL} term is determined in the regression analysis. Abrahamson et al. [2014] observed that at long periods, the scaling of PSA with V_{s30} became weaker for higher V_{s30} values, and, therefore, selected a model that does not scale with V_{s30} above some maximum value, V_1 = 1000 m/sec. Inclusion of this feature is based on evaluation of the data (Figure 3.1), which implies that above 1000 m/sec, the correlation between V_{s30} and the deeper profile no longer holds. Below 1000 m/sec, the linear site amplification terms approximately scales linearly with ln(V_{s30}), so the regional linear V_{s30}-based site amplification is modeled with a single frequency-dependent coefficient, c_8.

The nonlinear site amplification, f_{NL}, is constrained using a purely analytical model rather than obtaining it from the data. Empirical evaluations of the nonlinear effects are limited by the relatively sparse sampling of ground motions expected to be in the nonlinear range in the NGA-West2 database [Kamai et al. 2014]. Therefore, the Hashash et al. [2018] nonlinear site amplification term, f_{NL}, was adopted to model nonlinear soil amplification. This model was developed analytically by performing large-scale 1D site response simulations of input rock motions propagated through soil columns representative of WUS site conditions. Hashash et al. (2018) produced linear and nonlinear site amplification models for the PSA and FAS. Equations (3.6c) and (3.6d) are the nonlinear FAS amplification components of the Hashash et al. [2018] model developed for the WUS. In these equations, f_3, f_4, and f_5 are frequency-dependent coefficients, I_R is the peak ground acceleration (PGA, in units g) at rock outcrop, and V_{ref} is the limiting velocity beyond which there is no amplification relative to the reference rock condition, set to 760 m/sec [Hashash et al. 2018]. In this model, almost no nonlinearity is applied at frequencies below 1.0 Hz and the modification approaches zero for small values of the input motion (I_R) and as V_{s30} approaches V_{ref}.

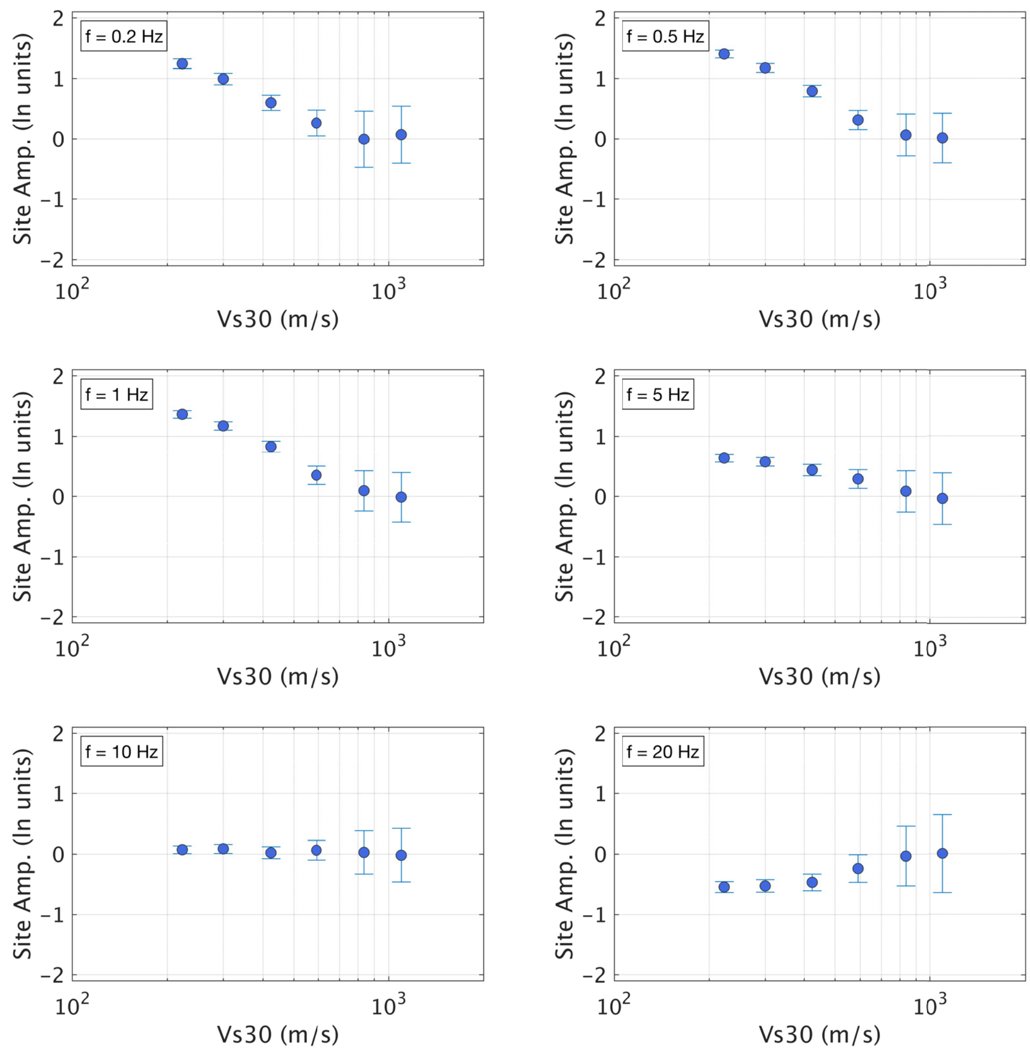

Figure 3.1 V_{s30} **scaling of the linear site amplification terms, at** f **= 0.2, 0.5, 1, 5, 10, and 20 Hz.**

To ensure smooth spectra in the GMM, a smoothed version of the Hashash et al. [2018] nonlinear site amplification model is implemented. The smoothing of coefficients f_3, f_4, and f_5 in frequency space are shown in Figure 3.2. The maximum frequency of the Hashash et al. [2018] model is 13.3 Hz, and the coefficients of the model reduce the nonlinear effect to zero for frequencies greater than this value simply due to the lack of FAS values at higher frequencies. Physically, this is not realistic behavior. To include nonlinear effects at the higher frequencies, the Hashash et al. [2018] model is modified by taking the minimum value of f_{NL} over all frequencies and constrain all higher frequencies to take the same value. An example of this method (for input values of V_{s30} = 300 m/sec and I_R = 0.8g) is shown in Figure 3.2.

To utilize the Hashash et al. [2018] nonlinear model requires the PGA on rock. Since the model is for the EAS, an estimate of the PGA (in units g) for the reference-site condition is developed as a function of the EAS for the reference site condition at f = 5 Hz (in units g-sec), given by Equation (3.6e). The EAS at f = 5 Hz is used to estimate PGA because this is approximately the predominant frequency of the ground motions and should correlate strongly with the PGA. In Figure 3.3, the data used to develop the I_R − EAS$_{ref}$ (f = 5 Hz) relationship are shown. Ground motions with $I_R > 0.01g$ are included, with symbols identifying data within unit **M** bins. In Figure 3.3, I_R is corrected to the reference site condition using the Abrahamson et al. [2014] linear site amplification model, and the EAS is corrected the reference V_{s30} condition using the linear site amplification model from this study. The least squares fit given by Equation (3.6e) is shown with the dashed line. Different **M** and distance ranges were evaluated similarly, with minimal differences in the slope of the relationship.

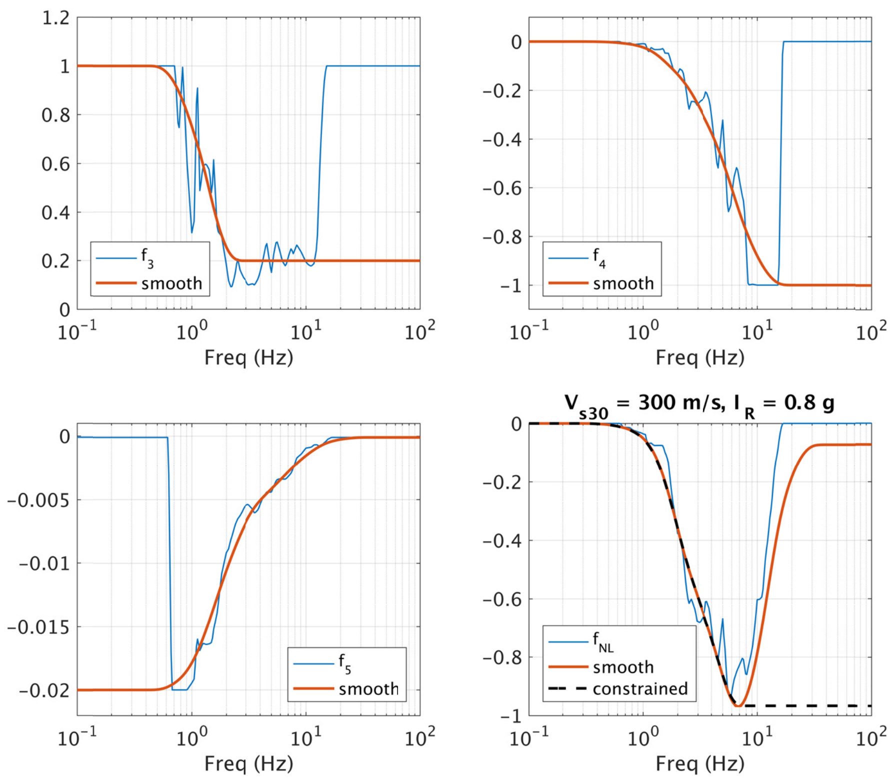

Figure 3.2 Smoothing of the Hashash et al. [2018] coefficients f_3, f_4, and f_5, and the smoothing procedure of term f_{NL} for example values of V_{s30} = 300 m/sec and I_R = 0.8g

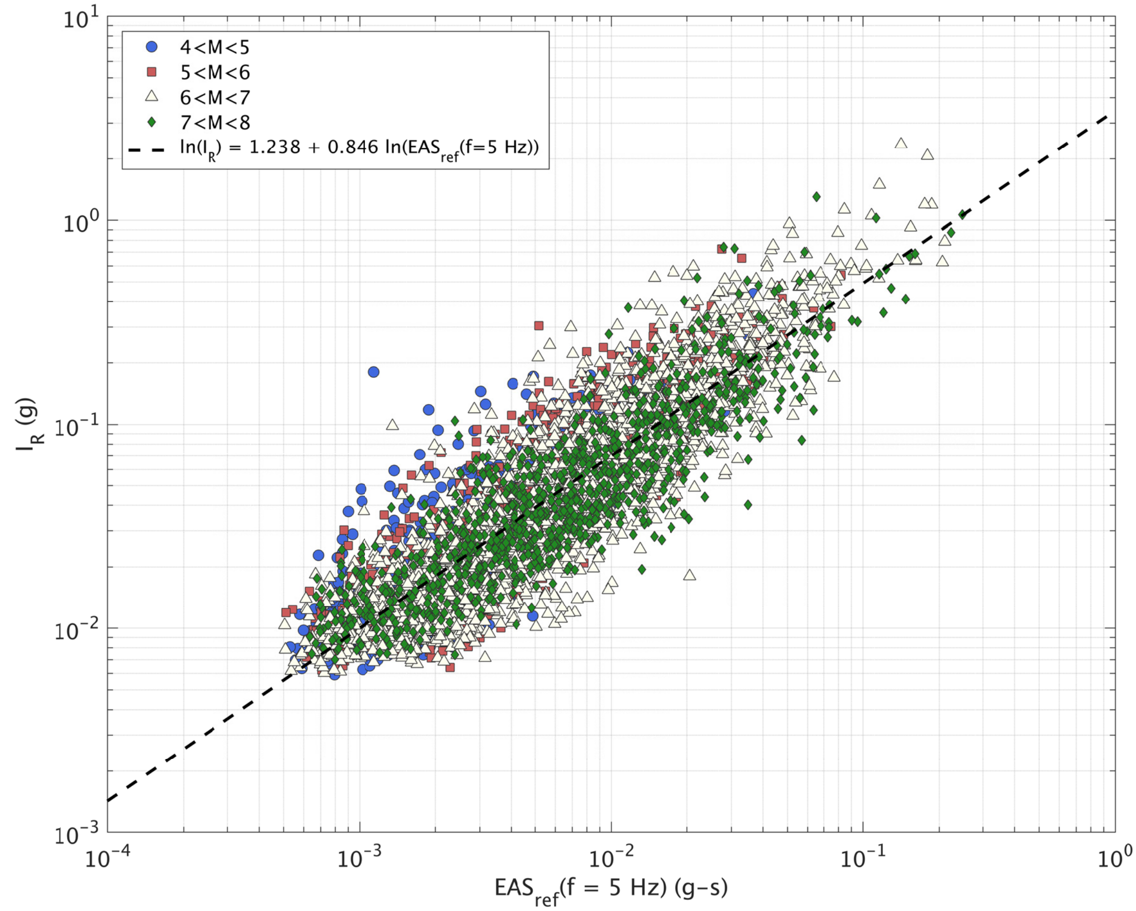

Figure 3.3 **Data used to develop the I_R – EAS$_{ref}$ (f = 5 Hz) relationship, where I_R is the peak ground acceleration on rock and EAS$_{ref}$ (f = 5 Hz) is the 5 Hz EAS on rock. Ground motions with I_R > 0.01g are included, with symbols identifying M bins. I_R is corrected to the reference site condition using the Abrahamson et al. [2014] linear site amplification model, and the EAS is corrected the reference V_{s30} condition using the linear site amplification model from this study.**

3.4 DEPTH TO TOP OF RUPTURE SCALING, f_{Ztor}

To model differences in the ground motions for surface and buried ruptures, the depth to the top of rupture scaling model takes the form of Equation (3.7):

$$f_{Z_{\text{tor}}} = c_9 \min\left(Z_{\text{tor}}, 20\right) \tag{3.7}$$

where c_9 c_9 is frequency dependent, and Z_{tor} is non-negative and measured in km. The Z_{tor} scaling is capped at 20 km to prevent unbounded scaling with Z_{tor}.

3.5 NORMAL STYLE OF FAULTING EFFECTS, f_{NM}

To model the differences in ground motions for normal style faults, the normal faulting term is:

$$f_{NM} = c_{10} F_{NM} \tag{3.8}$$

where F_{NM} is 1 for normal style faults and 0 for all others, and c_{10} is determined in the regression. A style of faulting term for reverse events was considered but not included, because this term was highly correlated with Z_{tor}. Therefore, the reverse style of faulting scaling is captured in $f_{Z_{\mathrm{tor}}}$.

3.6 SOIL DEPTH SCALING, f_{Z1}

To model the scaling with respect to sediment thickness, the Abrahamson et al. [2014] formulation is adopted, which is parameterized by the depth to shear wave velocity horizon of 1.0 km/sec, Z_1 (units of km). This model takes the form:

$$f_{Z_1} = c_{11} \ln\left[\frac{\min\left(Z_1, 2.0\right) + 0,01}{Z_{1_{\mathrm{ref}}} + 0.01}\right] \tag{3.9a}$$

$$c_{11} = \begin{cases} c_{11a} & \text{for } V_{s30} \le 200 \text{ m/sec} \\ c_{11b} & \text{for } 200 < V_{s30} \le 300 \text{ m/sec} \\ c_{11c} & \text{for } 300 < V_{s30} \le 500 \text{ m/sec} \\ c_{11d} & \text{for } V_{s30} > 500 \text{ m/sec} \end{cases} \tag{3.9b}$$

$$Z_{1_{\mathrm{ref}}} = \frac{1}{1000}\exp\left[\frac{-7.67}{4}\ln\left(\frac{V_{s30}{}^4 + 610^4}{1360^4 + 610^4}\right)\right] \tag{3.9c}$$

where $Z_{1_{\mathrm{ref}}}$ is the reference Z_1 for the regional model for California and Nevada. Equation (3.9c) was developed by Chiou and Youngs [2014] to account for regional differences in the $V_{s30} - Z_1$ relationships in the data. Abrahamson et al. [2014] showed that the Z_1 scaling is dependent on the V_{s30} value and used the V_{s30} bins in Equation (3.9b) to model this dependence; the same bins are used here. The soil depth scaling is capped to Z_1 = 2 km based on the range of the data and to avoid unconstrained extrapolation.

4 Regression Analysis

The random-effects model is used for the regression analysis following the procedure described by Abrahamson and Youngs [1992]. This procedure leads to the separation of total residuals into between-event residuals (δB) and within-event residuals (δW), following the notation of Al Atik et al. [2010]. For large numbers of recordings per earthquake, the between-event residual is approximately the average difference in logarithmic-space between the observed IM from a specific earthquake and the IM predicted by the GMM. The within-event residual (δW) is the difference between the IM at a specific site for a given earthquake and the median IM predicted by the GMM plus δB. By accounting for repeatable site effects, δW can further be partitioned into a site-to-site residual ($\delta S2S$) and the single-station within-event residual (δWS, also called the within site residual) (e.g., Villani and Abrahamson, 2015). Using this notation, the residuals take the following form:

$$Y = g\left(X_{es}, \theta\right) + \delta B_e + \delta S2S_s + \delta WS_{es} \tag{4.1}$$

$$\begin{aligned} \delta_{\text{total}} &= Y - g\left(X_{es}, \theta\right) + \delta B_e + \delta S2S_s + \delta WS_{es} \\ \delta_{\text{total}} &= Y - g\left(X_{es}, \theta\right) + \delta B_e + \delta S2S_s + \delta WS_{es} \\ \sigma &= \sqrt{\tau^2 + \phi_{S2S}^2 + \phi_{SS}^2} \end{aligned} \tag{4.2}$$

where Y is the natural log of the recorded ground motion IM, $g(X_{es}, \theta)$ is the median GMM, X_{es} is the vector of explanatory seismological parameters (magnitude, distance, site conditions, etc.), θ is the vector of GMM coefficients, and δ_{total} is the total residual for earthquake e and site s.

The residual components δB, $\delta S2S$, and δWS are well-represented as zero-mean, independent, normally distributed random variables with standard deviations τ, ϕ_{S2S}, and ϕ_{SS}, respectively [Al Atik et al. 2010]. The total standard deviation, σ, is expressed as:

$$\sigma = \sqrt{\tau^2 + \phi_{S2S}^2 + \phi_{SS}^2} \tag{4.3}$$

The regression is performed in a series of steps to prevent trade-off of correlated model coefficients and to constrain different components of the model using the data relevant to each piece. These steps are given in Table 4.1, along with the data used and parameters determined from each step. In Step 1-a, a dataset consisting of larger magnitudes and shorter distances is used to constrain the large magnitude scaling and near-source finite–fault saturation, using data from all regions. In Steps 1-b through 1-d, the same data set is used, and the remaining source effects are determined. In Step 2, the regionalized linear site amplification parameters are determined using the data from California and Nevada at distances within 100 km. In Steps 3-a through 3-c, data from California and Nevada are included out to 300 km distance. In these regression steps, the regional soil depth scaling, anelastic attenuation, and mean spectral shape coefficients are determined. For all steps the regression is performed independently at each of 239 log-spaced frequencies spanning 0.1–24 Hz.

Table 4.1 Regression steps.

Step	Data used	Parameters free in the regression	Parameters smoothed after the regression
1-a	$\mathbf{M} > 4$, $R_{\mathrm{RUP}} \leq 100$ km, all regions	c_1, c_2, c_3, c_n, c_M, c_4, c_7, c_8, c_9, c_{10}, c_{11}	c_2, c_4 (**M**, path)
1-b	Same as 1-a	c_1, c_3, c_n, c_M, c_7, c_8, c_9, c_{10}, c_{11}	c_3, c_n, c_M (**M**)
1-c	Same as 1-a	c_1, c_5, c_6, c_{hm}, c_7, c_8, c_9, c_{10}, c_{11}	c_5, c_6, c_{hm} (path)
1-d	Same as 1-a	c_1, c_7, c_8, c_9, c_{10}, c_{11}	c_9 (Z_{tor})
1-e	Same as 1-a	c_1, c_7, c_8, c_{10}, c_{11}	c_{10} (F_{NM})
2	$\mathbf{M} > 4$, $R_{\mathrm{RUP}} \leq 100$ km, from CA/Nevada	c_1, c_7, c_8, c_{11}	c_8 (V_{S30})
3-a	$\mathbf{M} > 3$, $R_{\mathrm{RUP}} \leq 300$ km, from CA/Nevada	c_1, c_7, c_{11}	c_{11} (Z_1)
3-b	Same as 3-a	c_1, c_7	c_7 (Q)
3-c	Same as 3-a	c_1	c_1

4.1 SMOOTHING

The model coefficients are smoothed in a series of steps as outlined in Table 4.1. Smoothing of the coefficients is performed to assure smooth spectra and, in some cases, to constrain the model to a more physical behavior where the data are sparse [Abrahamson et al. 2014]. Tables of the values of the final smoothed coefficients are available in Electronic Appendix B.

Figure 4.1 through Figure 4.10 show the regressed model coefficients plotted versus frequency, before and after smoothing. The coefficients c_2 and c_4 are frequency independent and are determined from regressions in the high frequency range. The coefficients c_3, c_n, and c_M require only minor smoothing to assure smooth spectra in the final model, including extrapolation outside the ranges well constrained by data. The smoothing of c_7 (the anelastic attenuation term) is constrained to be non-positive at all frequencies so that the model does not unintentionally increase in amplitude at very large distances. Minimal smoothing is required for the coefficient c_8 (the linear V_{S30} term). The coefficient c_9 (the Z_{tor} term) takes on negative values at low frequencies implying small de-amplification of low frequency ground motions with increasing Z_{tor}. The data lead to a large drop in c_{10} (the normal faulting term) at low frequencies, but this is not included in the model because the theoretical basis is not clear; instead a frequency-independent constant is used (uniform scaling across frequencies) for normal style-of-faulting earthquakes. The c_{11} terms are smoothed as shown in Figure 4.8, where the uncertainty is largest for $c_{11\text{a}}$, which corresponds to the lowest V_{S30} bin with relatively fewer data.

The c_1 coefficient works collectively with the c_3 term to represent the mean spectral shape after correcting for all other adjustments. In the regression, unexpected behavior of c_1 at low frequencies is observed, as shown in Figure 4.10. At frequencies below about 0.3 Hz, the regressed coefficient values are equal to or larger than the 0.3 Hz value. If unmodified and combined with the c_3 term, this would lead to an irregular spectral "bump" at $f < 0.3$ Hz. Following Aki [1967], the mean spectrum should be approximately linear with a slope = 2 in this frequency range. Therefore, the c_1 coefficient is modified at low frequencies by constraining the slope from $f \approx 1.0$ Hz down to 0.1 Hz, as shown in Figure 4.10. The difference between the regressed values of c_1 and the constrained values of c_1 is denoted c_{1a}; this adjustment coefficient is plotted in the lower portion of Figure 4.10. By introducing the c_{1a} term, the model predicts smooth, theoretically appropriate spectra at low frequencies. This also allows for residuals which are zero-centered, which is required for computing the correlations of the residuals between frequencies. To account for this modification, the c_{1a} term must be added to the total standard deviation using Equation (2.21). The standard deviation model is discussed further below.

This unexpected behavior of c_1 may be due to bias in the data. At low frequencies, the signal to noise ratio is commonly low [Douglas and Boore 2011]. This contributes to the drop off in data at low frequencies shown in Figure 2.1. Additionally, at low frequencies, the large epsilon (above average) ground motions are more likely to be above the signal to noise ratio, and therefore, be included in the database. Likewise, the below average ground motions are more likely to be below this ratio and be excluded. The net effect may be that, for the FAS at low frequencies, the database is biased towards higher ground motions. Observing the data, the mean spectra for certain binned magnitude and distance ranges contain this feature. As an example, Figure 4.11 shows the geometric mean spectra of a subset of the data used in the analysis. This figure is created using recordings from strike-slip earthquakes with $R_{\text{RUP}} < 50$ km, for **M** bins one unit wide, and adjusted to the reference V_{S30} condition. Below about 0.3 Hz, the bump in the spectral shape in the data that causes the increase of c_1 is evident, especially for the data with **M** > 7 and **M** < 5.

Other physical explanations of the cause of the increase in coefficient c_1 are not apparent. To check that long period basin effects are not the cause, the mean spectra are examined in the same way, but only including records with $Z_1 < 0.15$ km, and the same behavior is observed. To further test if basin effects are not adequately captured by the model, c_1 is fixed to the constrained shape and the residuals are mapped. We do not see regional or spatial trends in the mapped residuals, implying that basin effects are not the culprit. Understanding the physical cause of the long-period shape of the spectrum will be evaluated further in a future study.

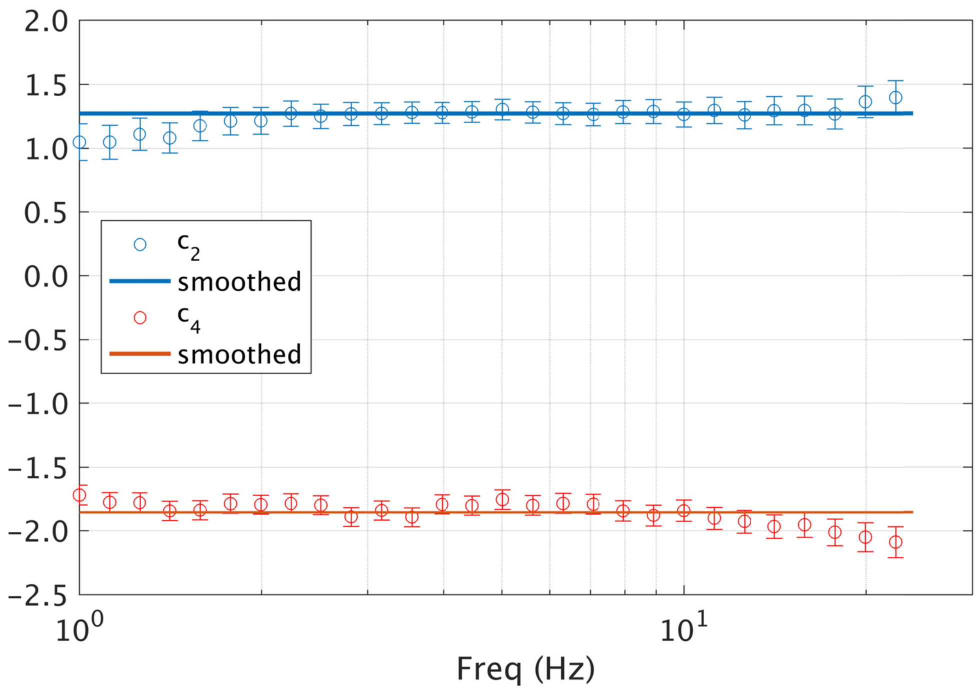

Figure 4.1 **Smoothing of source scaling (c_2) and near-source geometric spreading coefficients (c_4).**

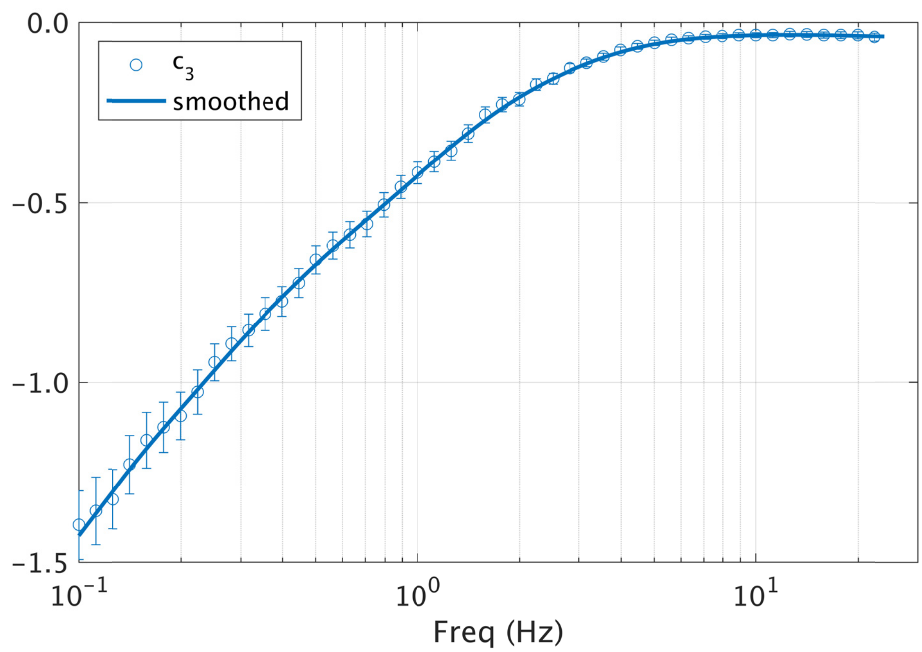

Figure 4.2 **Smoothing of the source scaling coefficient, c_3.**

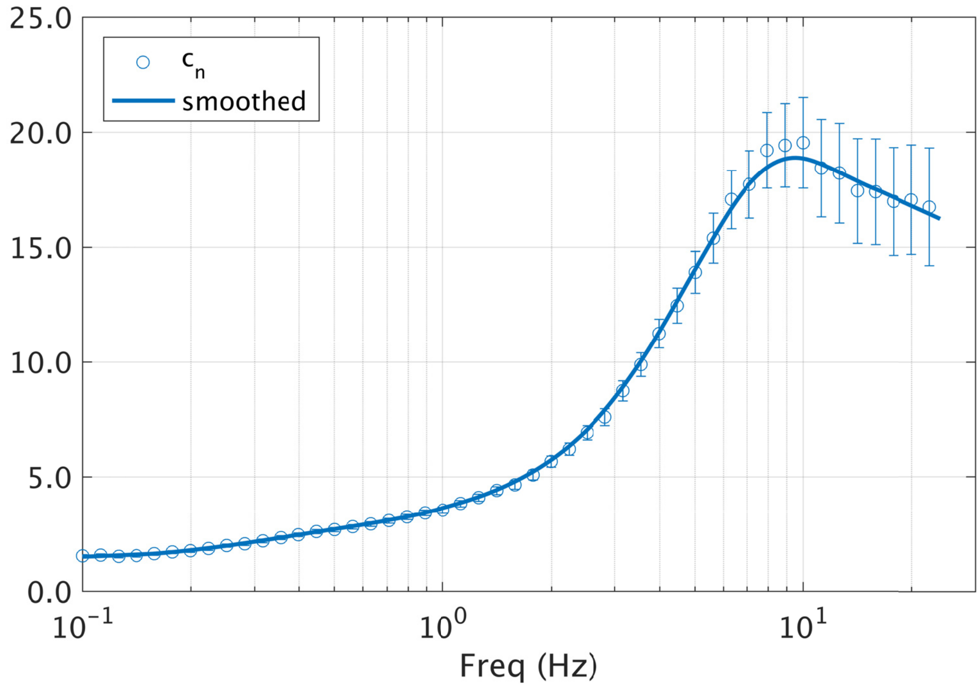

Figure 4.3 **Smoothing of the source scaling coefficient, c_n.**

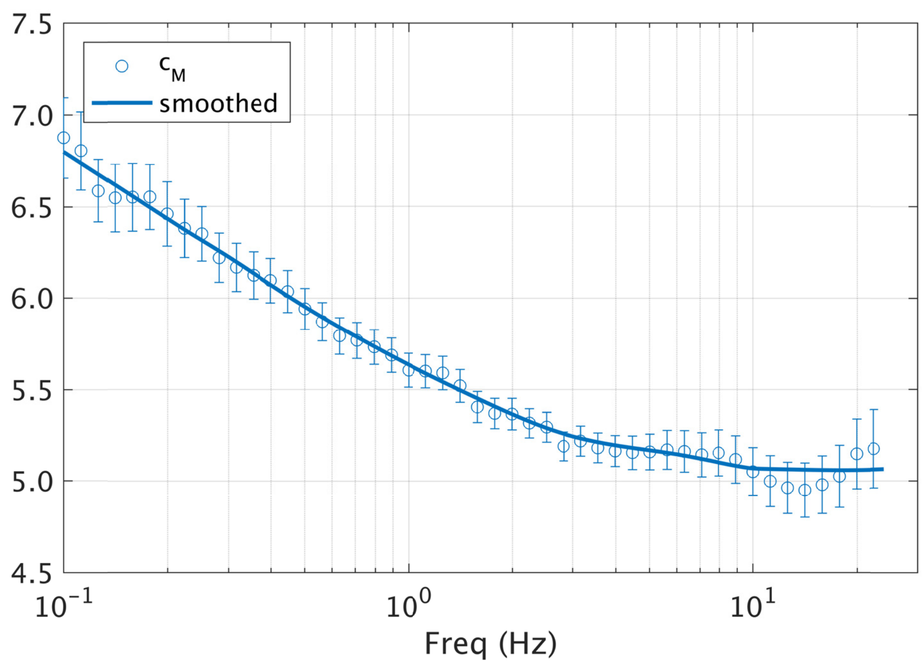

Figure 4.4 **Smoothing of the source scaling coefficient c_M.**

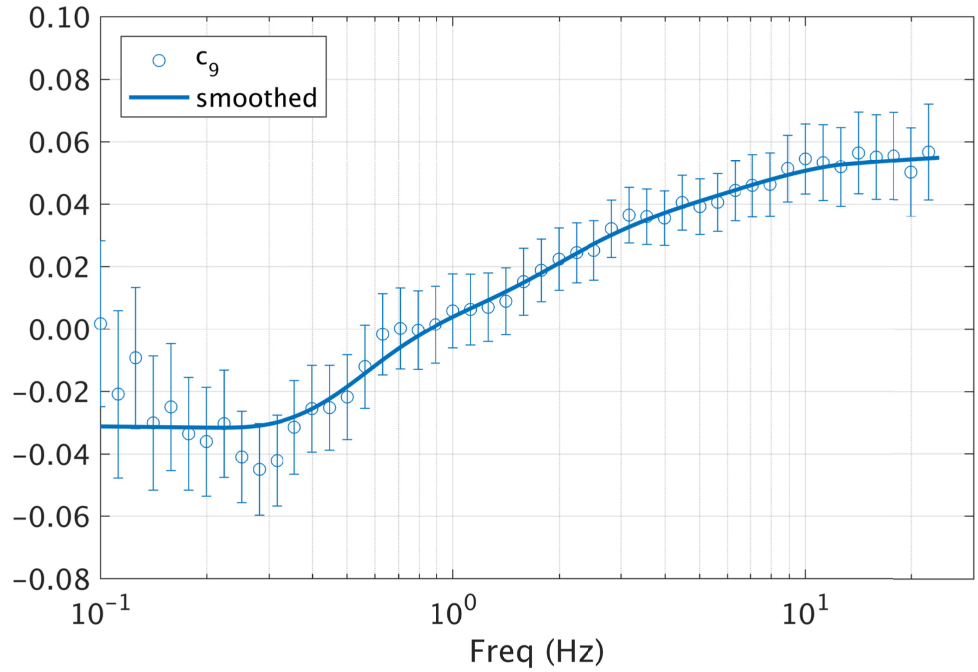

Figure 4.5 Smoothing of the Z_{tor} scaling coefficient, c_9.

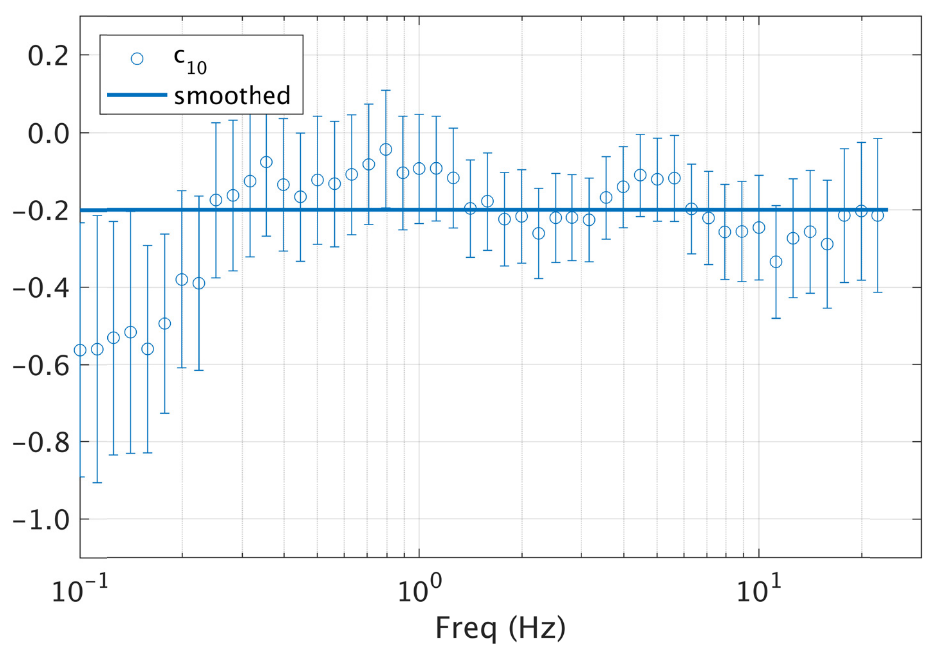

Figure 4.6 Smoothing of the F_{NM} style of faulting coefficient, c_{10}.

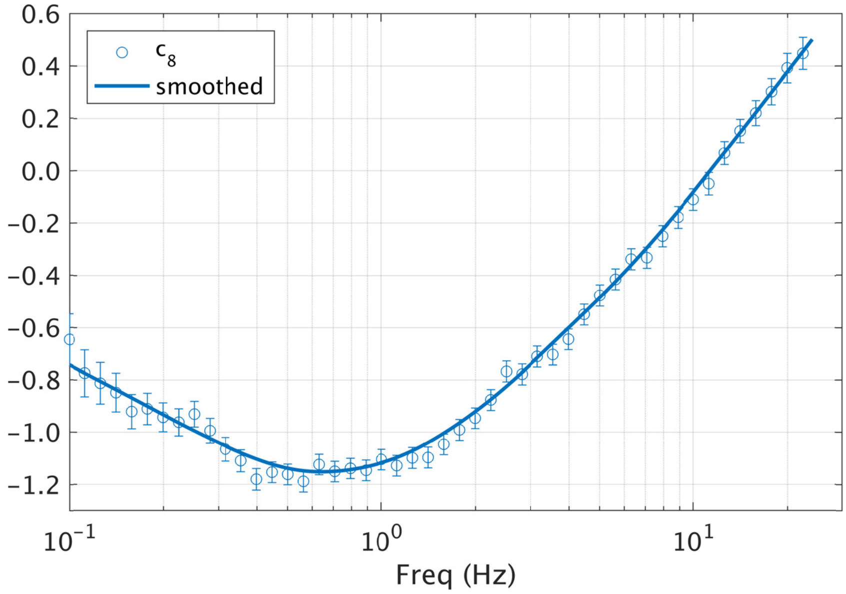

Figure 4.7 Smoothing of the linear V_{S30} scaling coefficient, c_8.

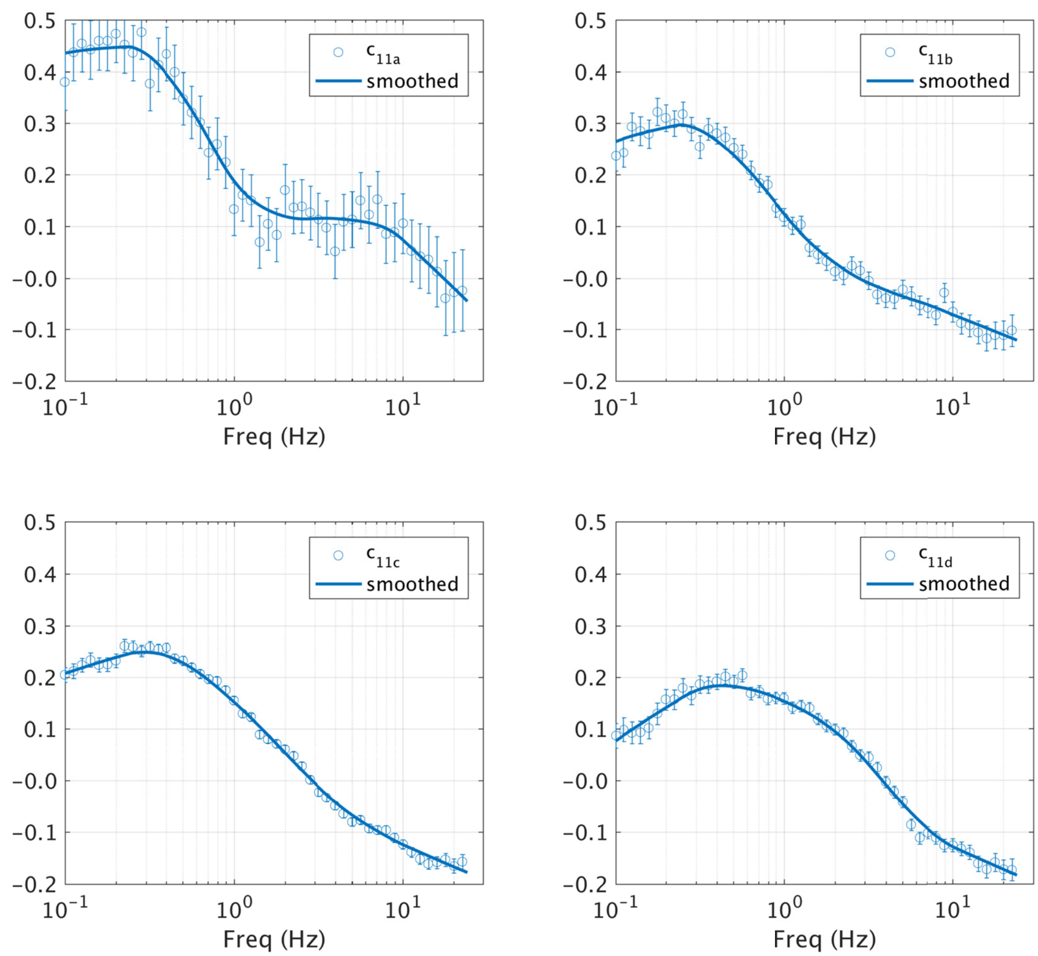

Figure 4.8 Smoothing of the Z_1 scaling coefficients, c_{11}.

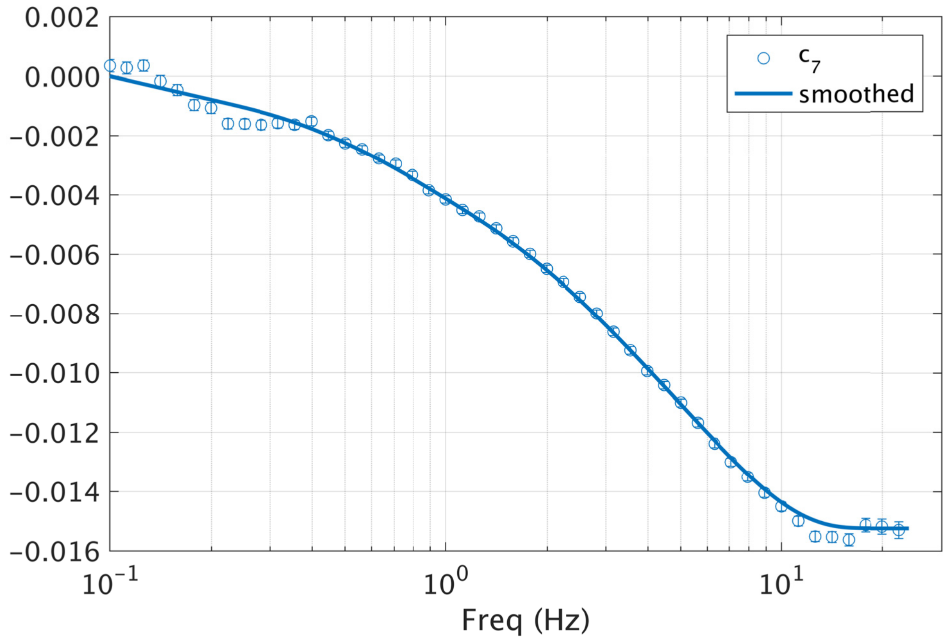

Figure 4.9 Smoothing of the anelastic attenuation coefficient, c_7.

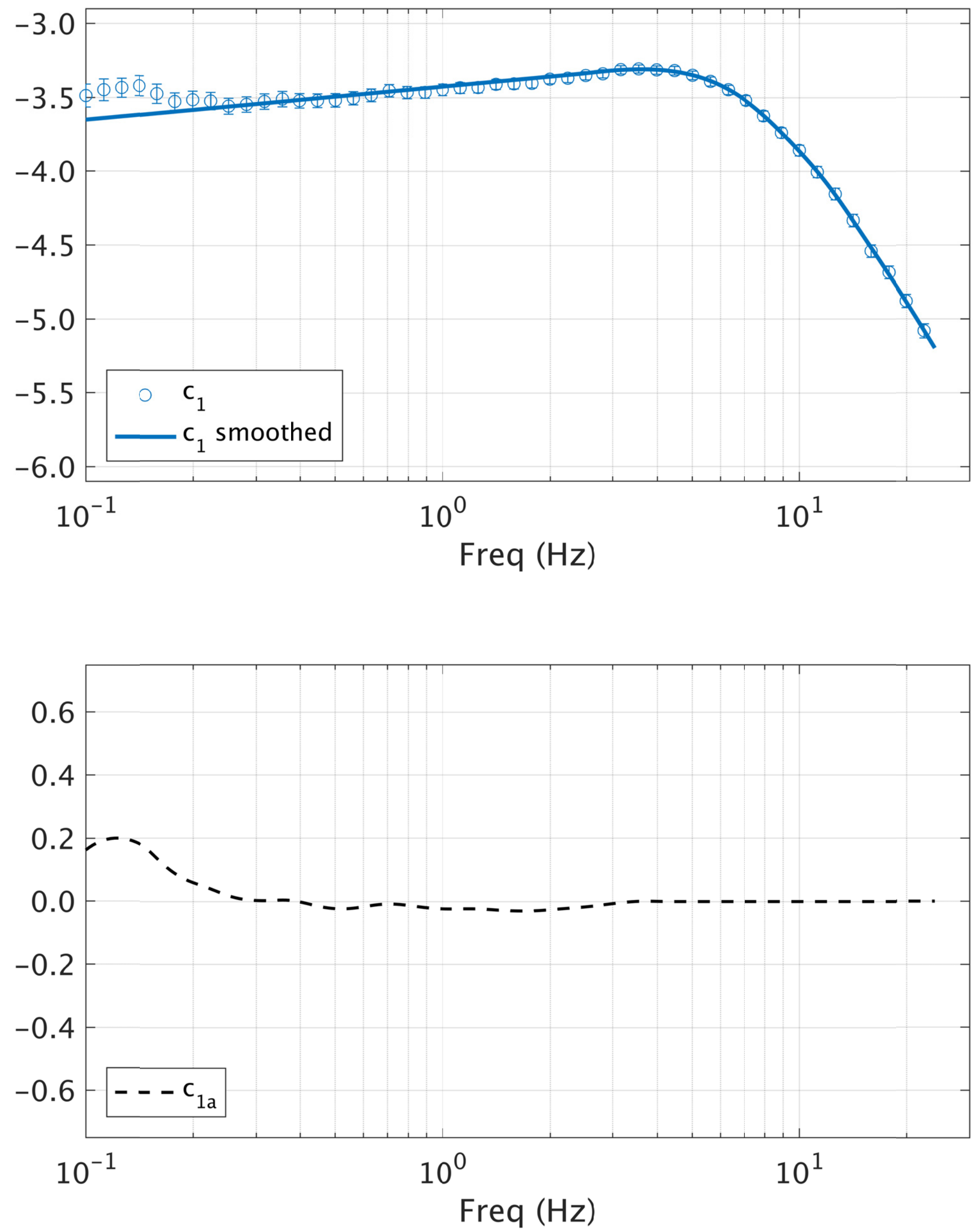

Figure 4.10 Smoothing of the coefficient, c_1, and adjustment coefficient c_{1a}.

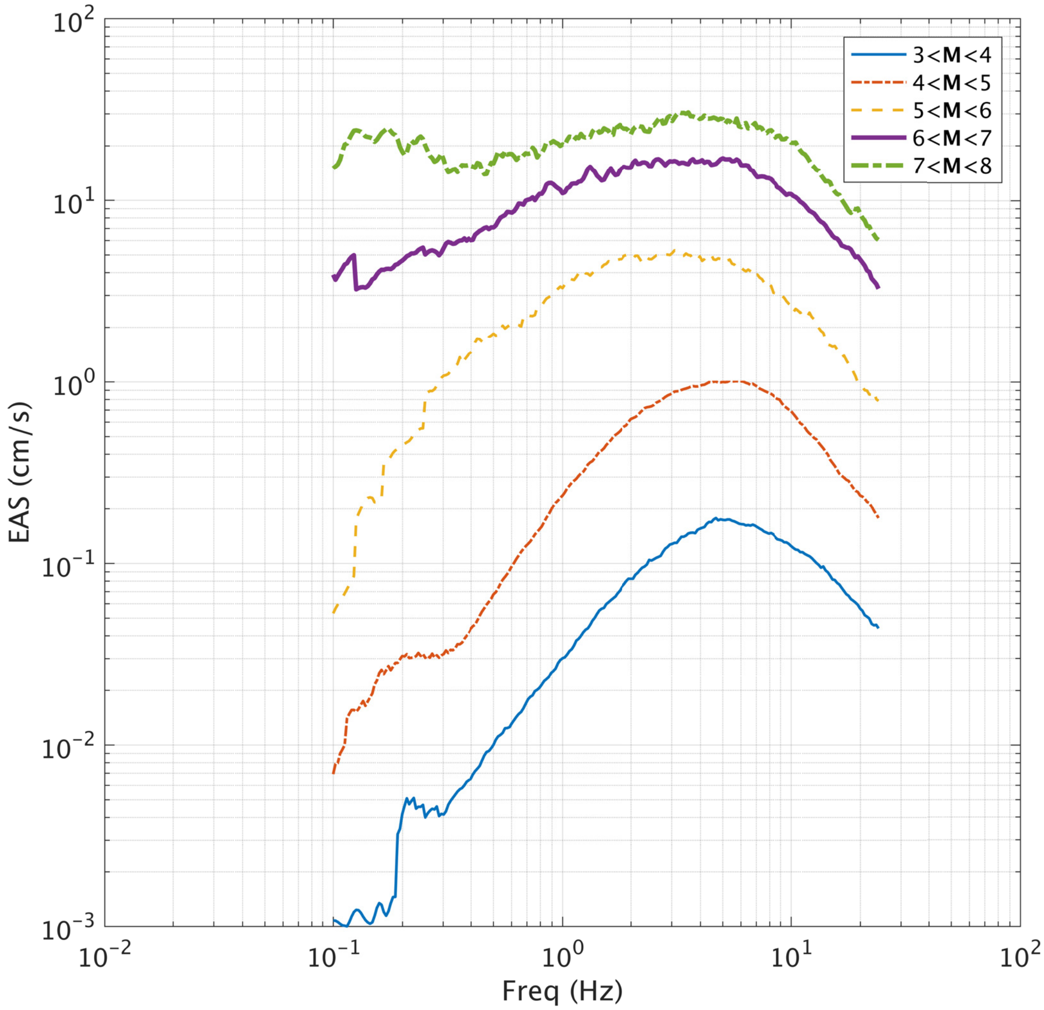

Figure 4.11 The geometric mean EAS spectra of the data used in the analysis, calculated using recordings from strike–slip earthquakes with R_{RUP} < 50 km, for M bins one unit wide, and adjusted to the reference V_{S30} condition.

4.2 EXTRAPOLATION TO 100 HZ

Model coefficients are obtained by regression for frequencies up to 24 Hz. At high frequencies, the FAS decays rapidly [Hanks 1982; Anderson and Hough 1984]. Anderson and Hough [1984] introduced the spectral decay factor kappa (κ) to model the rate of the decrease, where the amplitude of the log(FAS) decays linearly versus frequency (linear spaced), and κ is related to the slope. The total site amplification is the combined effect of crustal amplification and damping (κ and Q), but the effect of κ is so strong that it controls the spectral decay of the FAS at high frequencies and is the only parameter specified in the extrapolation. The model is extrapolated using Equations (4.4):

$$D(\kappa, f) = \exp\left(-\pi\kappa f\right) \tag{4.4a}$$

$$\ln\left(\kappa\right) = -0.4 * \ln\left(\frac{V_{s30}}{760}\right) - 3.5 \tag{4.4b}$$

$$\mathrm{EAS}\left(f > f_{\max}\right) = \mathrm{EAS}\left(f_{\max}\right) * D\left(\kappa, f - f_{\max}\right) \tag{4.4c}$$

where $D(\kappa, f)$ is the Anderson and Hough [1984] diminution operator, and f_{max} is the frequency beyond which the extrapolation occurs; f_{max} = 24 Hz. The parameter κ is estimated from κ is estimated from V_{S30} using the relationship given by Equation (4.4b). This relationship is selected based on the range of κ_0–V_{S30} correlation models presented in Figure 2 of Ktenidou et al. [2014]. The scatter observed in these correlations is large, as described in Ktenidou et al. [2014].

5 Residuals

The model is evaluated by checking the residuals from the regression analysis as functions of the main model parameters. Example figures are included below, and a larger set of residual figures are available in Electronic Appendix A.

5.1 BETWEEN-EVENT AND BETWEEN-SITE RESIDUALS

Examples of the dependence on the source parameters of the between-event residuals at f = 0.2, 1.0, and 5.0 Hz are given in Figure 5.1 through Figure 5.3. In these figures, the diamond-shaped markers represent events from California and Nevada, and circles represent events from all other regions. There is not a strong magnitude dependence of the δB. For Z_{tor}, there is no trend in the residuals at high frequencies, where the model increases the ground motion with increasing Z_{tor}. There is a potential difference in Z_{tor} scaling between regions at low to moderate frequencies, an effect which should be evaluated further in the future. For F_{NM}, there is also no trend in the residuals at high frequencies, but at the lower frequencies, potential regional differences exist. The normal faulting term is constrained by sparse data (only 10 events at 0.2 Hz, including six from Italy), so this term is not refined further. Figure 5.1 through Figure 5.3 also show the dependence of the between-site residuals on V_{S30}. Overall, there is no trend in $\delta S2S$ versus V_{S30}. The standard deviation of these residuals (ϕ_{S2S}) is comparable to τ at frequencies greater than about 2 Hz. The standard deviations are discussed further in Section 6.2.

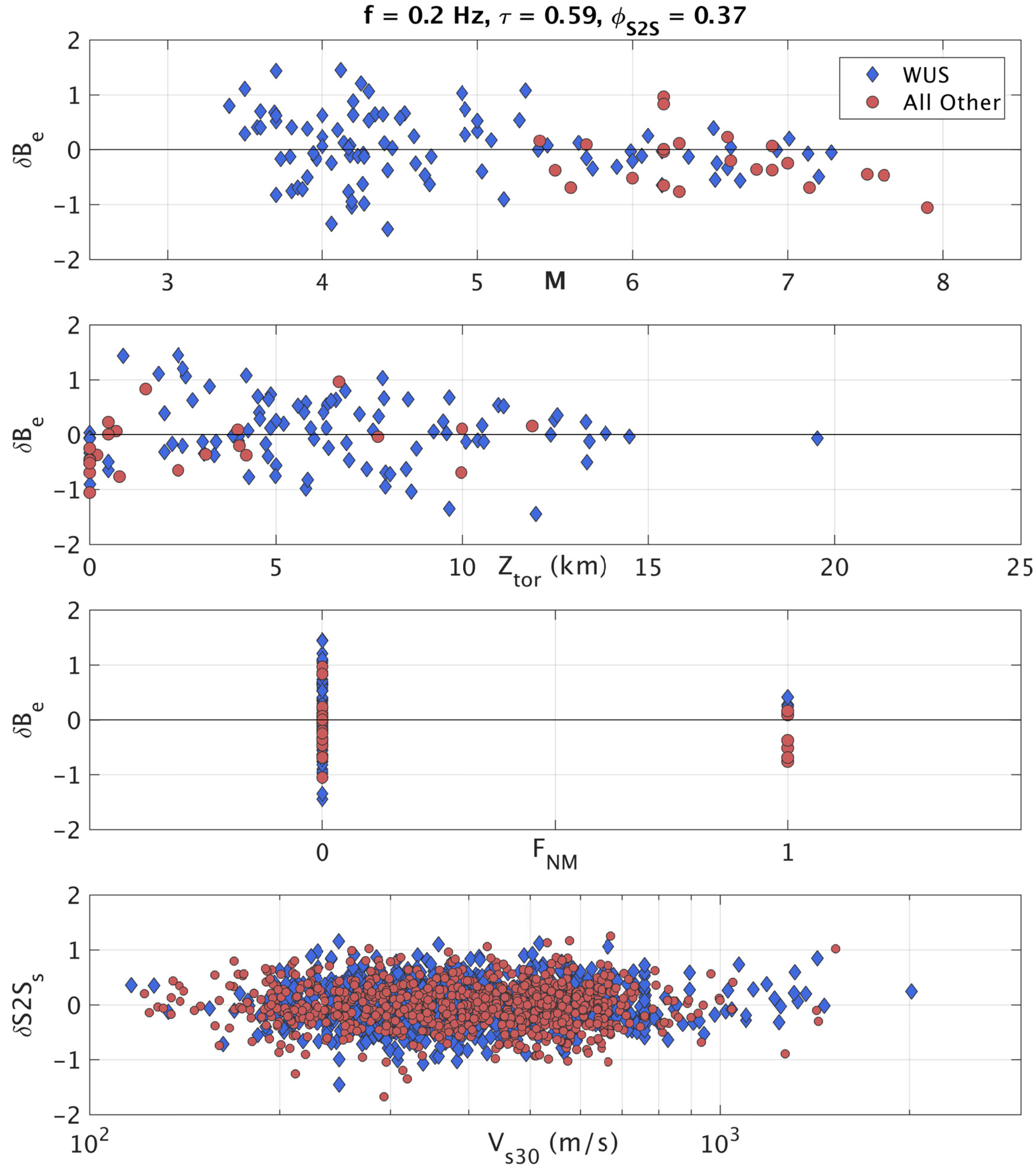

Figure 5.1 **Between-event residuals (δB_e) versus M, Z_{tor}, and F_{NM}, and between site residuals ($\delta S2S_s$) versus V_{s30}, f = 0.2 Hz.**

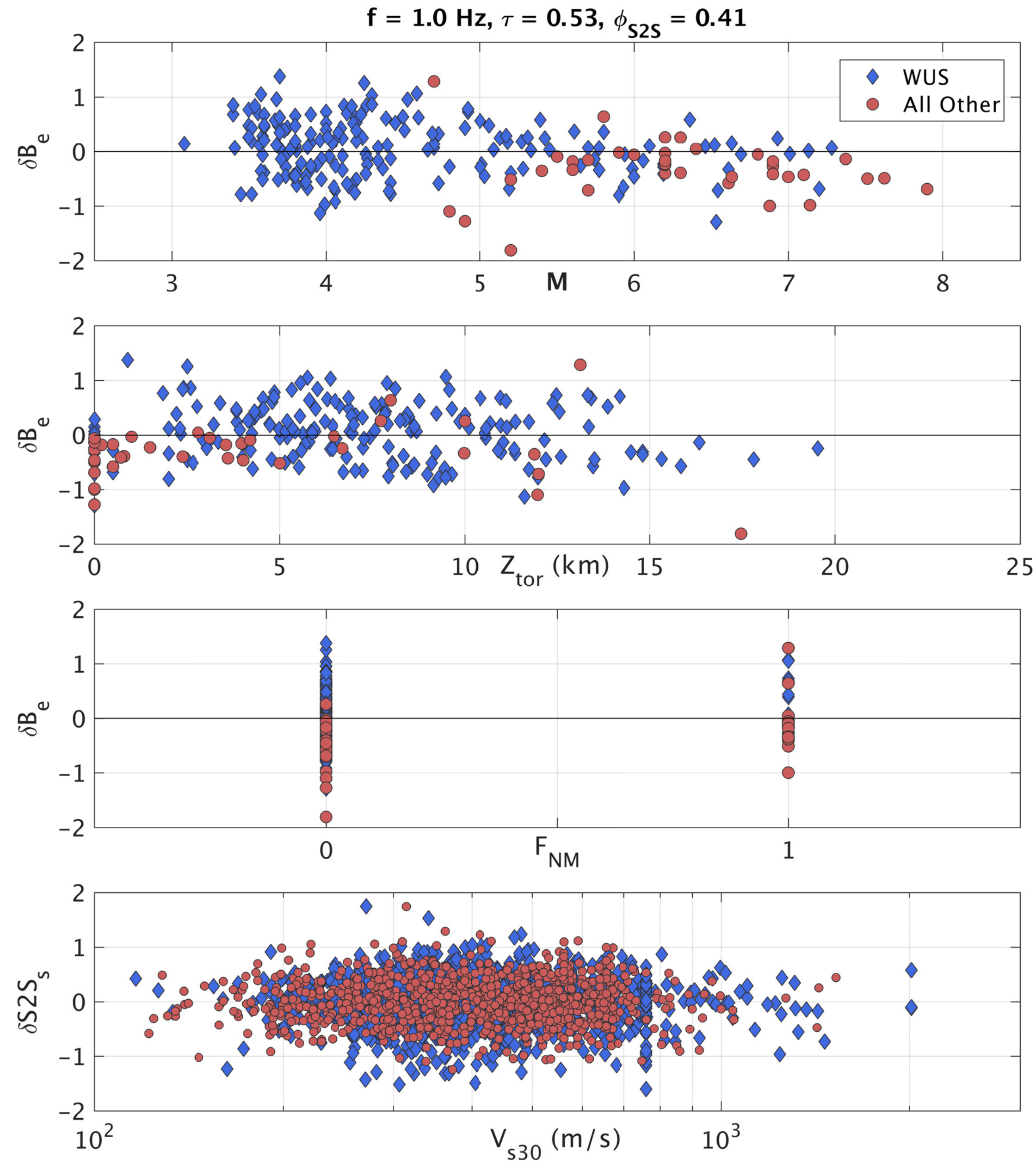

Figure 5.2 **Between-event residuals (δB_e) versus M, Z_{tor}, and F_{NM}, and between site residuals ($\delta S2S_s$) versus V_{s30}, f = 1 Hz.**

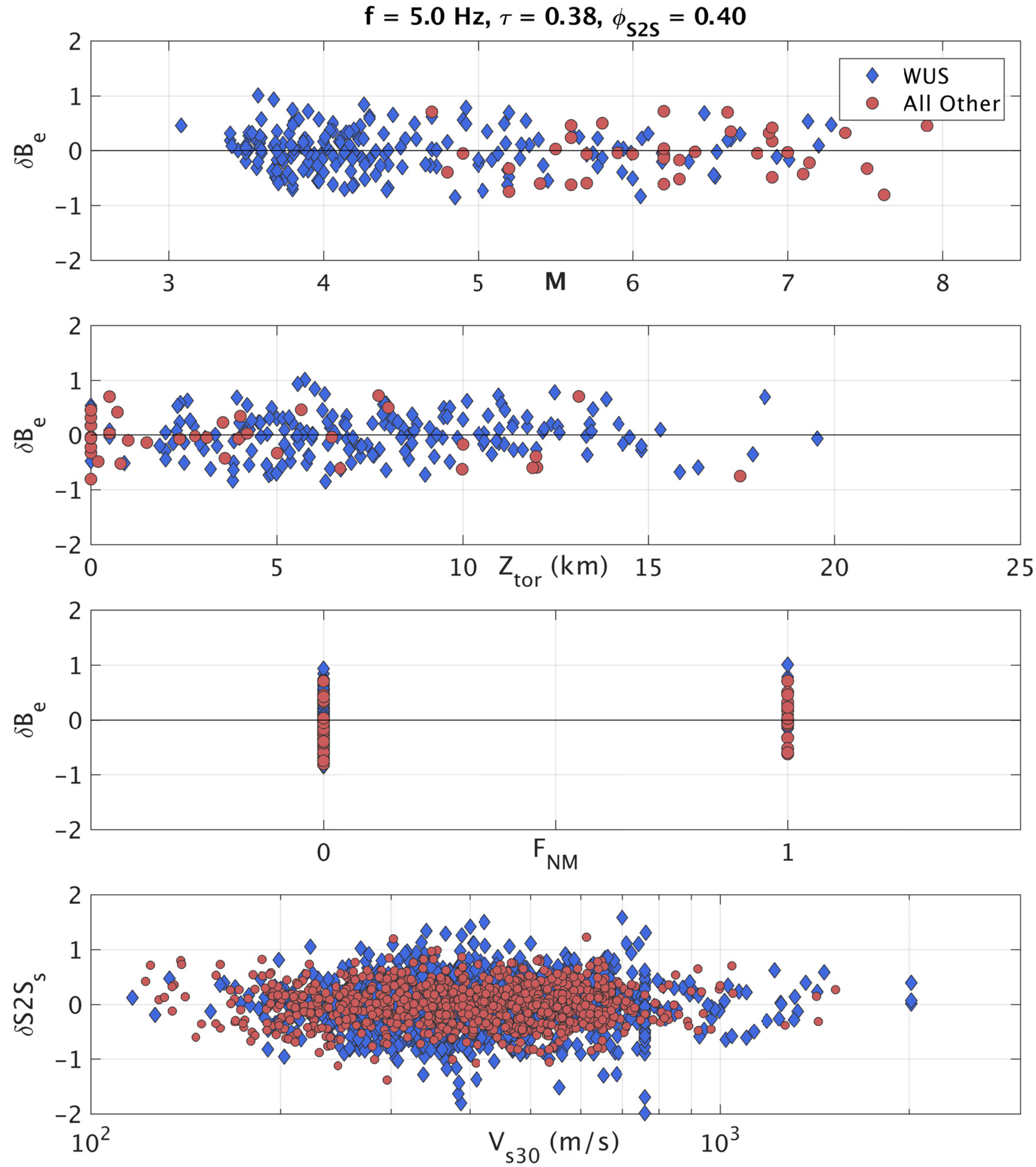

Figure 5.3 **Between-event residuals (δB_e) versus M, Z_{tor}, and F_{NM}, and between site residuals ($\delta S2S_s$) versus V_{s30}, f = 5 Hz.**

5.2 WITHIN-SITE RESIDUALS

Examples of the dependence on the model parameters of the within-site residuals at f = 0.2, 1.0, and 5.0 Hz are given in Figure 5.4 through Figure 5.6. The filled circles are individual residuals, and the black diamonds with whiskers represent the mean and 95% confidence interval of the mean for binned ranges of the model parameter. Overall, there is no trend observed in δWS versus moment magnitude. The linear site response model is evaluated through the V_{S30} and Z_1 dependence of the residuals. Overall, no strong trends are observed against V_{S30}, except for the highest V_{S30} values at low frequencies, where the residuals are slightly positive, indicating model under-prediction. The data are very sparse in this range (six records with V_{S30} > 1500 m/sec and 106 records with V_{S30} >1200 m/sec. No strong Z_1 dependencies on the residuals are observed.

The distance scaling of the model is evaluated using the distance-dependence of δWS as shown in Figure 5.4 through Figure 5.6. Additionally, the distance dependence is evaluated using magnitude binned residuals. Examples of the distance dependence binned by magnitude are shown in Figure 5.7 through Figure 5.9, where the magnitude bin ranges are given in the figure legends. In the distance range of about 5–100 km, there are no strong trends or biases of the residuals. At low frequencies, for distances beyond 100 km and in the **M** 5.5–6.5 bin, the δWS residuals are biased positive. This is likely due to the relatively limited data within this bin, and that the model scaling is appropriate even though these particular residuals are not zero-centered. Thus, neither the magnitude nor distance scaling are adjusted to center these residuals. At distances shorter than 1 km and for frequencies greater than about 2 Hz, there is a small systematic negative bias in the residuals (Figure 5.6). This means the near-fault saturation in this model is not as strong as indicated by the data. Graizer [2018] chose to incorporate oversaturation (a peak in the distance scaling at about 5 km) into his ground motion models. The oversaturation of distance scaling is intentionally avoided in this model. Because the available ground-motion data is extremely sparse at such close distances, this model is compared with the saturation from finite–fault earthquake simulations (see Model Summary section of this paper for more details). Based on these results, and on the sparsity of the data, the small bias in the short-distance residuals is accepted.

The distance dependence of the model is also compared with data from four well-recorded WUS earthquakes in Figure 5.10 through Figure 5.13: the 1989 **M** 6.9 Loma Prieta, 2010 **M** 7.2 El Mayor-Cucapah, 1992 **M** 7.3 Landers, and 1994 **M** 6.7 Northridge. In these figures, the top panels compare the recorded EAS with the model-predicted EAS at each site, including the event term for that earthquake. The lower panels show the within-event residuals for the same sites versus R_{RUP}. Residuals for El Mayor-Cucapah, the most well-recorded large earthquake in California, show no bias or trend at either frequency. Besides a few outliers, the remaining three events have attenuation which does not disagree with the median model and is captured on average.

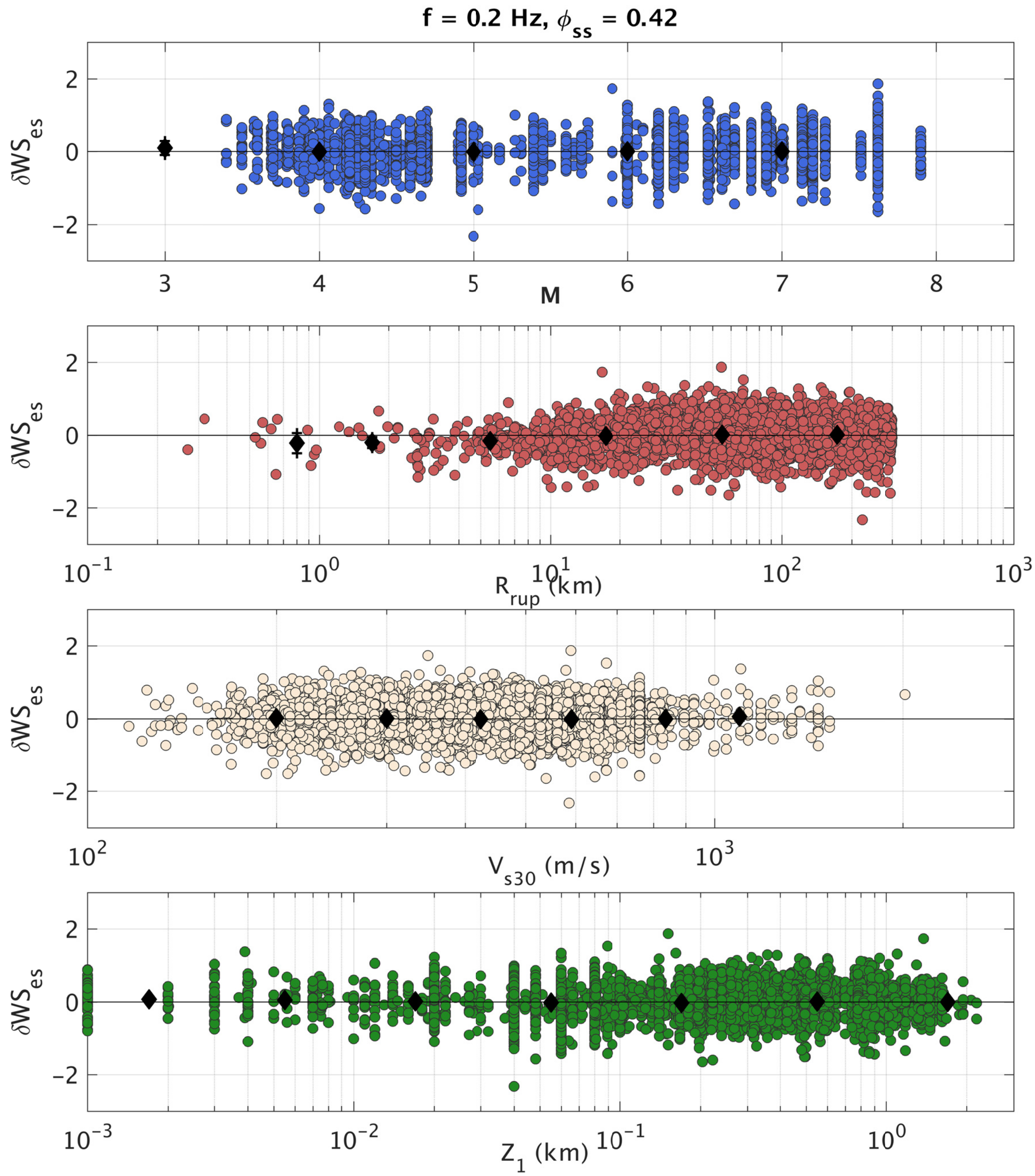

Figure 5.4 Within-site residuals (δWS_{es}) versus M, R_{RUP}, V_{s30}, and Z_1 for f = 0.2 Hz.

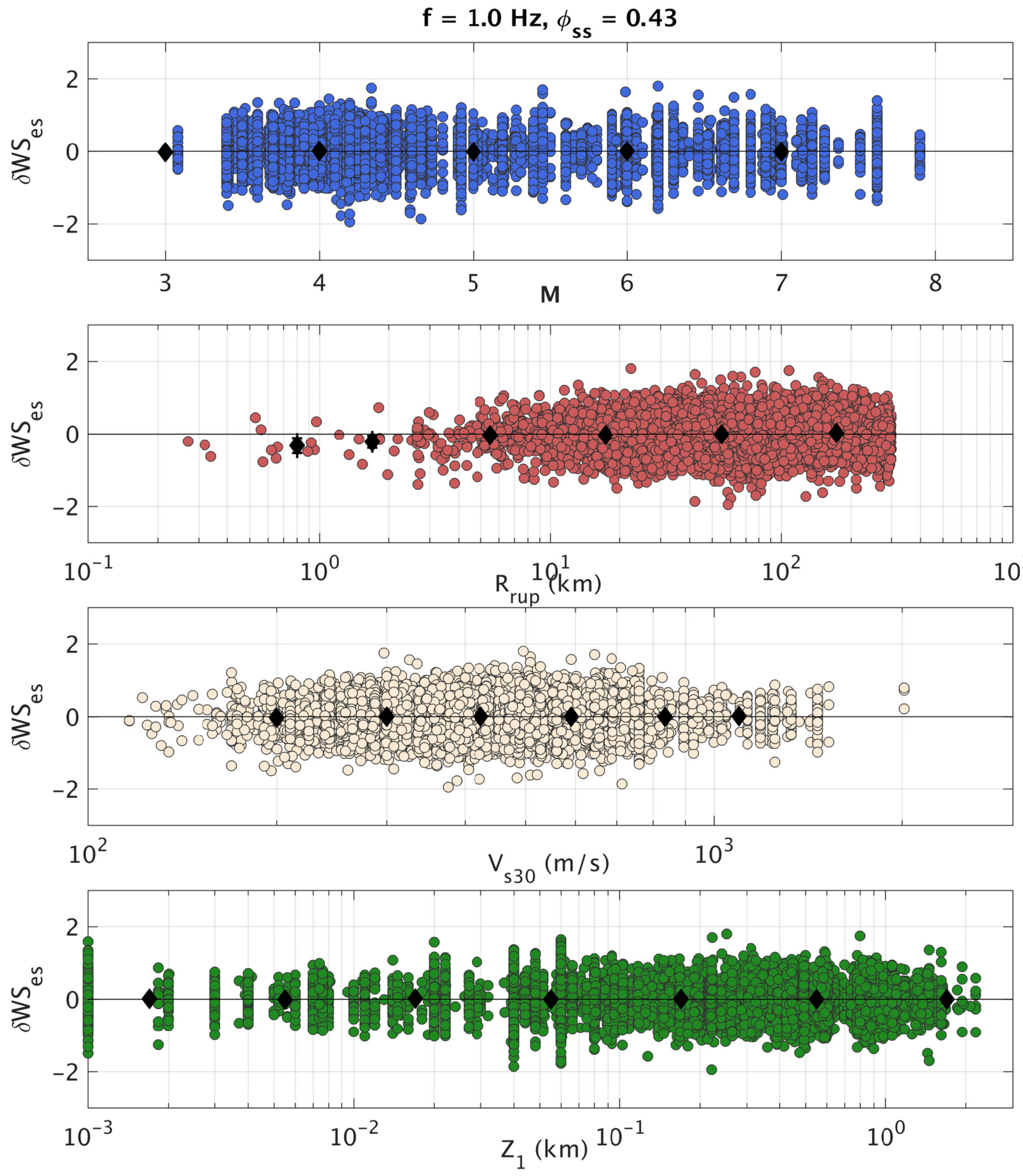

Figure 5.5 Within-site residuals (δWS_{es}) versus M, R_{RUP}, V_{s30}, and Z_1 for f =1 Hz.

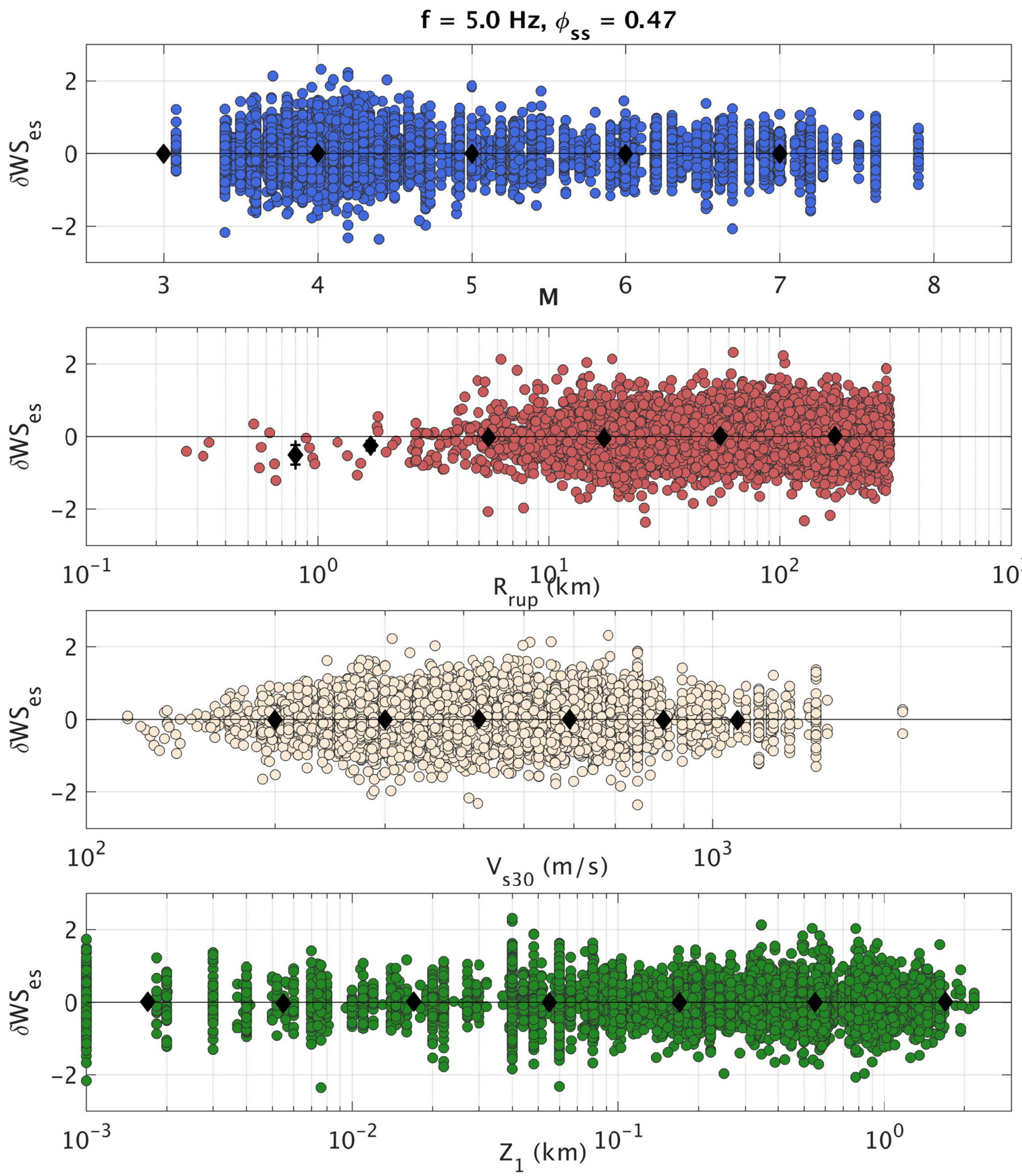

Figure 5.6 Within-site residuals (δWSes) versus M, RRUP, Vs30, and Z1 for f = 5 Hz.

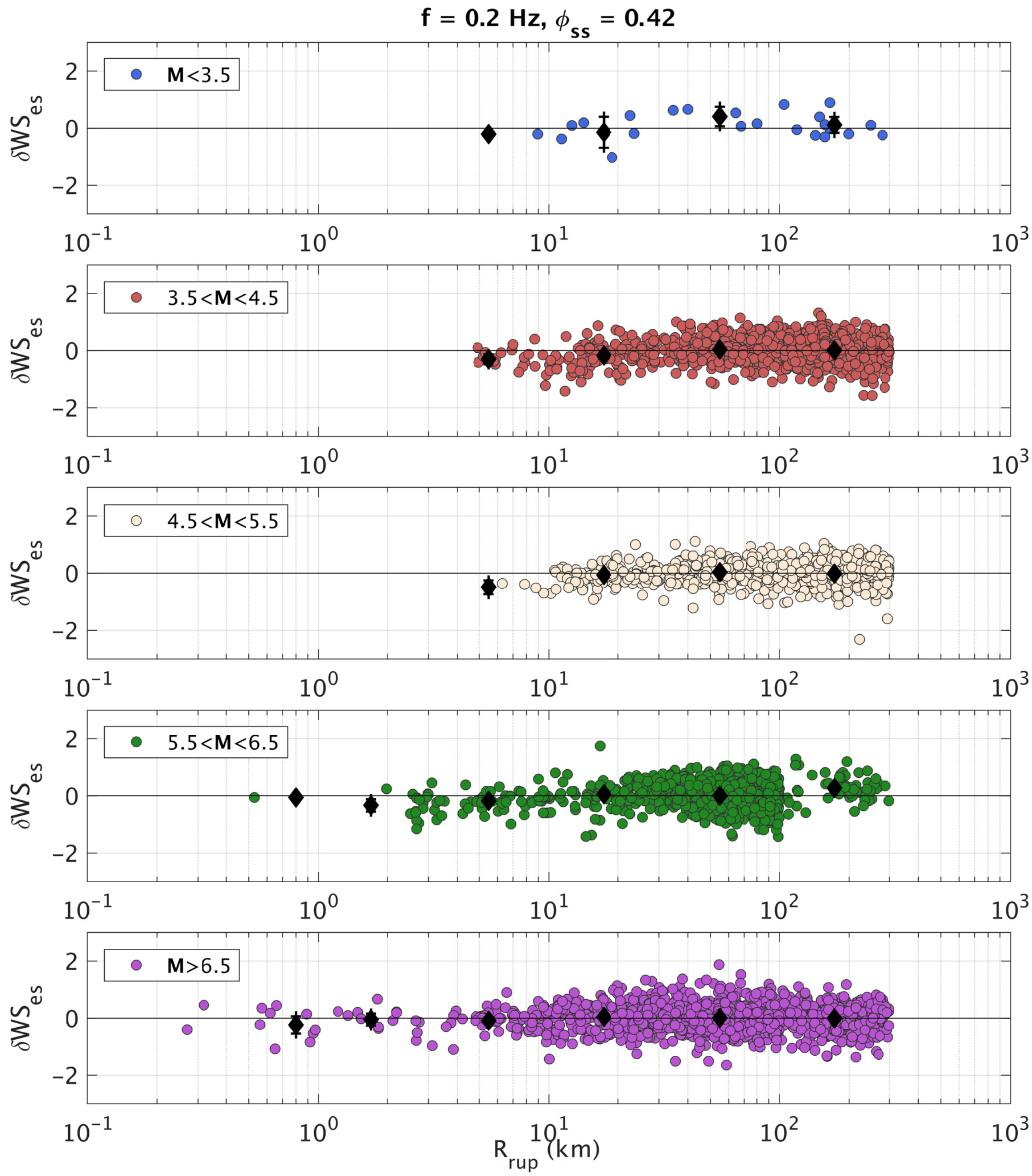

Figure 5.7 Within-site residuals (δWS_{es}) versus R_{RUP}, binned by M for f = 0.2 Hz.

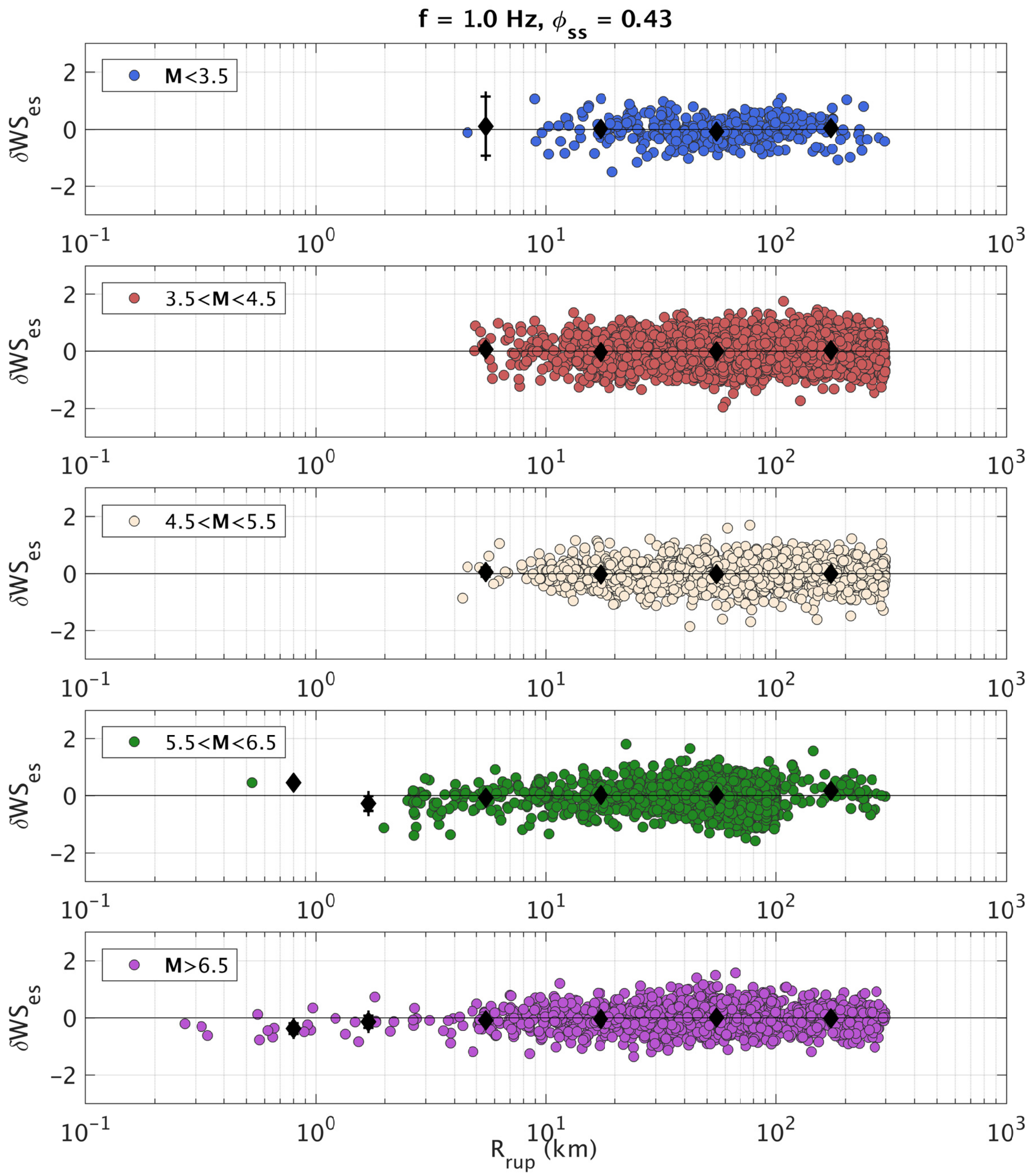

Figure 5.8 Within-site residuals (δWS_{es}) versus R_{RUP}, binned by M for f = 1 Hz.

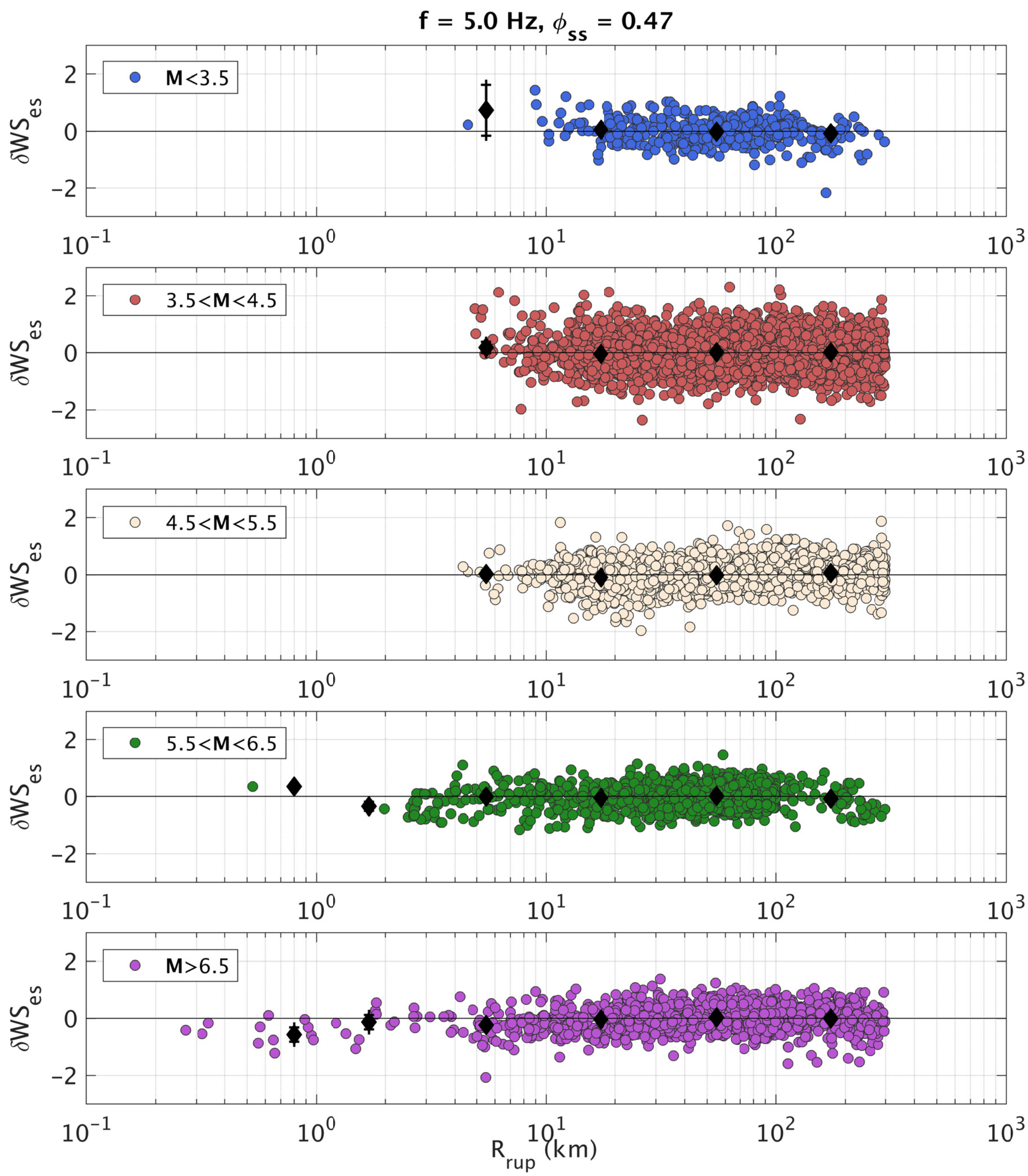

Figure 5.9 Within-site residuals (δWS_{es}) versus R_{RUP}, binned by M for f = 5 Hz.

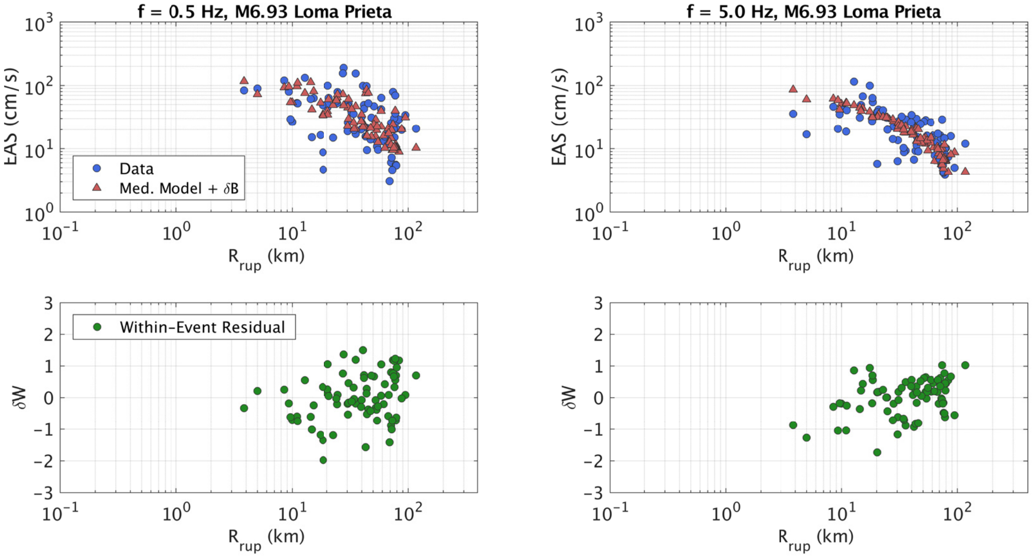

Figure 5.10 **Comparison of the model distance attenuation with the M 6.93 Loma Prieta data for (a) *f* = 0.5 Hz and (b) 5 Hz.**

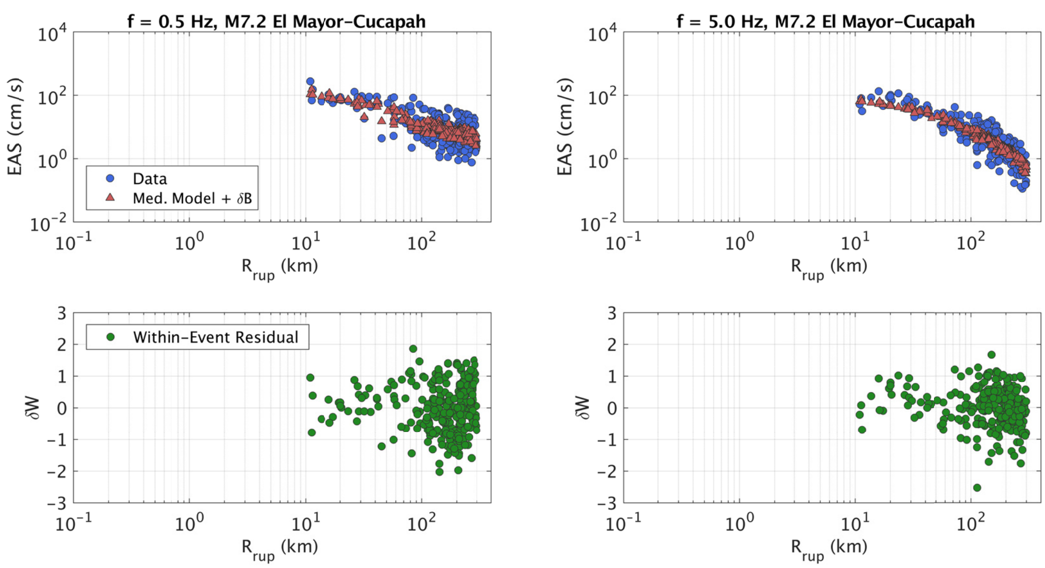

(a) **(b)**

Figure 5.11 **Comparison of the model distance attenuation with the M 7.2 El Mayor-Cucapah data for (a) *f* = 0.5 Hz and (b) 5 Hz.**

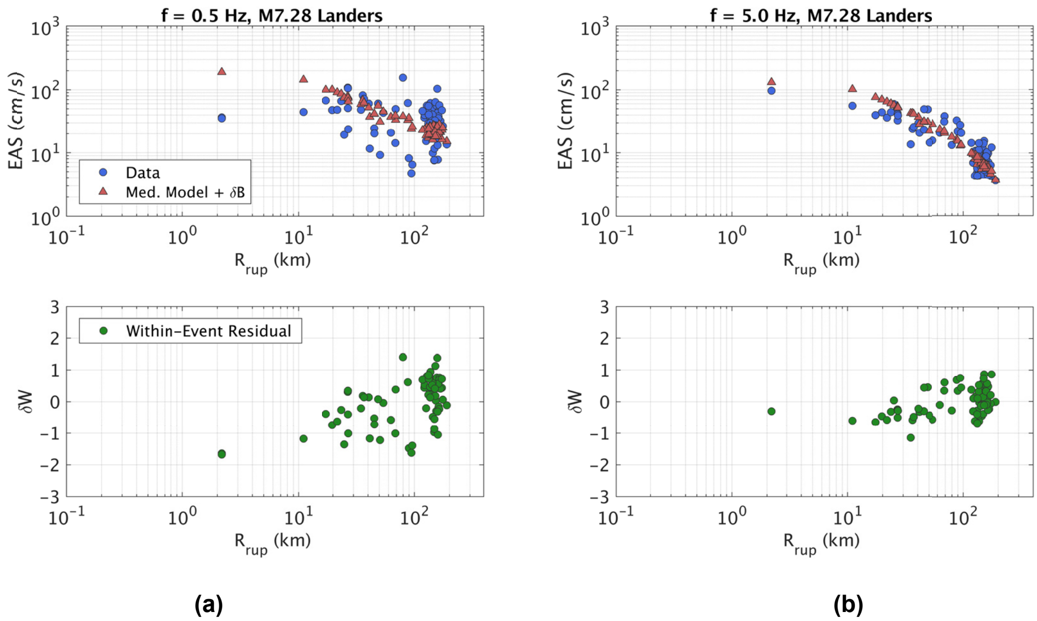

Figure 5.12 **Comparison of the model distance attenuation with the M 7.28 Landers data for (a) *f* = 0.5 Hz and (b) 5 Hz.**

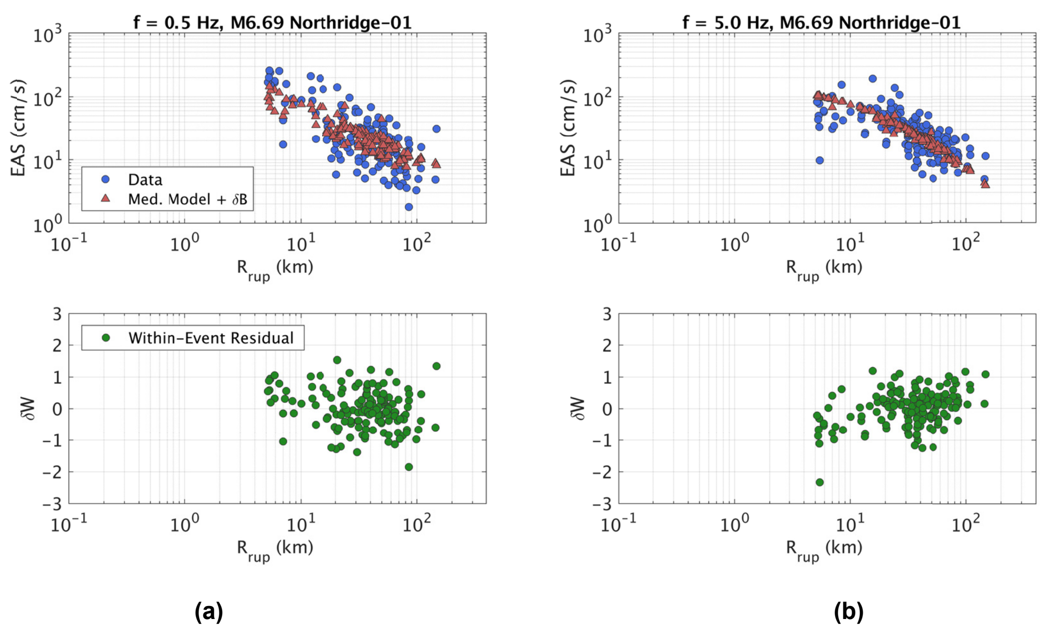

Figure 5.13 **Comparison of the model distance attenuation with the M 6.69 Northridge data for (a) *f* = 0.5 Hz and (b) 5 Hz.**

6 Model Summary

6.1 MEDIAN MODEL

In this section, the median model behavior is summarized. In Figure 6.1, the median EAS spectra from this model (solid lines) are compared with spectra from the additive double-corner-frequency source spectral model (dashed lines) described in Boore et al. [2014]. The double-corner-frequency spectra are computed using typical parameters for the WUS given by Boore [2003], including shear-wave velocity = 3.5 km/sec, density = 2.72 gm/cm^3, stress parameter $\Delta\sigma$ = 50 bars, and κ = 0.025 sec. Also used are the Boore and Thompson [2015] finite-fault distance adjustment, the Boore and Thompson [2014] path duration for western North America, and the Boore [2016] crustal amplification model. The point-source spectral models are calculated using the software package SMSIM [Boore 2005]. The median model spectra are computed for a strike-slip scenario at R_{RUP} = 30 km and Z_{tor} = 0 km, and with the reference Vs_{30} and Z_1 conditions. Figure 6.1 shows overall good agreement between the median model and the additive double-corner-frequency source spectral model with typical WUS parameters, including a well-defined decrease in corner frequency with increasing **M.** At frequencies well below the corner frequency, the spectra should be directly proportional to seismic moment (M_0), and since M_0 = $10^{1.5\mathbf{M}-16.05}$, the spectra in this range should scale by $10^{1.5} \approx 31.6$ for one magnitude unit. This approximate scaling is evident in Figure 6.1. At frequencies between 10–30 Hz, there is a dip in the model spectra compared with the point source spectra. This may be related to the region-specific attenuation parameters (geometric spreading and Q), where the point source spectra use generalized models for these attenuation parameters. The κ-based extrapolation in the model spectra begins at 24 Hz.

In Figure 6.2, the median EAS spectra from this model are shown for a set of scenarios. Panels (a) and (b) show the spectra for a vertical strike–slip scenario at R_{RUP} = 30 km with Vs_{30} = 1000 and 500 m/sec, respectively. In (c) and (d) are the spectra for the same Vs_{30} but at V_{s30} but at R_{RUP} = 1 km.

In Figure 6.3, the distance scaling of the median model is shown for f = 0.2, 1, 5, and 20 Hz. All spectra in this figure are from a strike–slip earthquake rupturing the ground surface with reference Vs_{30} and Z_1 conditions. The distance scaling is compared with the Chiou and Youngs [2014] model for PSA (dashed lines) by scaling the PSA values to the R_{RUP} = 0.1 km EAS values. At 0.2 Hz, where the Q term coefficient (c_7) is very small, the distance scaling is controlled by the geometric spreading terms, which includes a transition to $R^{-0.5}$ scaling to model surface wave geometric spreading at larger distances. At increasing frequencies, the effect of the Q term becomes more pronounced. In Figure 6.3(d), the distance scaling is shown to deviate significantly from the Chiou and Youngs [2014] model, which has a magnitude dependence on Q. This difference can be explained by the differences between EAS and PSA. At high frequencies, the PSA is strongly influenced by the predominant ground-motion frequency, as discussed above. Because of this, the PSA scaling at 20 Hz and 5 Hz are similar, but since the EAS at 20 Hz is directly representative of the ground motions in that frequency range, the distance scaling is much stronger for 20 Hz than for 5 Hz.

The **M** scaling of the median EAS is shown in Figure 6.4 for a strike–slip surface rupturing scenario with reference Vs_{30} and $Z1$ conditions, for $f = 0.2$, 1, 5, and 20. In Figure 6.5 through Figure 6.7, the median **M** scaling is compared with that from a set of broadband finite-fault simulations. The simulations were performed on the SCEC Broadband Platform, [Maechling et al. 2015] version 17.3, using simulation methods Graves and Pitarka [2015] (also known as GP) and Atkinson and Assatourians [2015] (also known as EXSIM). Both simulation methods were used to develop broadband time histories for vertical strike–slip scenarios with a range of **M** 6.5 to 8 and with stations arranged on constant R_{RUP} bands. In these figures, the **M** scaling is shown for $R_{\text{RUP}} = 3$, 10, 20, and 30 km for the median EAS model, the GP simulations, the EXSIM simulations, and for the Chiou and Youngs [2014] (CY14 hereafter) model for PSA. For the CY14 PSA, the amplitudes are scaled to the EAS model values at **M** 6.5 for this comparison. The symbols identified in the legend represent the mean simulated EAS over all stations on a given R_{RUP} band, and the standard error of the mean.

The simulations are used to evaluate the near-source saturation of the **M** scaling and to compare with the scaling implied by the data. Overall, there is less saturation in this GMM than there is in CY14 at all frequencies. At very close distances, there is stronger high-frequency saturation in EXSIM than in GP. Interestingly, this relationship is inverted at low frequencies. Based on these and other comparisons, it is determined the EAS saturation in this model is not inconsistent with the saturation from the simulations. The EAS should have some scaling at zero distance even though the PSA is nearly fully saturated at high frequencies because the PSA procedure involves selecting the peak response of the oscillator over all time, meaning it is not affected by duration. Conversely, the EAS will continue to scale for large magnitudes at short distance due to the longer source durations.

The site response scaling of the median model is summarized for a set of example scenarios in Figure 6.8. Panel (a) shows the V_{s30} scaling of the median model for a **M** 7 strike–slip earthquake rupturing the surface with reference Z_1 conditions at $R_{\text{RUP}} = 30$ km. The solid lines represent the total (linear and nonlinear) V_{s30} scaling and the dashed lines represent only the linear portion of the V_{s30} scaling. Panel (b) shows the Z_1 scaling of the median model for the same scenario with $V_{s30} = 300$ m/sec. Panel (c) shows the scaling of the modified Hashash et al. [2018] nonlinear site term with **M,** for a scenario with $R_{\text{RUP}} = 30$ km and $V_{s30} = 300$ m/sec. Similarly, panel (d) shows the scaling of the modified Hashash et al. [2018] nonlinear site term with R_{RUP}, for a scenario with **M** 7 and $V_{s30} = 300$ m/sec.

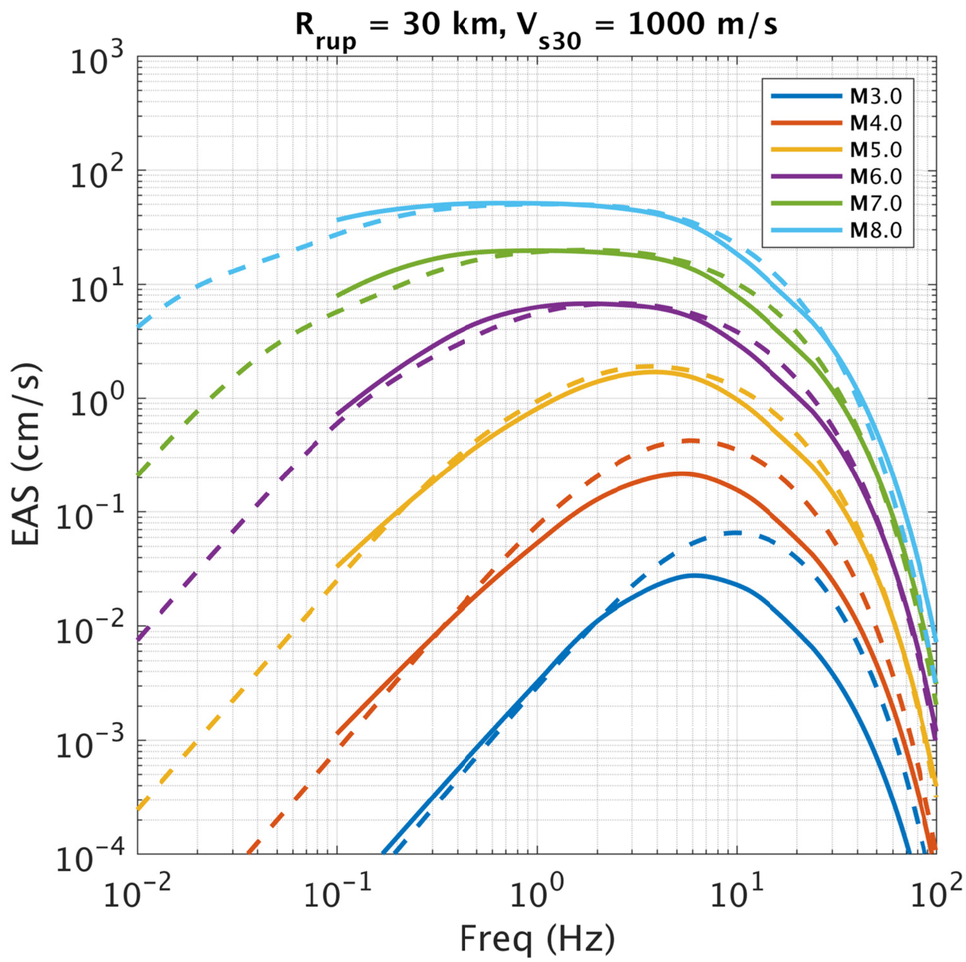

Figure 6.1 **Median model spectra for a strike-slip scenario at R_{RUP} = 30 km, Z_{tor} = 0 km and with reference Vs_{30} and Z_1 conditions (solid lines) compared with the additive double-corner frequency source spectral model with typical WUS parameters (dashed lines).**

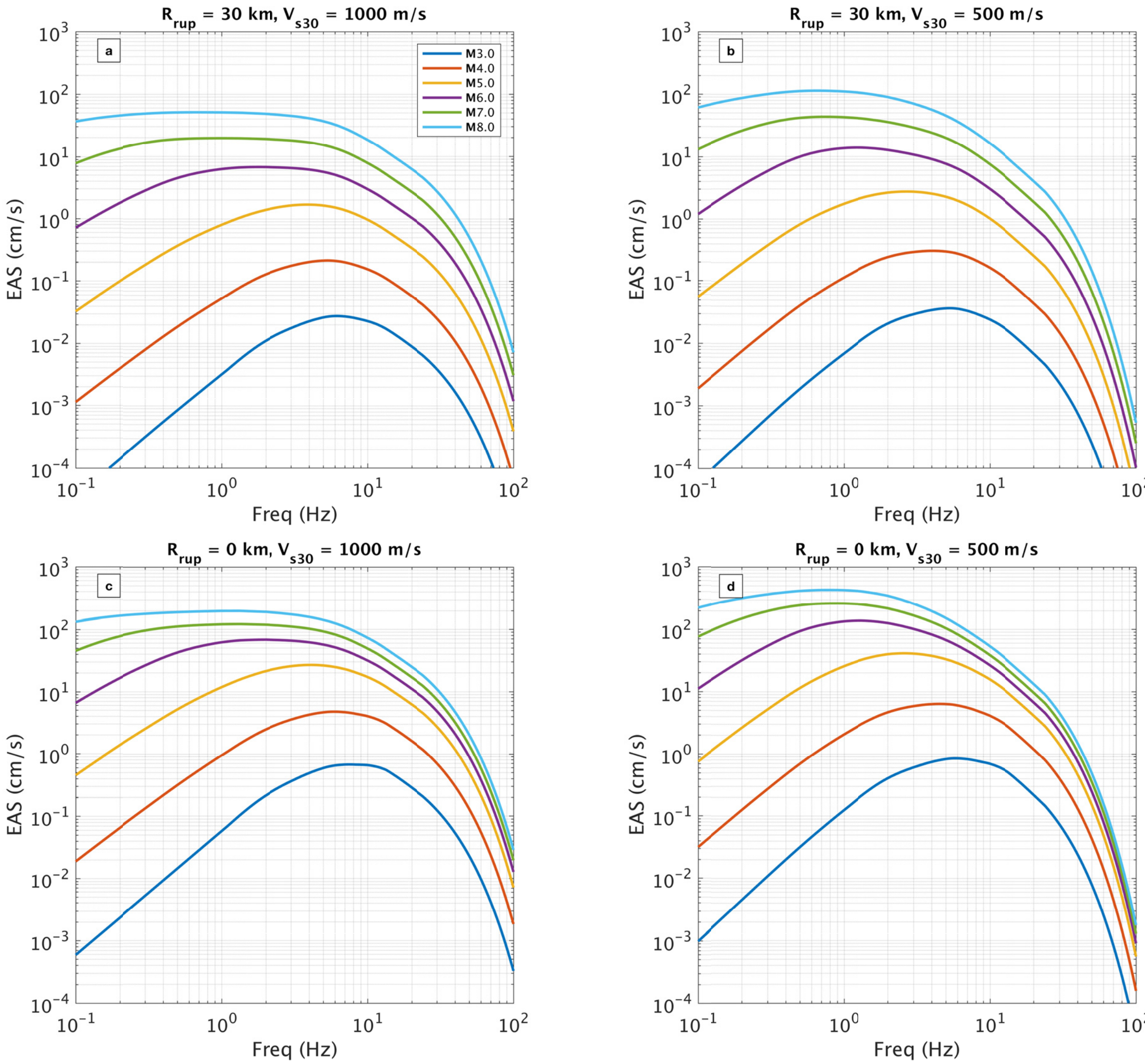

Figure 6.2 Median model EAS spectra for a set of scenarios described by the parameters in each title.

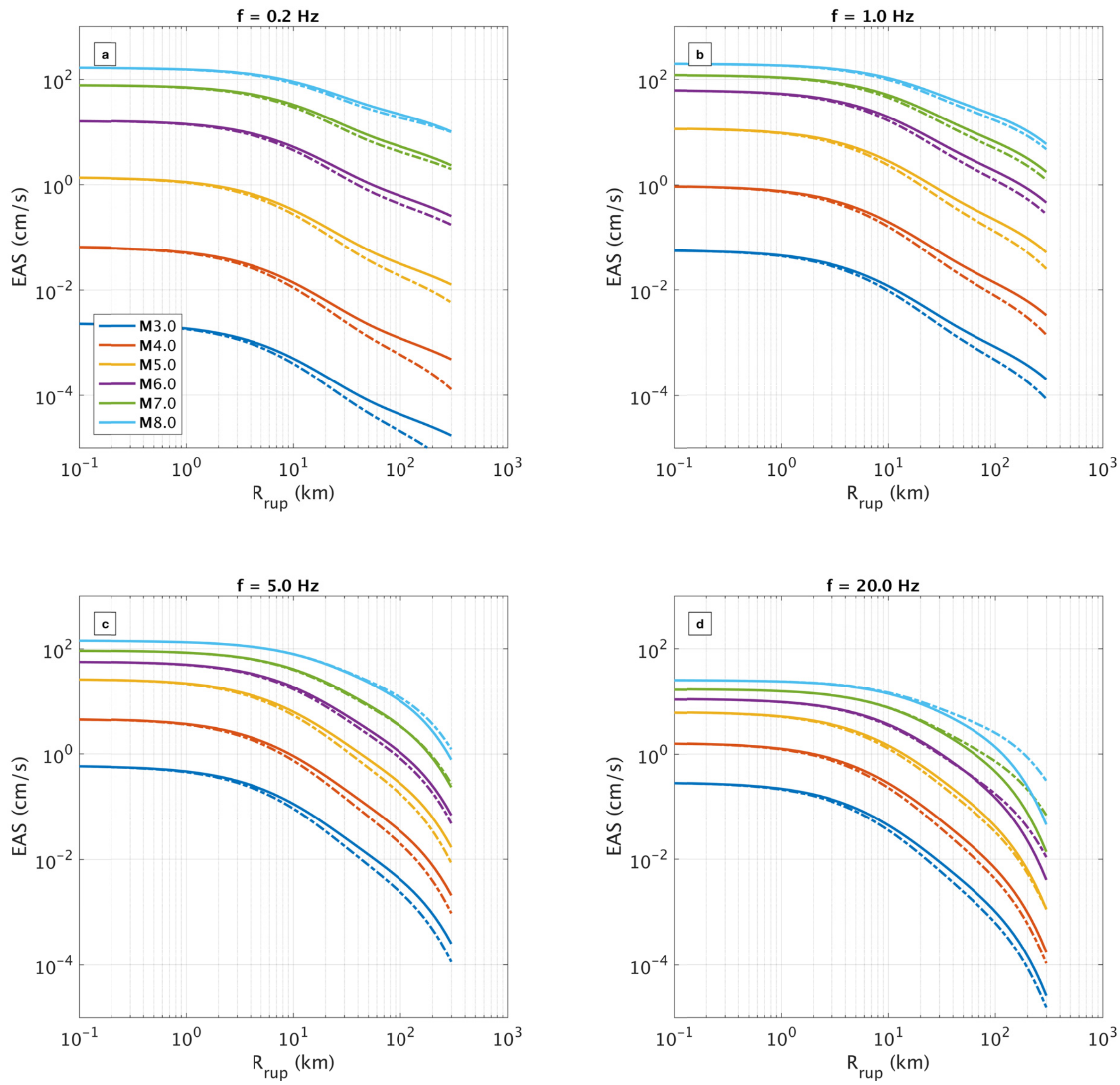

Figure 6.3 **Distance scaling of the median EAS (solid lines) for a strike-slip scenario with reference Vs_{30} and Z_1 conditions, for four frequencies. For reference, the distance scaling of the Chiou and Youngs [2014] model for PSA is shown for the same scenarios with the dash-dotted lines, where the PSA values have been scaled to the $R_{RUP\,=}$ 0.1 km EAS values.**

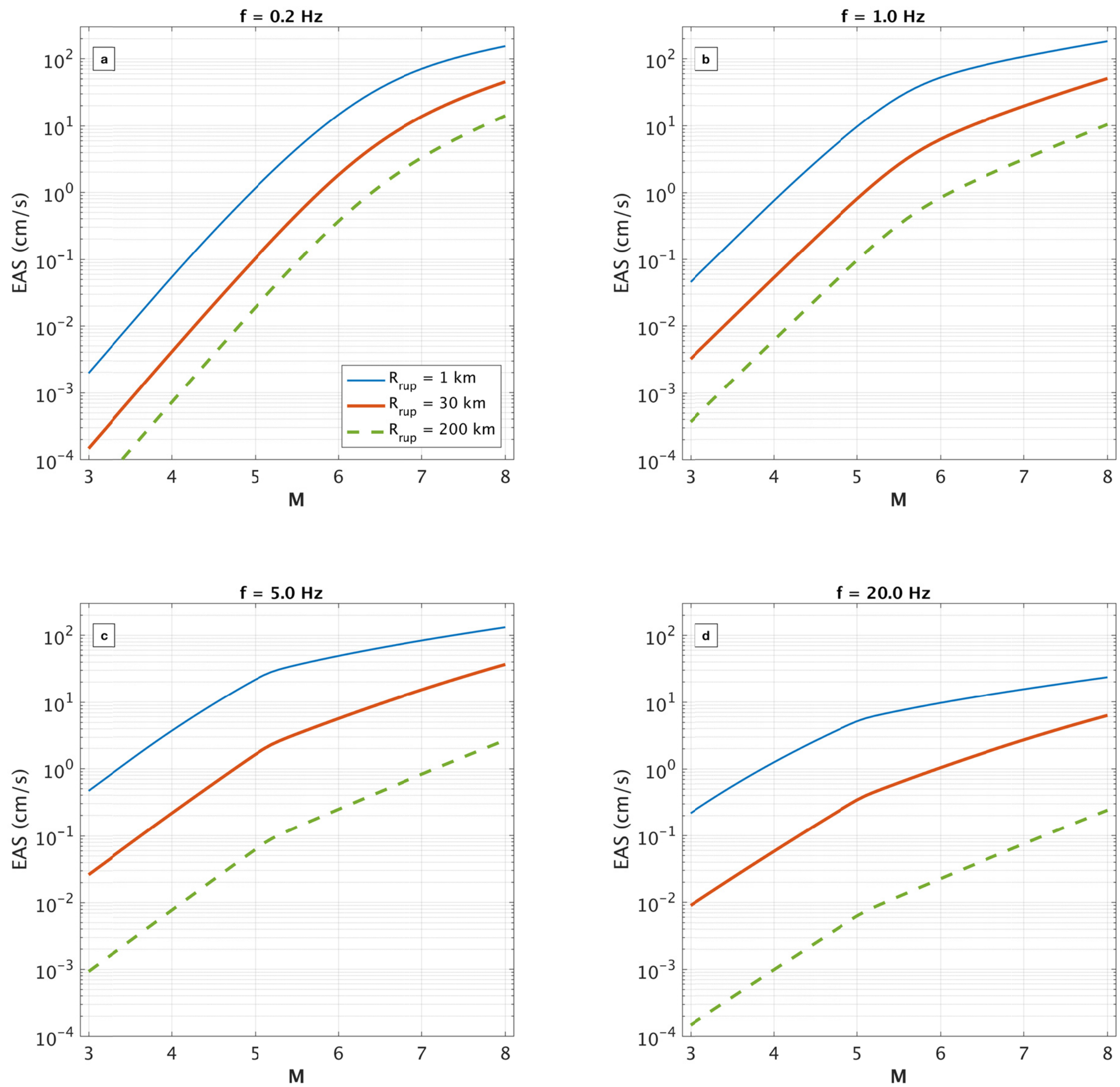

Figure 6.4 **M scaling of the median EAS for a strike–slip surface rupturing scenario with reference V_{S30} and Z_1 conditions for *f* = 0.2, 1, 5, and 20 Hz.**

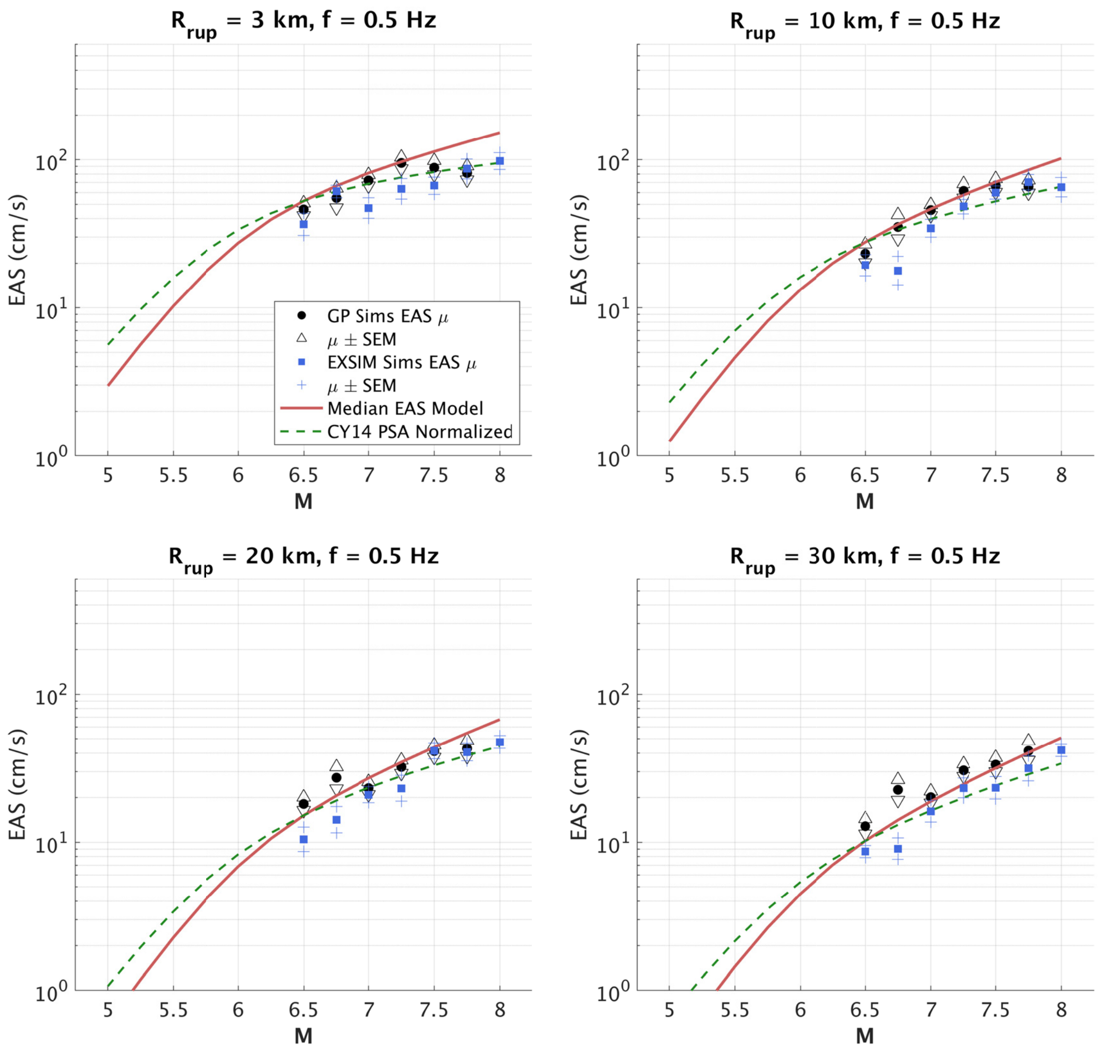

Figure 6.5 **M scaling of the median model for four distances, at *f* = 0.5 Hz for a strike–slip earthquake rupturing the surface with reference Vs_{30} and Z_1 conditions, compared with results from finite-fault simulations.**

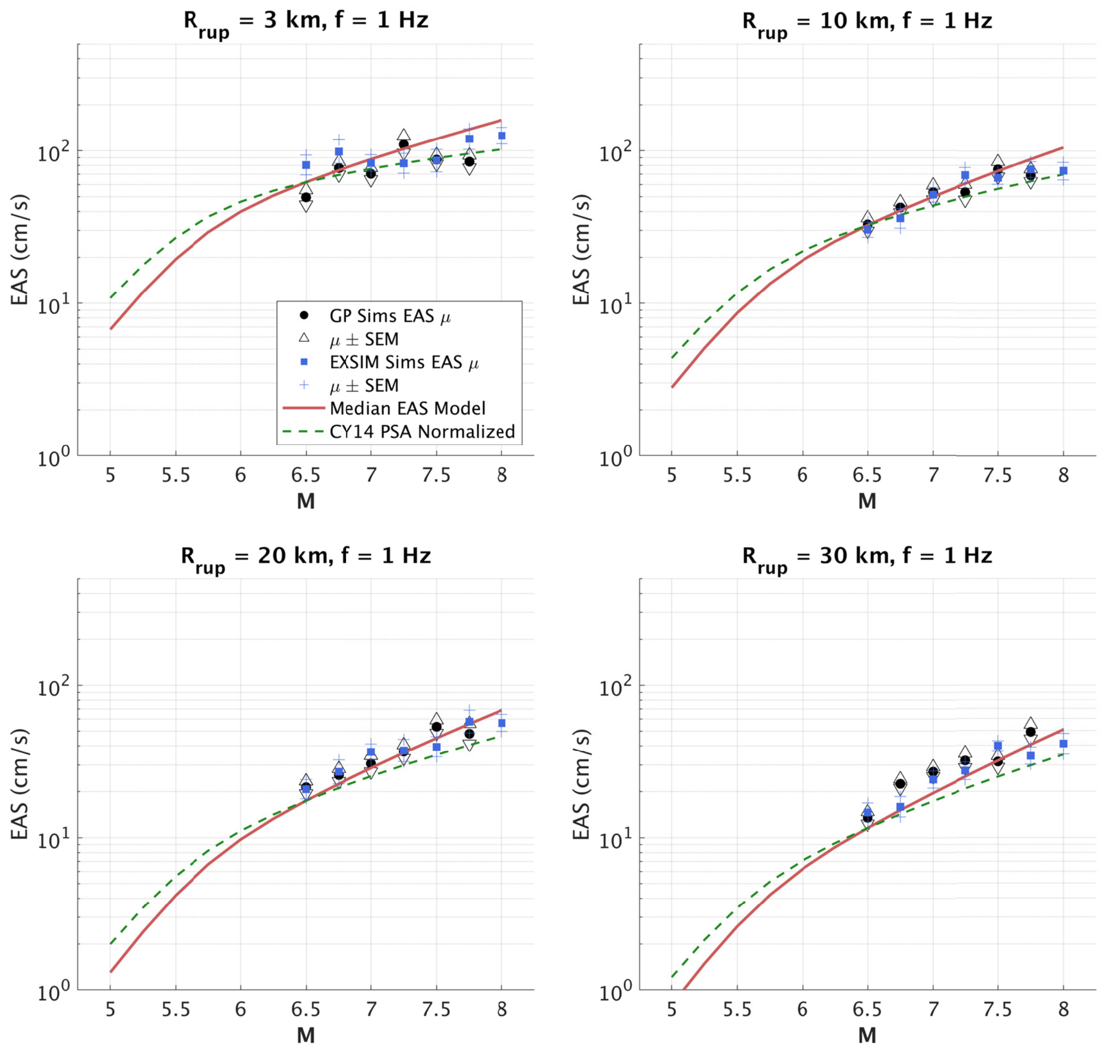

Figure 6.6 **M scaling of the median model for four distances, at *f* = 1 Hz for a strike-slip earthquake rupturing the surface with reference Vs_{30} and Z_1 conditions compared with results from finite-fault simulations.**

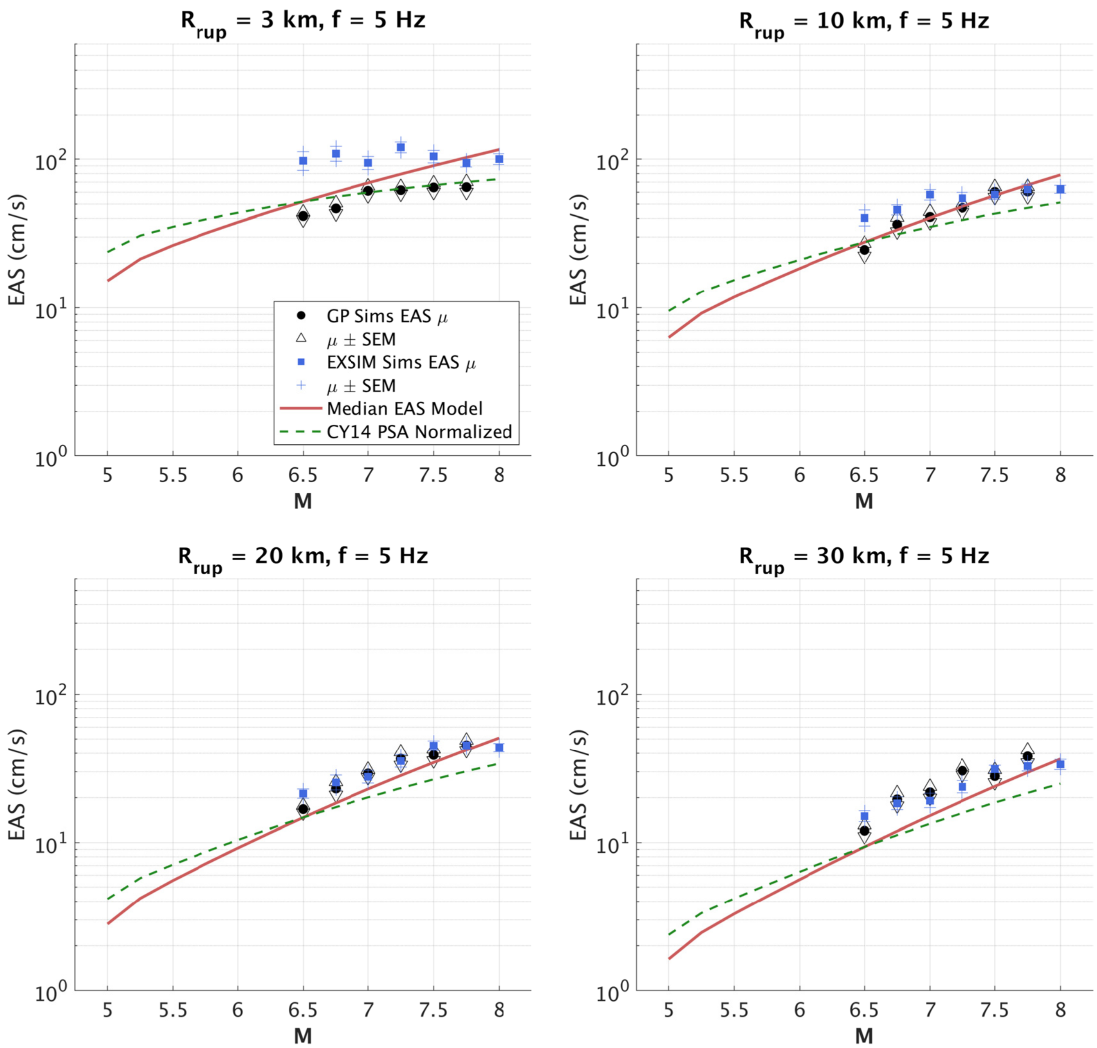

Figure 6.7 **M scaling of the median model for four distances, at *f* = 5 Hz for a strike-slip earthquake rupturing the surface with reference V_{S30} and Z_1 conditions, compared with results from finite-fault simulations.**

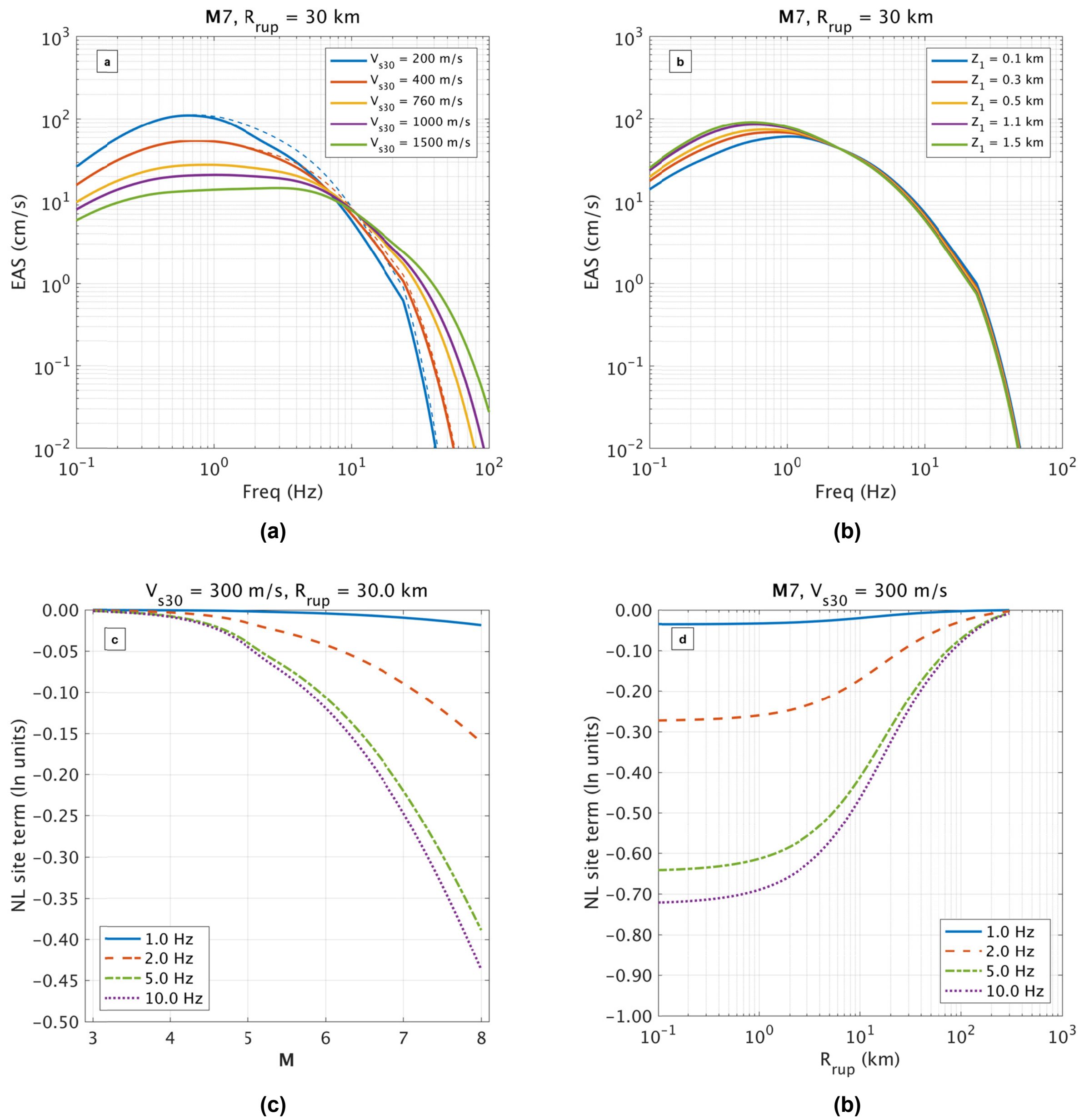

Figure 6.8 (a) V_{s30} scaling of the median model for a M 7 strike–slip earthquake rupturing the surface with reference Z_1 conditions at R_{RUP} = 30 km. The solid lines represent the total (linear and nonlinear) V_{s30} scaling and the dashed lines represent only the linear portion of the V_{s30} scaling; (b) Z_1 scaling of the median model for the same scenario with V_{s30} = 300 m/sec; (c) scaling of the modified Hashash et al. [2018] nonlinear site term with M, for R_{RUP} = 30 km and V_{s30} = 300 m/sec; and (d) scaling of the modified Hashash et al. [2018] nonlinear site term with R_{RUP}, for M 7 and V_{s30} = 300 m/sec.

6.2 STANDARD DEVIATION MODEL

Prediction of the EAS [Equation (3.1)] requires a model for the aleatory variability. The random-effects method employed leads to the separation of total residuals into between-event residuals (δB) site-to-site residuals ($\delta S2S$) and single-station within-event residuals (δWS), which have variance components τ, ϕ_{S2S}^2, and ϕ_{SS}^2, respectively. The total standard deviation model (natural logarithm units) is given by Equation (6.1).

$$\sigma = \sqrt{\tau^2 + \phi_{S2S}^2 + \phi_{SS}^2 c_{1a}^2} \tag{6.1}$$

In Equation (6.1), c_{1a} is the spectral shape adjustment coefficient (Figure 4.10) which has been added to the total standard deviation, as described previously. Figure 6.9 shows the standard deviations for each component of Equation (6.1), as calculated directly from the regression analysis (all magnitudes). The increase observed in τ at frequencies greater than about 3 Hz is consistent with the behavior of response spectrum models (e.g., Abrahamson et al. [2014] and Chiou and Youngs [2014]). This is believed to be the effect of κ, which is related to regional crustal damping, being mapped into the between-event terms. For a given earthquake, recordings in close proximity to the source will have similar κ, and the high frequencies of these recordings may be systematically above or below average. If there is a regional difference in kappa, then the regression treats this as an event-specific variation, which artificially increases τ. Stafford [2017] also observed an increase in the variance components of the FAS with increasing frequency and hypothesized that the increase of ϕ_{S2S} reflects variations in κ across different sites.

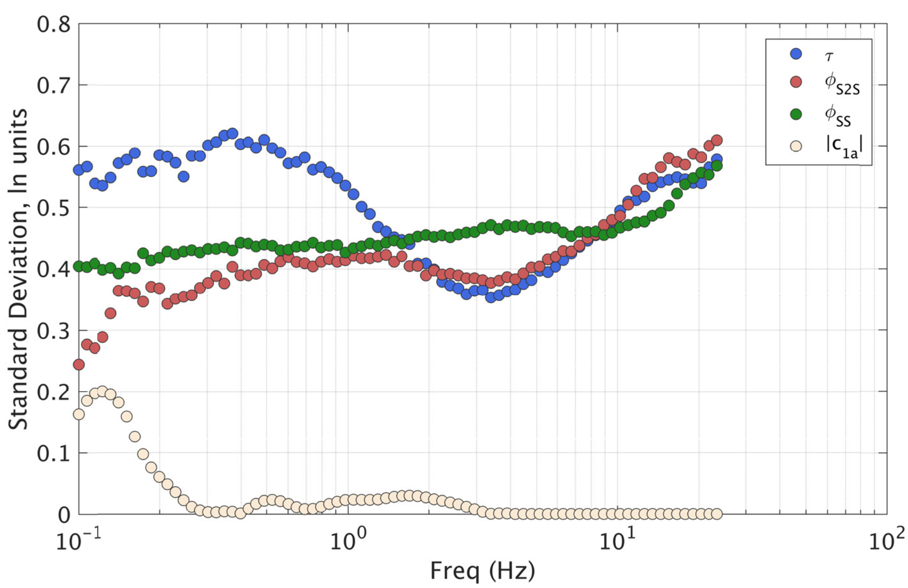

Figure 6.9 Standard deviation components calculated directly from the regression analysis for all magnitudes.

The magnitude dependence of each aleatory term is fit as shown in Figure 6.10 and is given by Equation (6.2). At low frequencies, the small-magnitude data have higher between-event standard deviation. This is also consistent with the Abrahamson et al. [2014] response spectrum model, and could be related to the steeper magnitude scaling slope at low magnitudes and the uncertainty in small-magnitude source measurements [Abrahamson et al. 2014]. The standard deviations of the two within-event residuals do not have strong magnitude dependence at low frequencies. At higher frequencies, τ does not show strong magnitude dependence, but ϕ_{S2S} and ϕ_{SS} are larger for the small-magnitude data, which is again consistent with the Abrahamson et al., [2014] and Chiou and Youngs [2014] models. Higher within-event variability for small magnitudes may be related to the increased effect of the high-frequency radiation pattern, which is reduced for larger magnitude events due to destructive interference [Abrahamson et al. 2014].

$$\tau = \begin{cases} s_1 & \text{for } \mathbf{M} < 4.0 \\ s_3 + \dfrac{s_2 - s_1}{2}(\mathbf{M} - 4) & \text{for } 4.0 \le \mathbf{M} \le 6.0 \\ s_2 & \text{for } \mathbf{M} > 6.0 \end{cases} \tag{6.2a}$$

$$\phi_{S2S} = \begin{cases} s_3 & \text{for } \mathbf{M} < 4.0 \\ s_3 + \dfrac{s_4 - s_3}{2}(\mathbf{M} - 4) & \text{for } 4.0 \le \mathbf{M} \le 6.0 \\ s_4 & \text{for } \mathbf{M} > 5.5 \end{cases} \tag{6,2b}$$

$$\phi_{SS} = \begin{cases} s_5 & \text{for } \mathbf{M} < 4.0 \\ s_5 + \dfrac{s_6 - s_5}{2}(\mathbf{M} - 4) & \text{for } 4.0 \le \mathbf{M} \le 6.0 \\ s_6 & \text{for } \mathbf{M} > 6.0 \end{cases} \tag{6.2c}$$

At frequencies above approximately 20 Hz, the model is constrained to smoothly transition to be flat in frequency space for all components of σ. The frequency dependence of the standard deviation model is shown in Figure 6.11, and examples of the total standard deviation model for a set of scenarios are shown in Figure 6.12. Coefficients s_2 through s_2 are given in Appendix B. In Figure 6.13, the components of the standard deviation model are compared with those from Bora et al. [2015] and Stafford [2017]. The Bora et al. [2015] model was developed for smoothed FAS from data in Europe, the Mediterranean, and the Middle-East, and the Stafford [2017] model was developed for unsmoothed FAS from a subset of the NGA-West1 database [Chiou et al. 2008].

The standard deviation model developed here is linear, meaning it does not account for the effects of nonlinear site response. As discussed in Al Atik and Abrahamson [2010] and Abrahamson et al., [2014], the nonlinear effects on the standard deviation are influenced by the variability of the rock motion, leading to a reduction in the soil motion variability at high frequencies. In Abrahamson et al. [2014], the standard deviation of the rock motion is estimated by removing the site amplification variability (determined analytically) from the surface motion, and the variability of the soil motion is computed using propagation of errors. In a future update of the model, similar steps will be taken to account for the effects of nonlinear site response on the standard deviation.

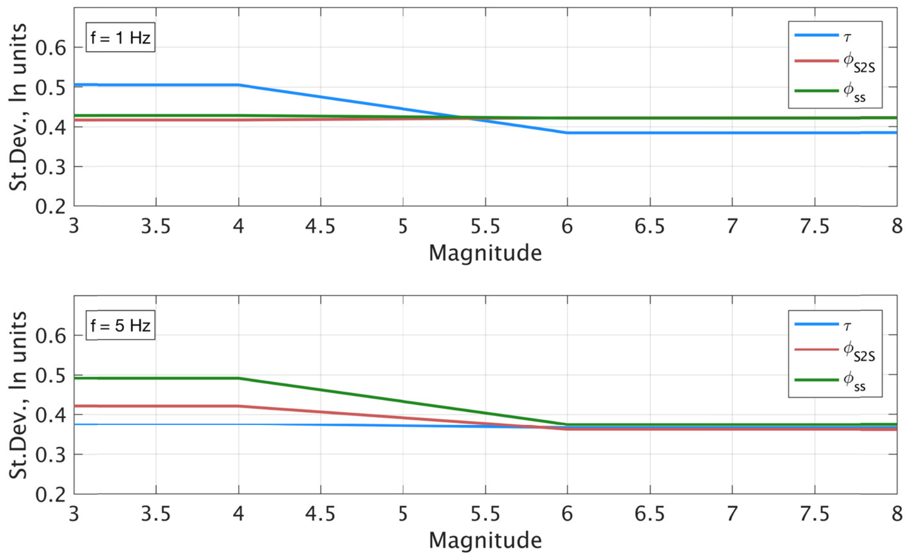

Figure 6.10 Magnitude scaling of the standard deviation terms for *f* = 1 and 5 Hz.

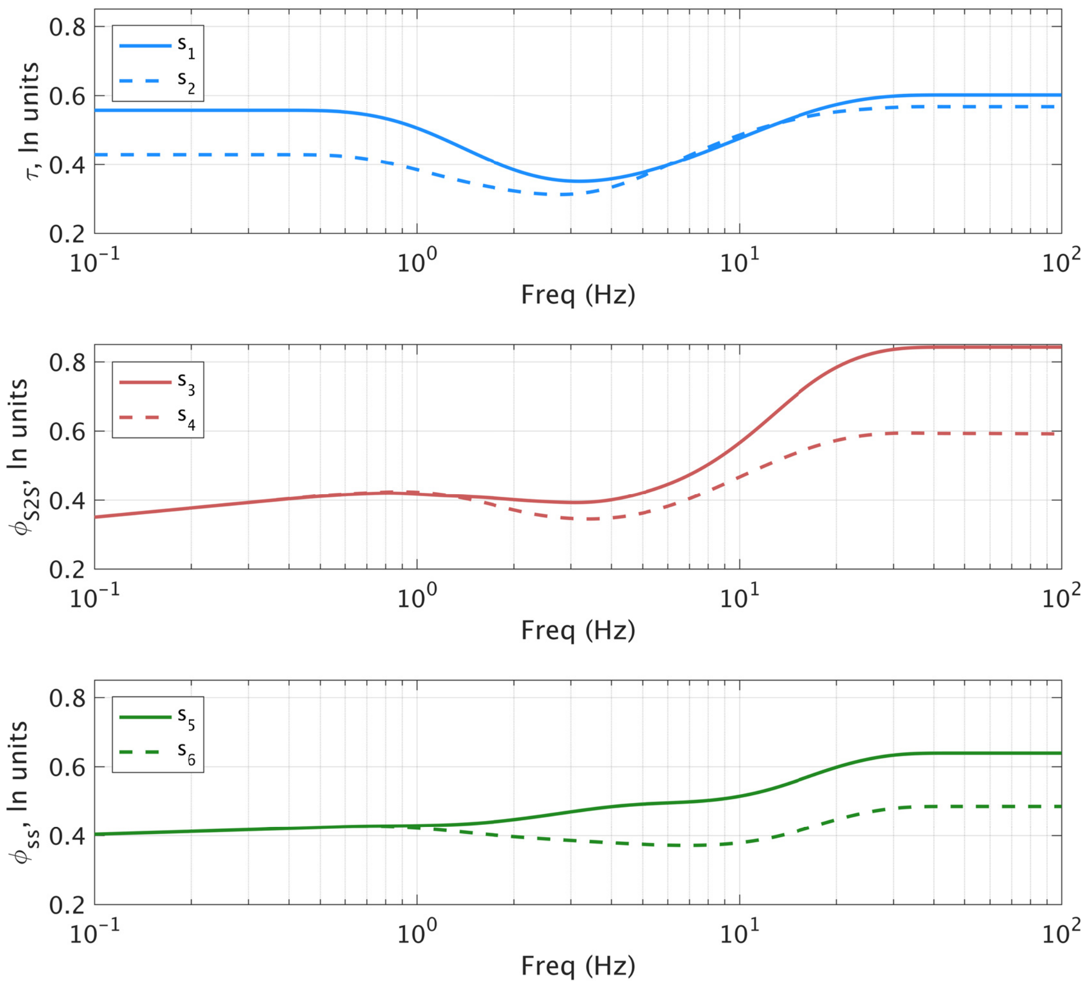

Figure 6.11 Frequency dependence of the standard deviation model.

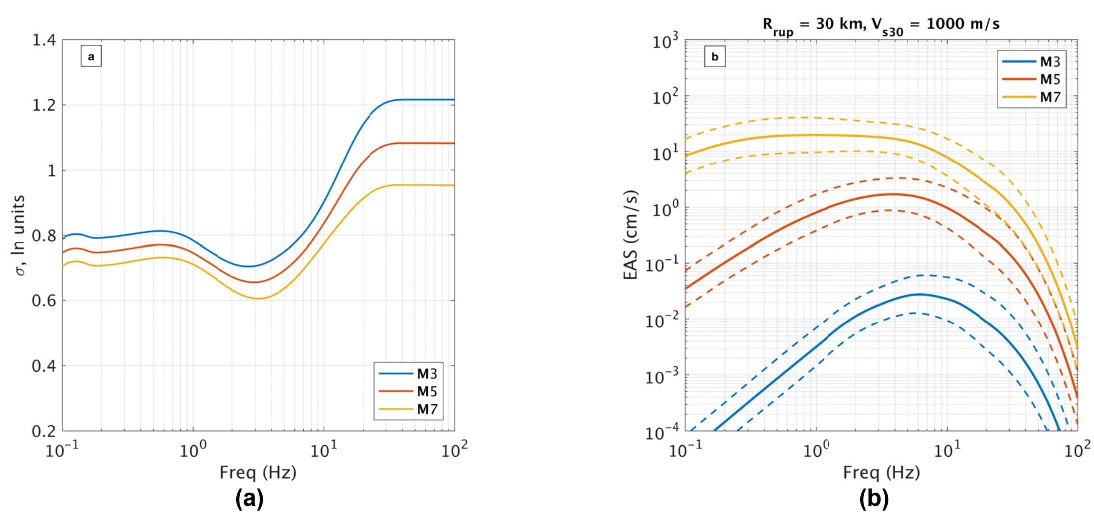

Figure 6.12 (a) Total standard deviation model for M 3, 5, and 7; and (b) median (solid lines) and median plus and minus one σ (dashed lines) EAS spectra for M 3, 5, and 7 scenarios.

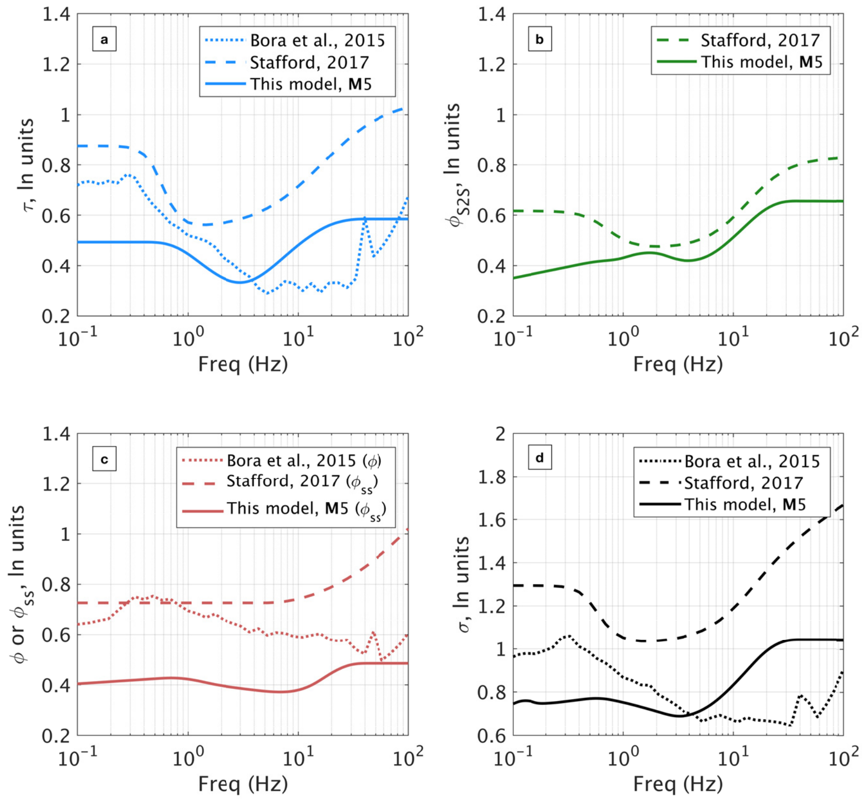

Figure 6.13 Comparison of the standard deviation components between the Bora et al. [2015], Stafford [2017] models and this model, for a M 5 earthquake. Panels (a) through (d) show the comparison of τ, *ϕ_{S2S}*, *and* *ϕ_{SS}*, and σ, - respectively.

6.3 RANGE OF APPLICABILITY

The model is applicable for shallow crustal earthquakes in California and Nevada. The model is developed using a database dominated by California earthquakes, but uses data worldwide to constrain the magnitude scaling and geometric spreading. The model is applicable for rupture distances of 0–300 km, **M** 3.0–8.0, and over the frequency range 0.1–100 Hz. The V_{s30} range of applicability is 18–1500 m/sec, although the model is not well constrained for V_{s30} values greater than 1000 m/sec. Models for the median and the aleatory variability of the EAS are developed. Regional models for Japan and Taiwan will be developed in a future update of the model. A model for the inter-frequency correlation of $\varepsilon_{\mathrm{EAS}}$ is presented in Bayless and Abrahamson [2018].

6.4 LIMITATIONS AND FUTURE CONSIDERATIONS

The model presented uses the ergodic assumption, as introduced by Anderson and Brune [1999]. This means that the variability in the data from a broad geographic region (in this case, globally for the magnitude scaling and geometric spreading, and over the California and Nevada for the remaining parameters) are assumed to represent the variability of the ground motions over time for a given site in the target region. With this approach, the model is expected to be appropriate for general use in California and Nevada but will be biased for a particular site. In an ergodic model, systematic site, path, and source effects are the dominant parts of the aleatory variability, making fully or partially non-ergodic models attractive [Abrahamson 2017]. Developing a partially non-ergodic model requires repeated observations of source, path, or site effects. For example, in this model, with multiple recordings at a site, the median site-specific amplification for the site is separated and the intra-event residual is partitioned, shifting that component of aleatory variability into an epistemic uncertainty [Walling 2009]. To get a fully non-ergodic model, all of the components of the total ground-motion variability that are not representative of the variability of future observations of ground motion at a single site must be removed [Abrahamson and Hollenback 2012].

Incorporating regional differences into a GMM is a first step towards a partially non-ergodic assumption [Kuehn and Scherbaum 2016]. To account for the known differences in regional crustal structure, regionalized models for Japan and Taiwan can be developed in a future model update. This will involve regionalizing the linear V_{s30} scaling (c_8), soil depth scaling (c_{11}), anelastic attenuation (c_7) and spectral shape (c_1) coefficients.

At frequencies above 24 Hz, this model uses a κ-based extrapolation. This approach required selecting a $\kappa - V_{s30}$ relationship from the literature. Future improvements to the model relationship, or calculating one directly from the database used.

The effects of rupture directivity and hanging-wall scaling are not explicitly included in the model. Therefore, these effects are accounted for in the total aleatory variability. The hanging-wall effect, characterized by increased ground motion amplitudes on the hanging-wall side of dipping ruptures, is not well constrained by the data. For NGA-West2, Donahue and Abrahamson [2013] investigated these effects for response spectra using finite-fault simulations, and the results were incorporated in the Abrahamson et al. [2014] model. In a future update, a similar study for the EAS could be incorporated into this model. The effects of rupture directivity on the EAS is also a potential future research topic. Finally, the effects of nonlinear site response on the standard deviation are not accounted for in this model, which can be addressed in a future update.

REFERENCES

Abrahamson N.A. (2017). Recent advances in seismic hazard, *Presentation*, Pacific Rim Forum, January 23–23, Pacific Earthquake Engineering Research Center, Berkeley, CA.

Abrahamson N.A., Hollenback J.C. (2012). Application of single-site sigma ground motion prediction equations in practice, *Proceedings*, 15th World Conference on Earthquake Engineering, Paper No. 2536, Lisbon, Portugal.

Abrahamson N.A., Silva W.J. (1997). Empirical response spectral attenuation relations for shallow crustal earthquakes, *Seismol. Res. Lett*., 68(1): 94–127.

Abrahamson N. Silva W.J. (2008). Summary of the Abrahamson & Silva NGA ground-motion relations, Earthq. Spectra, 24: 67–97, doi: 10.1193/1.2924360.

Abrahamson N.A., Silva W.J., Kamai R. (2014). Summary of the ASK14 ground motion relation for active crustal regions. *Earthq. Spectra*, 30:1025–1055.

Abrahamson N.A., Youngs R.R. (1992). A stable algorithm for regression analyses using the random effects model, *Bull. Seismol. Soc. Am*., 82: 505–510.

Aki K. (1967), Scaling law of seismic spectrum, *J. Geophys. Res*., 72: 1217–1231.

Al Atik L., Abrahamson N.A. (2010). Nonlinear site response effects on the standard deviations of predicted ground motions, *Bull. Seismol. Soc. Am*., 100: 1288–1292.

Al Atik L., Abrahamson N.A., Cotton F., Scherbaum F., Bommer J.J., Kuehn N. (2010). The variability of ground-motion prediction models and its components, *Seismol. Res. Lett*., 81(5): 794–801.

Ancheta T.D., Darragh R.B., Stewart J.P., Seyhan E., Silva W.J., Chiou B.S.-J., Wooddell K.E., Graves R.W., Kottke A.R., Boore D.M., Kishida T., Donahue J.L. (2014). NGA-West2 database, *Earthq. Spectra,* 30: 989–1005.

Anderson J.G., Brune J.N. (1999). Probabilistic seismic hazard assessment without the ergodic assumption, *Seismol. Res. Lett*., 70(1): 19–28.

Anderson J.G., Hough S.E. (1984) A model for the shape of the Fourier amplitude spectrum of acceleration at high frequencies, *Bull. Seismol. Soc. Am*., 74: 1969–1993.

Atkinson G.M., Assatourians K. (2015) Implementation and validation of EXSIM (a stochastic finite-fault ground-motion simulation algorithm) on the SCEC broadband platform, *Seismol. Res. Lett*., 86(1): 48–60, doi: 10.1785/0220140097.

Bayless J., Abrahamson N.A. (2018). An empirical model for the inter-frequency correlation of epsilon for Fourier amplitude spectra, in review.

Boore D.M. (2003). Simulation of ground motion using the stochastic method, *P&A Geophysics.* 160: 635–675.

Boore D.M. (2005). SMSIM-Fortran programs for simulating ground motions from earthquakes: Version 2.3—A Revision of OFR 96-80-A, *U.S. Geological Survey Open-File Rept. 00-509,* revised 15 August 2005, 55 pgs.

Boore D.M. (2016). Determining generic velocity and density models for crustal amplification calculations, with an update of the Boore and Joyner (1997) Generic Site Amplification for VS(Z)=760 m/sec, *Bull. Seismol. Soc. Am.*, 106: 316–320.

Boore D.M., Di Alessandro C., Abrahamson N.A. (2014). A generalization of the double-corner-frequency source spectral model and its use in the SCEC BBP validation exercise, *Bull. Seismol. Soc. Am*., 104: 2387–2398.

Boore D.M., Thompson E.M. (2014). Path durations for use in the stochastic-method simulation of ground motions, *Bull. Seismol. Soc. Am.*, 104: 2541–2552.

Boore D.M., Thompson E.M. (2015). Revisions to some parameters used in stochastic-method simulations of ground motion, *Bull. Seismol. Soc. Am.*, 105: 1029–1041.

Bora S. S., Scherbaum F., Kuehn N., Stafford P.J (2016). On the relationship between Fourier and response spectra: Implications for the adjustment of empirical ground-motion prediction equations (GMPEs), *Bull. Seismol. Soc. Am.*, 106(3):, doi: 10.1785/0120150129.

Bora S. S., Scherbaum F., Kuehn N., Stafford P.J., Edwards B. (2015). Development of a response spectral ground-motion prediction equation (GMPE) for seismic hazard analysis from empirical Fourier spectral and duration models, *Bull. Seismol. Soc. Am.,* 105(4): 2192–2218.

Brune J.N. (1970). Tectonic stress and spectra of seismic shear waves from earthquakes, *J. Geophys. Res*. 75: 4997–5009.

Chiou B. S.-J., Darragh R.B., Gregor N., Silva W.J. (2008). NGA project strong-motion database, *Earthq. Spectra* 24(1): 23–44.

Chiou B.S.-J., Youngs R.R. (2008). An NGA model for the average horizontal component of peak ground motion and response spectra, *Earthq. Spectra*, 24: 173–216.

Chiou,B.S.-J., Youngs R.R. (2014). Update of the Chiou and Youngs NGA model for the average horizontal component of peak ground motion and response spectra, *Earthq. Spectra,* 30: 1117–1153.

Chopra A.K. (2007) *Dynamics of Structures, Theory and Applications to Earthquake Engineering*, Pearson, Higher Education Press, Beijing.

Donahue J.L., Abrahamson N.A. (2013). Hanging wall scaling using finite-fault simulations, *PEER Report No. 2013/14*, Pacific Earthquake Engineering Research Center, University of California, Berkeley, CA.

Douglas J., Boore D.M. (2011). High-frequency filtering of strong-motion records, *Bull. Earthq. Eng*. 9: 395–409.

Goulet C.A., Kottke A., Hollenback J., Kuehn N., Kishida T., Boore D.M., Abrahamson N.A., Bozorgnia Y., Der Kiureghian A., Ktenidou O-J., Rathje E.M., Silva W.J., Thompson E.M., Wang, X. (2018). Effective amplitude spectrum and smoothing optimization for the development of ground motion models based on Fourier amplitudes, *Earthq. Spectra*, in preparation.

Graizer V. (2018). GK17 ground-motion prediction equation for horizontal PGA and 5% damped PSA from Shallow crustal continental earthquakes, *Bull. Seismol. Soc. Am*., 108(1): 380–398, doi: 10.1785/0120170158.

Graves R.W., Pitarka A. (2015) Refinements to the Graves and Pitarka (2010) broadband ground-motion simulation method, *Seismol. Res. Lett.,* 86: 75-80, doi: 10.1785/0220140101.

Hanks T.C. (1982). fmax, *Bull. Seismol. Soc. Am*., 72: 1867–1879.

Hashash Y.M.A., Harmon J., Ilhan O., Stewart J.P., Rathje E.M., Campbell K.W., Silva W.J., Goulet C.G. (2018). Modelling of site amplification via large scale nonlinear simulations with applications to North America, ASCE, *Proceedings*, Geotechnical Earthquake Engineering and Soil Dynamics V, doi: 10.1061/9780784481462.051.

Kamai R., Abrahamson N.A., SilvaW. J., (2014). Nonlinear horizontal site amplification for constraining the NGA-West2 GMPEs, *Earthq. Spectra*, 30: 1223–1240.

Kishida T., Ktenidou O., Darragh R.B., Silva W.J. (2016). Semi-automated procedure for windowing time series and computing Fourier amplitude spectra for the NGA-West2 database, *PEER Report No. 2016/02*, Pacific Earthquake Engineering Research Center, University of California, Berkeley, CA.

Konno K., Ohmachi, T., (1998). Ground-motion characteristics estimated from spectral ratio between horizontal and vertical components of microtremor, *Bull. Seismol. Soc. Am*. 88: 228–241.

Kottke A., Abrahamson N.A., Boore D.M., Bozorgnia Y., Goulet C.A., Holleback J., Kishida T., Der Kiureghian A., Ktenidou O-.J., Kuehn N., Rathje E.M., Silva W.J., Thompson E., Wang X. (2018). Selection of random vibration procedures for the NGA East Project, *PEER Report No. 2018/05*, Pacific Earthquake Engineering Research Center, University of California, Berkeley, CA.

Ktenidou O., Cotton F., Abrahamson N.A., Anderson J.G. (2014). Taxonomy of κ: A review of definition and estimation approaches targeted to applications, *Seismol. Res. Lett*., 85(1): 135–146, doi: 10.1785/0220130027

Kuehn N.M, Scherbaum F. (2016). A partially non-ergodic ground-motion prediction equation for Europe and the Middle East, *Bull Earthq. Eng.,* 14(10): 2629–2642, doi: 10.1007/s10518-016-9911-x

Maechling P.J., Silva F., Callaghan S., Jordan T.H. (2015). SCEC broadband platform: System architecture and software implementation, *Seismol. Res. Lett.*, 86(1): 27–38, doi: 10.1785/0220140125.

PEER (2015) NGA-East: Median ground-motion models for the Central and Eastern North America region, *PEER Report No. 2014/05*, Pacific Earthquake Engineering Research Center, University of California, Berkeley, CA.

Stafford P.J. (2017). Inter-frequency correlations among Fourier spectral ordinates and implications for stochastic ground-motion simulation, *Bull Seismol. Soc. of Am.,* 107(6): 2774–2791, doi: 10.1785/01210170081.

Villani M., Abrahamson N. (2015). Repeatable site and path effects on the ground-motion sigma based on empirical data from southern California and simulated waveforms from the CyberShake platforms, *Bull. Seimol. Soc. Am*., 104: 2681–2695.

Walling M.A. (2009). Non-*Ergodic Probabilistic Seismic Hazard Analysis and Spatial Simulation of Variation in Ground Motion*, PhD dissertation, Department of Civil and Environmental Engineering, University of California, Berkeley, CA.

Appendix A Residual Figures (Electronic)

This appendix contains a larger set of residual figures. Between-event, between-site, and within-site residuals are shown for the following frequencies: 0.1, 0.15, 0.2, 0.3, 0.5, 0.8, 1, 1.5, 2, 3, 5, 8, 10, 15, 20, and 24 Hz.

A.1 Between-Event and Between-Site Residuals

A.2 Within-Site Residuals

A.3 Within-Site Residuals Binned by M

Appendix B MATLAB Program for the Effective Amplitude Spectrum GMM (Electronic)

This appendix contains a MATLAB program to implement the EAS GMM. The program includes tables of model coefficients. The program is included as an electronic appendix.

PEER REPORTS

PEER reports are available as a free PDF download from https://peer.berkeley.edu/peer-reports. In addition, printed hard copies of PEER reports can be ordered directly from our printer by following the instructions at https://peer.berkeley.edu/peer-reports. For other related questions about the PEER Report Series, contact the Pacific Earthquake Engineering Research Center, 325 Davis Hall, Mail Code 1792, Berkeley, CA 94720. Tel.: (510) 642-3437; and Email: peer_center@berkeley.edu.

PEER 2018/06 *Estimation of Shear Demands on Rock-Socketed Drilled Shafts subjected to Lateral Loading*. Pedro Arduino, Long Chen, and Christopher R. McGann. December 2018.

PEER 2018/05 *Selection of Random Vibration Procedures for the NGA-East Project*. Albert Kottke, Norman A. Abrahamson, David M. Boore, Yousef Bozorgnia, Christine Goulet, Justin Hollenback, Tadahiro Kishida, Armen Der Kiureghian, Olga-Joan Ktenidou, Nicolas Kuehn, Ellen M. Rathje, Walter J. Silva, Eric Thompson, and Xiaoyue Wang. December 2018.

PEER 2018/04 *Capturing Directivity Effects in the Mean and Aleatory Variability of the NGA-West 2 Ground Motion Prediction Equations.* Jennie A. Watson-Lamprey. November 2018.

PEER 2018/03 *Probabilistic Seismic Hazard Analysis Code Verification*. Christie Hale, Norman Abrahamson, and Yousef Bozorgnia. July 2018.

PEER 2018/02 *Update of the BCHydro Subduction Ground-Motion Model using the NGA-Subduction Dataset.* Norman Abrahamson, Nicolas Kuehn, Zeynep Gulerce, Nicholas Gregor, Yousef Bozorgnia, Grace Parker, Jonathan Stewart, Brian Chiou, I. M. Idriss, Kenneth Campbell, and Robert Youngs. June 2018.

PEER 2018/01 *PEER Annual Report 2017–2018*. Khalid Mosalam, Amarnath Kasalanati, and Selim Günay. June 2018.

PEER 2017/12 *Experimental Investigation of the Behavior of Vintage and Retrofit Concentrically Braced Steel Frames under Cyclic Loading*. Barbara G. Simpson, Stephen A. Mahin, and Jiun-Wei Lai, December 2017.

PEER 2017/11 *Preliminary Studies on the Dynamic Response of a Seismically Isolated Prototype Gen-IV Sodium-Cooled Fast Reactor* (*PGSFR*). Benshun Shao, Andreas H. Schellenberg, Matthew J. Schoettler, and Stephen A. Mahin. December 2017.

PEER 2017/10 *Development of Time Histories for IEEE693 Testing and Analysis (including Seismically Isolated Equipment).* Shakhzod M. Takhirov, Eric Fujisaki, Leon Kempner, Michael Riley, and Brian Low. December 2017.

PEER 2017/09 *“”R” Package for Computation of Earthquake Ground-Motion Response Spectra.* Pengfei Wang, Jonathan P. Stewart, Yousef Bozorgnia, David M. Boore, and Tadahiro Kishida. December 2017.

PEER 2017/08 *Influence of Kinematic SSI on Foundation Input Motions for Bridges on Deep Foundations*. Benjamin J. Turner, Scott J. Brandenberg, and Jonathan P. Stewart. November 2017.

PEER 2017/07 *A Nonlinear Kinetic Model for Multi-Stage Friction Pendulum Systems*. Paul L. Drazin and Sanjay Govindjee. September 2017.

PEER 2017/06 *Guidelines for Performance-Based Seismic Design of Tall Buildings, Version 2.02*. TBI Working Group led by co-chairs Ron Hamburger and Jack Moehle: Jack Baker, Jonathan Bray, C.B. Crouse, Greg Deierlein, John Hooper, Marshall Lew, Joe Maffei, Stephen Mahin, James Malley, Farzad Naeim, Jonathan Stewart, and John Wallace. May 2017.

PEER 2017/05 *Recommendations for Ergodic Nonlinear Site Amplification in Central and Eastern North America*. Youssef M.A. Hashash, Joseph A. Harmon, Okan Ilhan, Grace A. Parker, and Jonathan P. Stewart. March 2017.

PEER 2017/04 *Expert Panel Recommendations for Ergodic Site Amplification in Central and Eastern North America*. Jonathan P. Stewart, Grace A. Parker, Joseph P. Harmon, Gail M. Atkinson, David M. Boore, Robert B. Darragh, Walter J. Silva, and Youssef M.A. Hashash. March 2017.

PEER 2017/03 *NGA-East Ground-Motion Models for the U.S. Geological Survey National Seismic Hazard Maps*. Christine A. Goulet, Yousef Bozorgnia, Nicolas Kuehn, Linda Al Atik, Robert R. Youngs, Robert W. Graves, and Gail M. Atkinson. March 2017.

PEER 2017/02 *U.S.–New Zealand–Japan Workshop: Liquefaction-Induced Ground Movements Effects, University of California, Berkeley, California, 2–4 November 2016.* Jonathan D. Bray, Ross W. Boulanger, Misko Cubrinovski, Kohji Tokimatsu, Steven L. Kramer, Thomas O’Rourke, Ellen Rathje, Russell A. Green, Peter K. Robinson, and Christine Z. Beyzaei. March 2017.

PEER 2017/01 *2016 PEER Annual Report.* Khalid M. Mosalam, Amarnath Kasalanati, and Grace Kang. March 2017.

PEER 2016/10 *Performance-Based Robust Nonlinear Seismic Analysis with Application to Reinforced Concrete Bridge Systems*. Xiao Ling and Khalid M. Mosalam. December 2016.

PEER 2017/09 *Segmental Displacement Control Design for Seismically Isolated Bridges,* Kenneth A. Ogorzalek and Stephen A. Mahin. December 2016.

PEER 2016/08 *Resilience of Critical Structures, Infrastructure, and Communities*. Gian Paolo Cimellaro, Ali Zamani-Noori, Omar Kamouh, Vesna Terzic, and Stephen A. Mahin. December 2016.

PEER 2016/07 *Hybrid Simulation Theory for a Classical Nonlinear Dynamical System*. Paul L. Drazin and Sanjay Govindjee. September 2016.

PEER 2016/06 *California Earthquake Early Warning System Benefit Study*. Laurie A. Johnson, Sharyl Rabinovici, Grace S. Kang, and Stephen A. Mahin. July 2006.

PEER 2016/05 *Ground-Motion Prediction Equations for Arias Intensity Consistent with the NGA-West2 Ground-Motion Models*. Charlotte Abrahamson, Hao-Jun Michael Shi, and Brian Yang. July 2016.

PEER 2016/04 *The M_W 6.0 South Napa Earthquake of August 24, 2014: A Wake-Up Call for Renewed Investment in Seismic Resilience Across California.* Prepared for the California Seismic Safety Commission, Laurie A. Johnson and Stephen A. Mahin. May 2016.

PEER 2016/03 *Simulation Confidence in Tsunami-Driven Overland Flow*. Patrick Lynett. May 2016.

PEER 2016/02 *Semi-Automated Procedure for Windowing time Series and Computing Fourier Amplitude Spectra for the NGA-West2 Database.* Tadahiro Kishida, Olga-Joan Ktenidou, Robert B. Darragh, and Walter J. Silva. May 2016.

PEER 2016/01 *A Methodology for the Estimation of Kappa (κ) from Large Datasets: Example Application to Rock Sites in the NGA-East Database and Implications on Design Motions.* Olga-Joan Ktenidou, Norman A. Abrahamson, Robert B. Darragh, and Walter J. Silva. April 2016.

PEER 2015/13 *Self-Centering Precast Concrete Dual-Steel-Shell Columns for Accelerated Bridge Construction: Seismic Performance, Analysis, and Design*. Gabriele Guerrini, José I. Restrepo, Athanassios Vervelidis, and Milena Massari. December 2015.

PEER 2015/12 *Shear-Flexure Interaction Modeling for Reinforced Concrete Structural Walls and Columns under Reversed Cyclic Loading*. Kristijan Kolozvari, Kutay Orakcal, and John Wallace. December 2015.

PEER 2015/11 *Selection and Scaling of Ground Motions for Nonlinear Response History Analysis of Buildings in Performance-Based Earthquake Engineering*. N. Simon Kwong and Anil K. Chopra. December 2015.

PEER 2015/10 *Structural Behavior of Column-Bent Cap Beam-Box Girder Systems in Reinforced Concrete Bridges Subjected to Gravity and Seismic Loads. Part II: Hybrid Simulation and Post-Test Analysis*. Mohamed A. Moustafa and Khalid M. Mosalam. November 2015.

PEER 2015/09 *Structural Behavior of Column-Bent Cap Beam-Box Girder Systems in Reinforced Concrete Bridges Subjected to Gravity and Seismic Loads. Part I: Pre-Test Analysis and Quasi-Static Experiments*. Mohamed A. Moustafa and Khalid M. Mosalam. September 2015.

PEER 2015/08 *NGA-East: Adjustments to Median Ground-Motion Models for Center and Eastern North America*. August 2015.

PEER 2015/07 *NGA-East: Ground-Motion Standard-Deviation Models for Central and Eastern North America*. Linda Al Atik. June 2015.

PEER 2015/06 *Adjusting Ground-Motion Intensity Measures to a Reference Site for which V_{S30} = 3000 m/sec*. David M. Boore. May 2015.

PEER 2015/05 *Hybrid Simulation of Seismic Isolation Systems Applied to an APR-1400 Nuclear Power Plant.* Andreas H. Schellenberg, Alireza Sarebanha, Matthew J. Schoettler, Gilberto Mosqueda, Gianmario Benzoni, and Stephen A. Mahin. April 2015.

PEER 2015/04 *NGA-East: Median Ground-Motion Models for the Central and Eastern North America Region*. April 2015.

PEER 2015/03 *Single Series Solution for the Rectangular Fiber-Reinforced Elastomeric Isolator Compression Modulus*. James M. Kelly and Niel C. Van Engelen. March 2015.

PEER 2015/02 *A Full-Scale, Single-Column Bridge Bent Tested by Shake-Table Excitation.* Matthew J. Schoettler, José I. Restrepo, Gabriele Guerrini, David E. Duck, and Francesco Carrea. March 2015.

PEER 2015/01 *Concrete Column Blind Prediction Contest 2010: Outcomes and Observations.* Vesna Terzic, Matthew J. Schoettler, José I. Restrepo, and Stephen A Mahin. March 2015.

PEER 2014/20 *Stochastic Modeling and Simulation of Near-Fault Ground Motions for Performance-Based Earthquake Engineering*. Mayssa Dabaghi and Armen Der Kiureghian. December 2014.

PEER 2014/19 *Seismic Response of a Hybrid Fiber-Reinforced Concrete Bridge Column Detailed for Accelerated Bridge Construction*. Wilson Nguyen, William Trono, Marios Panagiotou, and Claudia P. Ostertag. December 2014.

PEER 2014/18 *Three-Dimensional Beam-Truss Model for Reinforced Concrete Walls and Slabs Subjected to Cyclic Static or Dynamic Loading*. Yuan Lu, Marios Panagiotou, and Ioannis Koutromanos. December 2014.

PEER 2014/17 *PEER NGA-East Database.* Christine A. Goulet, Tadahiro Kishida, Timothy D. Ancheta, Chris H. Cramer, Robert B. Darragh, Walter J. Silva, Youssef M.A. Hashash, Joseph Harmon, Jonathan P. Stewart, Katie E. Wooddell, and Robert R. Youngs. October 2014.

PEER 2014/16 *Guidelines for Performing Hazard-Consistent One-Dimensional Ground Response Analysis for Ground Motion Prediction*. Jonathan P. Stewart, Kioumars Afshari, and Youssef M.A. Hashash. October 2014.

PEER 2014/15 *NGA-East Regionalization Report: Comparison of Four Crustal Regions within Central and Eastern North America using Waveform Modeling and 5%-Damped Pseudo-Spectral Acceleration Response*. Jennifer Dreiling, Marius P. Isken, Walter D. Mooney, Martin C. Chapman, and Richard W. Godbee. October 2014.

PEER 2014/14 *Scaling Relations between Seismic Moment and Rupture Area of Earthquakes in Stable Continental Regions*. Paul Somerville. August 2014.

PEER 2014/13 *PEER Preliminary Notes and Observations on the August 24, 2014, South Napa Earthquake*. Grace S. Kang and Stephen A. Mahin, Editors. September 2014.

PEER 2014/12 *Reference-Rock Site Conditions for Central and Eastern North America: Part II – Attenuation (Kappa) Definition*. Kenneth W. Campbell, Youssef M.A. Hashash, Byungmin Kim, Albert R. Kottke, Ellen M. Rathje, Walter J. Silva, and Jonathan P. Stewart. August 2014.

PEER 2014/11 *Reference-Rock Site Conditions for Central and Eastern North America: Part I - Velocity Definition*. Youssef M.A. Hashash, Albert R. Kottke, Jonathan P. Stewart, Kenneth W. Campbell, Byungmin Kim, Ellen M. Rathje, Walter J. Silva, Sissy Nikolaou, and Cheryl Moss. August 2014.

PEER 2014/10 *Evaluation of Collapse and Non-Collapse of Parallel Bridges Affected by Liquefaction and Lateral Spreading*. Benjamin Turner, Scott J. Brandenberg, and Jonathan P. Stewart. August 2014.

PEER 2014/09 *PEER Arizona Strong-Motion Database and GMPEs Evaluation*. Tadahiro Kishida, Robert E. Kayen, Olga-Joan Ktenidou, Walter J. Silva, Robert B. Darragh, and Jennie Watson-Lamprey. June 2014.

PEER 2014/08 *Unbonded Pretensioned Bridge Columns with Rocking Detail*. Jeffrey A. Schaefer, Bryan Kennedy, Marc O. Eberhard, and John F. Stanton. June 2014.

PEER 2014/07 *Northridge 20 Symposium Summary Report: Impacts, Outcomes, and Next Steps*. May 2014.

PEER 2014/06 *Report of the Tenth Planning Meeting of NEES/E-Defense Collaborative Research on Earthquake Engineering*. December 2013.

PEER 2014/05 *Seismic Velocity Site Characterization of Thirty-One Chilean Seismometer Stations by Spectral Analysis of Surface Wave Dispersion*. Robert Kayen, Brad D. Carkin, Skye Corbet, Camilo Pinilla, Allan Ng, Edward Gorbis, and Christine Truong. April 2014.

PEER 2014/04 Effect of Vertical Acceleration on Shear Strength of Reinforced Concrete Columns. Hyerin Lee and Khalid M. Mosalam. April 2014.

PEER 2014/03 *Retest of Thirty-Year-Old Neoprene Isolation Bearings.* James M. Kelly and Niel C. Van Engelen. March 2014.

PEER 2014/02 *Theoretical Development of Hybrid Simulation Applied to Plate Structures.* Ahmed A. Bakhaty, Khalid M. Mosalam, and Sanjay Govindjee. January 2014.

PEER 2014/01 *Performance-Based Seismic Assessment of Skewed Bridges.* Peyman Kaviani, Farzin Zareian, and Ertugrul Taciroglu. January 2014.

PEER 2013/26 *Urban Earthquake Engineerin*g. Proceedings of the U.S.-Iran Seismic Workshop. December 2013.

PEER 2013/25 *Earthquake Engineering for Resilient Communities: 2013 PEER Internship Program Research Report Collection.* Heidi Tremayne (Editor), Stephen A. Mahin (Editor), Jorge Archbold Monterossa, Matt Brosman, Shelly Dean, Katherine deLaveaga, Curtis Fong, Donovan Holder, Rakeeb Khan, Elizabeth Jachens, David Lam, Daniela Martinez Lopez, Mara Minner, Geffen Oren, Julia Pavicic, Melissa Quinonez, Lorena Rodriguez, Sean Salazar, Kelli Slaven, Vivian Steyert, Jenny Taing, and Salvador Tena. December 2013.

PEER 2013/24 *NGA-West2 Ground Motion Prediction Equations for Vertical Ground Motions*. September 2013.

PEER 2013/23 *Coordinated Planning and Preparedness for Fire Following Major Earthquakes*. Charles Scawthorn. November 2013.

PEER 2013/22 *GEM-PEER Task 3 Project: Selection of a Global Set of Ground Motion Prediction Equations.* Jonathan P. Stewart, John Douglas, Mohammad B. Javanbarg, Carola Di Alessandro, Yousef Bozorgnia, Norman A. Abrahamson, David M. Boore, Kenneth W. Campbell, Elise Delavaud, Mustafa Erdik, and Peter J. Stafford. December 2013.

PEER 2013/21 *Seismic Design and Performance of Bridges with Columns on Rocking Foundations*. Grigorios Antonellis and Marios Panagiotou. September 2013.

PEER 2013/20 *Experimental and Analytical Studies on the Seismic Behavior of Conventional and Hybrid Braced Frames*. Jiun-Wei Lai and Stephen A. Mahin. September 2013.

PEER 2013/19 *Toward Resilient Communities: A Performance-Based Engineering Framework for Design and Evaluation of the Built Environment.* Michael William Mieler, Bozidar Stojadinovic, Robert J. Budnitz, Stephen A. Mahin, and Mary C. Comerio. September 2013.

PEER 2013/18 *Identification of Site Parameters that Improve Predictions of Site Amplification*. Ellen M. Rathje and Sara Navidi. July 2013.

PEER 2013/17 *Response Spectrum Analysis of Concrete Gravity Dams Including Dam-Water-Foundation Interaction*. Arnkjell Løkke and Anil K. Chopra. July 2013.

PEER 2013/16 *Effect of Hoop Reinforcement Spacing on the Cyclic Response of Large Reinforced Concrete Special Moment Frame Beams.* Marios Panagiotou, Tea Visnjic, Grigorios Antonellis, Panagiotis Galanis, and Jack P. Moehle. June 2013.

PEER 2013/15 *A Probabilistic Framework to Include the Effects of Near-Fault Directivity in Seismic Hazard Assessment*. Shrey Kumar Shahi, Jack W. Baker. October 2013.

PEER 2013/14 *Hanging-Wall Scaling using Finite-Fault Simulations.* Jennifer L. Donahue and Norman A. Abrahamson. September 2013.

PEER 2013/13 *Semi-Empirical Nonlinear Site Amplification and its Application in NEHRP Site Factors*. Jonathan P. Stewart and Emel Seyhan. November 2013.

PEER 2013/12 *Nonlinear Horizontal Site Response for the NGA-West2 Project.* Ronnie Kamai, Norman A. Abramson, Walter J. Silva. May 2013.

PEER 2013/11 *Epistemic Uncertainty for NGA-West2 Models.* Linda Al Atik and Robert R. Youngs. May 2013.

PEER 2013/10 *NGA-West 2 Models for Ground-Motion Directionality.* Shrey K. Shahi and Jack W. Baker. May 2013.

PEER 2013/09 *Final Report of the NGA-West2 Directivity Working Group.* Paul Spudich, Jeffrey R. Bayless, Jack W. Baker, Brian S.J. Chiou, Badie Rowshandel, Shrey Shahi, and Paul Somerville. May 2013.

PEER 2013/08 *NGA-West2 Model for Estimating Average Horizontal Values of Pseudo-Absolute Spectral Accelerations Generated by Crustal Earthquakes*. I. M. Idriss. May 2013.

PEER 2013/07 *Update of the Chiou and Youngs NGA Ground Motion Model for Average Horizontal Component of Peak Ground Motion and Response Spectra*. Brian Chiou and Robert Youngs. May 2013.

PEER 2013/06 *NGA-West2 Campbell-Bozorgnia Ground Motion Model for the Horizontal Components of PGA, PGV, and 5%-Damped Elastic Pseudo-Acceleration Response Spectra for Periods Ranging from 0.01 to 10 sec.* Kenneth W. Campbell and Yousef Bozorgnia. May 2013.

PEER 2013/05 *NGA-West 2 Equations for Predicting Response Spectral Accelerations for Shallow Crustal Earthquakes*. David M. Boore, Jonathan P. Stewart, Emel Seyhan, and Gail M. Atkinson. May 2013.

PEER 2013/04 *Update of the AS08 Ground-Motion Prediction Equations Based on the NGA-West2 Data Set*. Norman Abrahamson, Walter Silva, and Ronnie Kamai. May 2013.

PEER 2013/03 *PEER NGA-West2 Database.* Timothy D. Ancheta, Robert B. Darragh, Jonathan P. Stewart, Emel Seyhan, Walter J. Silva, Brian S.J. Chiou, Katie E. Wooddell, Robert W. Graves, Albert R. Kottke, David M. Boore, Tadahiro Kishida, and Jennifer L. Donahue. May 2013.

PEER 2013/02 *Hybrid Simulation of the Seismic Response of Squat Reinforced Concrete Shear Walls*. Catherine A. Whyte and Bozidar Stojadinovic. May 2013.

PEER 2013/01 *Housing Recovery in Chile: A Qualitative Mid-program Review*. Mary C. Comerio. February 2013.

PEER 2012/08 *Guidelines for Estimation of Shear Wave Velocity.* Bernard R. Wair, Jason T. DeJong, and Thomas Shantz. December 2012.

PEER 2012/07 *Earthquake Engineering for Resilient Communities: 2012 PEER Internship Program Research Report Collection.* Heidi Tremayne (Editor), Stephen A. Mahin (Editor), Collin Anderson, Dustin Cook, Michael Erceg, Carlos

Esparza, Jose Jimenez, Dorian Krausz, Andrew Lo, Stephanie Lopez, Nicole McCurdy, Paul Shipman, Alexander Strum, Eduardo Vega. December 2012.

PEER 2012/06 *Fragilities for Precarious Rocks at Yucca Mountain.* Matthew D. Purvance, Rasool Anooshehpoor, and James N. Brune. December 2012.

PEER 2012/05 *Development of Simplified Analysis Procedure for Piles in Laterally Spreading Layered Soils.* Christopher R. McGann, Pedro Arduino, and Peter Mackenzie–Helnwein. December 2012.

PEER 2012/04 *Unbonded Pre-Tensioned Columns for Bridges in Seismic Regions.* Phillip M. Davis, Todd M. Janes, Marc O. Eberhard, and John F. Stanton. December 2012.

PEER 2012/03 *Experimental and Analytical Studies on Reinforced Concrete Buildings with Seismically Vulnerable Beam-Column Joints*. Sangjoon Park and Khalid M. Mosalam. October 2012.

PEER 2012/02 *Seismic Performance of Reinforced Concrete Bridges Allowed to Uplift during Multi-Directional Excitation*. Andres Oscar Espinoza and Stephen A. Mahin. July 2012.

PEER 2012/01 *Spectral Damping Scaling Factors for Shallow Crustal Earthquakes in Active Tectonic Regions.* Sanaz Rezaeian, Yousef Bozorgnia, I. M. Idriss, Kenneth Campbell, Norman Abrahamson, and Walter Silva. July 2012.

PEER 2011/10 *Earthquake Engineering for Resilient Communities: 2011 PEER Internship Program Research Report Collection*. Heidi Faison and Stephen A. Mahin, Editors. December 2011.

PEER 2011/09 *Calibration of Semi-Stochastic Procedure for Simulating High-Frequency Ground Motions*. Jonathan P. Stewart, Emel Seyhan, and Robert W. Graves. December 2011.

PEER 2011/08 *Water Supply in regard to Fire Following Earthquake*. Charles Scawthorn. November 2011.

PEER 2011/07 *Seismic Risk Management in Urban Areas*. Proceedings of a U.S.-Iran-Turkey Seismic Workshop. September 2011.

PEER 2011/06 *The Use of Base Isolation Systems to Achieve Complex Seismic Performance Objectives*. Troy A. Morgan and Stephen A. Mahin. July 2011.

PEER 2011/05 *Case Studies of the Seismic Performance of Tall Buildings Designed by Alternative Means.* Task 12 Report for the Tall Buildings Initiative. Jack Moehle, Yousef Bozorgnia, Nirmal Jayaram, Pierson Jones, Mohsen Rahnama, Nilesh Shome, Zeynep Tuna, John Wallace, Tony Yang, and Farzin Zareian. July 2011.

PEER 2011/04 *Recommended Design Practice for Pile Foundations in Laterally Spreading Ground.* Scott A. Ashford, Ross W. Boulanger, and Scott J. Brandenberg. June 2011.

PEER 2011/03 *New Ground Motion Selection Procedures and Selected Motions for the PEER Transportation Research Program*. Jack W. Baker, Ting Lin, Shrey K. Shahi, and Nirmal Jayaram. March 2011.

PEER 2011/02 *A Bayesian Network Methodology for Infrastructure Seismic Risk Assessment and Decision Support*. Michelle T. Bensi, Armen Der Kiureghian, and Daniel Straub. March 2011.

PEER 2011/01 *Demand Fragility Surfaces for Bridges in Liquefied and Laterally Spreading Ground.* Scott J. Brandenberg, Jian Zhang, Pirooz Kashighandi, Yili Huo, and Minxing Zhao. March 2011.

PEER 2010/05 *Guidelines for Performance-Based Seismic Design of Tall Buildings.* Developed by the Tall Buildings Initiative. November 2010.

PEER 2010/04 *Application Guide for the Design of Flexible and Rigid Bus Connections between Substation Equipment Subjected to Earthquakes.* Jean-Bernard Dastous and Armen Der Kiureghian. September 2010.

PEER 2010/03 *Shear Wave Velocity as a Statistical Function of Standard Penetration Test Resistance and Vertical Effective Stress at Caltrans Bridge Sites.* Scott J. Brandenberg, Naresh Bellana, and Thomas Shantz. June 2010.

PEER 2010/02 *Stochastic Modeling and Simulation of Ground Motions for Performance-Based Earthquake Engineering.* Sanaz Rezaeian and Armen Der Kiureghian. June 2010.

PEER 2010/01 *Structural Response and Cost Characterization of Bridge Construction Using Seismic Performance Enhancement Strategies.* Ady Aviram, Božidar Stojadinović, Gustavo J. Parra-Montesinos, and Kevin R. Mackie. March 2010.

PEER 2009/03 *The Integration of Experimental and Simulation Data in the Study of Reinforced Concrete Bridge Systems Including Soil-Foundation-Structure Interaction.* Matthew Dryden and Gregory L. Fenves. November 2009.

PEER 2009/02 *Improving Earthquake Mitigation through Innovations and Applications in Seismic Science, Engineering, Communication, and Response*. Proceedings of a U.S.-Iran Seismic Workshop. October 2009.

PEER 2009/01 *Evaluation of Ground Motion Selection and Modification Methods: Predicting Median Interstory Drift Response of Buildings*. Curt B. Haselton, Editor. June 2009.

PEER 2008/10 *Technical Manual for Strata.* Albert R. Kottke and Ellen M. Rathje. February 2009.

PEER 2008/09 *NGA Model for Average Horizontal Component of Peak Ground Motion and Response Spectra.* Brian S.-J. Chiou and Robert R. Youngs. November 2008.

PEER 2008/08 *Toward Earthquake-Resistant Design of Concentrically Braced Steel Structures*. Patxi Uriz and Stephen A. Mahin. November 2008.

PEER 2008/07 *Using OpenSees for Performance-Based Evaluation of Bridges on Liquefiable Soils*. Stephen L. Kramer, Pedro Arduino, and HyungSuk Shin. November 2008.

PEER 2008/06 *Shaking Table Tests and Numerical Investigation of Self-Centering Reinforced Concrete Bridge Columns*. Hyung IL Jeong, Junichi Sakai, and Stephen A. Mahin. September 2008.

PEER 2008/05 *Performance-Based Earthquake Engineering Design Evaluation Procedure for Bridge Foundations Undergoing Liquefaction-Induced Lateral Ground Displacement*. Christian A. Ledezma and Jonathan D. Bray. August 2008.

PEER 2008/04 *Benchmarking of Nonlinear Geotechnical Ground Response Analysis Procedures.* Jonathan P. Stewart, Annie On-Lei Kwok, Youssef M. A. Hashash, Neven Matasovic, Robert Pyke, Zhiliang Wang, and Zhaohui Yang. August 2008.

PEER 2008/03 *Guidelines for Nonlinear Analysis of Bridge Structures in California.* Ady Aviram, Kevin R. Mackie, and Božidar Stojadinović. August 2008.

PEER 2008/02 *Treatment of Uncertainties in Seismic-Risk Analysis of Transportation Systems*. Evangelos Stergiou and Anne S. Kiremidjian. July 2008.

PEER 2008/01 *Seismic Performance Objectives for Tall Buildings.* William T. Holmes, Charles Kircher, William Petak, and Nabih Youssef. August 2008.

PEER 2007/12 *An Assessment to Benchmark the Seismic Performance of a Code-Conforming Reinforced Concrete Moment-Frame Building.* Curt Haselton, Christine A. Goulet, Judith Mitrani-Reiser, James L. Beck, Gregory G. Deierlein, Keith A. Porter, Jonathan P. Stewart, and Ertugrul Taciroglu. August 2008.

PEER 2007/11 *Bar Buckling in Reinforced Concrete Bridge Columns.* Wayne A. Brown, Dawn E. Lehman, and John F. Stanton. February 2008.

PEER 2007/10 *Computational Modeling of Progressive Collapse in Reinforced Concrete Frame Structures*. Mohamed M. Talaat and Khalid M. Mosalam. May 2008.

PEER 2007/09 *Integrated Probabilistic Performance-Based Evaluation of Benchmark Reinforced Concrete Bridges*. Kevin R. Mackie, John-Michael Wong, and Božidar Stojadinović. January 2008.

PEER 2007/08 *Assessing Seismic Collapse Safety of Modern Reinforced Concrete Moment-Frame Buildings*. Curt B. Haselton and Gregory G. Deierlein. February 2008.

PEER 2007/07 *Performance Modeling Strategies for Modern Reinforced Concrete Bridge Columns*. Michael P. Berry and Marc O. Eberhard. April 2008.

PEER 2007/06 *Development of Improved Procedures for Seismic Design of Buried and Partially Buried Structures*. Linda Al Atik and Nicholas Sitar. June 2007.

PEER 2007/05 *Uncertainty and Correlation in Seismic Risk Assessment of Transportation Systems*. Renee G. Lee and Anne S. Kiremidjian. July 2007.

PEER 2007/04 *Numerical Models for Analysis and Performance-Based Design of Shallow Foundations Subjected to Seismic Loading.* Sivapalan Gajan, Tara C. Hutchinson, Bruce L. Kutter, Prishati Raychowdhury, José A. Ugalde, and Jonathan P. Stewart. May 2008.

PEER 2007/03 *Beam-Column Element Model Calibrated for Predicting Flexural Response Leading to Global Collapse of RC Frame Buildings*. Curt B. Haselton, Abbie B. Liel, Sarah Taylor Lange, and Gregory G. Deierlein. May 2008.

PEER 2007/02 *Campbell-Bozorgnia NGA Ground Motion Relations for the Geometric Mean Horizontal Component of Peak and Spectral Ground Motion Parameters*. Kenneth W. Campbell and Yousef Bozorgnia. May 2007.

PEER 2007/01 *Boore-Atkinson NGA Ground Motion Relations for the Geometric Mean Horizontal Component of Peak and Spectral Ground Motion Parameters*. David M. Boore and Gail M. Atkinson. May 2007.

PEER 2006/12 Societal Implications of Performance-Based Earthquake Engineering. Peter J. May. May 2007.

PEER 2006/11 *Probabilistic Seismic Demand Analysis Using Advanced Ground Motion Intensity Measures, Attenuation Relationships, and Near-Fault Effects*. Polsak Tothong and C. Allin Cornell. March 2007.

PEER 2006/10 *Application of the PEER PBEE Methodology to the I-880 Viaduct*. Sashi Kunnath. February 2007.

PEER 2006/09 *Quantifying Economic Losses from Travel Forgone Following a Large Metropolitan Earthquake*. James Moore, Sungbin Cho, Yue Yue Fan, and Stuart Werner. November 2006.

PEER 2006/08 *Vector-Valued Ground Motion Intensity Measures for Probabilistic Seismic Demand Analysis*. Jack W. Baker and C. Allin Cornell. October 2006.

PEER 2006/07 *Analytical Modeling of Reinforced Concrete Walls for Predicting Flexural and Coupled–Shear-Flexural Responses*. Kutay Orakcal, Leonardo M. Massone, and John W. Wallace. October 2006.

PEER 2006/06 *Nonlinear Analysis of a Soil-Drilled Pier System under Static and Dynamic Axial Loading*. Gang Wang and Nicholas Sitar. November 2006.

PEER 2006/05 *Advanced Seismic Assessment Guidelines.* Paolo Bazzurro, C. Allin Cornell, Charles Menun, Maziar Motahari, and Nicolas Luco. September 2006.

PEER 2006/04 *Probabilistic Seismic Evaluation of Reinforced Concrete Structural Components and Systems*. Tae Hyung Lee and Khalid M. Mosalam. August 2006.

PEER 2006/03 *Performance of Lifelines Subjected to Lateral Spreading.* Scott A. Ashford and Teerawut Juirnarongrit. July 2006.

PEER 2006/02 *Pacific Earthquake Engineering Research Center Highway Demonstration Project.* Anne Kiremidjian, James Moore, Yue Yue Fan, Nesrin Basoz, Ozgur Yazali, and Meredith Williams. April 2006.

PEER 2006/01 *Bracing Berkeley. A Guide to Seismic Safety on the UC Berkeley Campus.* Mary C. Comerio, Stephen Tobriner, and Ariane Fehrenkamp. January 2006.

PEER 2005/17 *Earthquake Simulation Tests on Reducing Residual Displacements of Reinforced Concrete Bridges.* Junichi Sakai, Stephen A Mahin, and Andres Espinoza. December 2005.

PEER 2005/16 *Seismic Response and Reliability of Electrical Substation Equipment and Systems.* Junho Song, Armen Der Kiureghian, and Jerome L. Sackman. April 2006.

PEER 2005/15 *CPT-Based Probabilistic Assessment of Seismic Soil Liquefaction Initiation.* R. E. S. Moss, R. B. Seed, R. E. Kayen, J. P. Stewart, and A. Der Kiureghian. April 2006.

PEER 2005/14 *Workshop on Modeling of Nonlinear Cyclic Load-Deformation Behavior of Shallow Foundations.* Bruce L. Kutter, Geoffrey Martin, Tara Hutchinson, Chad Harden, Sivapalan Gajan, and Justin Phalen. March 2006.

PEER 2005/13 *Stochastic Characterization and Decision Bases under Time-Dependent Aftershock Risk in Performance-Based Earthquake Engineering*. Gee Liek Yeo and C. Allin Cornell. July 2005.

PEER 2005/12 *PEER Testbed Study on a Laboratory Building: Exercising Seismic Performance Assessment.* Mary C. Comerio, Editor. November 2005.

PEER 2005/11 *Van Nuys Hotel Building Testbed Report: Exercising Seismic Performance Assessment.* Helmut Krawinkler, Editor. October 2005.

PEER 2005/10 *First NEES/E-Defense Workshop on Collapse Simulation of Reinforced Concrete Building Structures.* September 2005.

PEER 2005/09 *Test Applications of Advanced Seismic Assessment Guidelines.* Joe Maffei, Karl Telleen, Danya Mohr, William Holmes, and Yuki Nakayama. August 2006.

PEER 2005/08 *Damage Accumulation in Lightly Confined Reinforced Concrete Bridge Columns.* R. Tyler Ranf, Jared M. Nelson, Zach Price, Marc O. Eberhard, and John F. Stanton. April 2006.

PEER 2005/07 *Experimental and Analytical Studies on the Seismic Response of Freestanding and Anchored Laboratory Equipment.* Dimitrios Konstantinidis and Nicos Makris. January 2005.

PEER 2005/06 *Global Collapse of Frame Structures under Seismic Excitations*. Luis F. Ibarra and Helmut Krawinkler. September 2005.

PEER 2005//05 *Performance Characterization of Bench- and Shelf-Mounted Equipment.* Samit Ray Chaudhuri and Tara C. Hutchinson. May 2006.

PEER 2005/04 *Numerical Modeling of the Nonlinear Cyclic Response of Shallow Foundations.* Chad Harden, Tara Hutchinson, Geoffrey R. Martin, and Bruce L. Kutter. August 2005.

PEER 2005/03 *A Taxonomy of Building Components for Performance-Based Earthquake Engineering.* Keith A. Porter. September 2005.

PEER 2005/02 *Fragility Basis for California Highway Overpass Bridge Seismic Decision Making*. Kevin R. Mackie and Božidar Stojadinović. June 2005.

PEER 2005/01 *Empirical Characterization of Site Conditions on Strong Ground Motion.* Jonathan P. Stewart, Yoojoong Choi, and Robert W. Graves. June 2005.

PEER 2004/09 *Electrical Substation Equipment Interaction: Experimental Rigid Conductor Studies.* Christopher Stearns and André Filiatrault. February 2005.

PEER 2004/08 *Seismic Qualification and Fragility Testing of Line Break 550-kV Disconnect Switches.* Shakhzod M. Takhirov, Gregory L. Fenves, and Eric Fujisaki. January 2005.

PEER 2004/07 *Ground Motions for Earthquake Simulator Qualification of Electrical Substation Equipment.* Shakhzod M. Takhirov, Gregory L. Fenves, Eric Fujisaki, and Don Clyde. January 2005.

PEER 2004/06 *Performance-Based Regulation and Regulatory Regimes.* Peter J. May and Chris Koski. September 2004.

PEER 2004/05 *Performance-Based Seismic Design Concepts and Implementation: Proceedings of an International Workshop.* Peter Fajfar and Helmut Krawinkler, Editors. September 2004.

PEER 2004/04 *Seismic Performance of an Instrumented Tilt-up Wall Building.* James C. Anderson and Vitelmo V. Bertero. July 2004.

PEER 2004/03 *Evaluation and Application of Concrete Tilt-up Assessment Methodologies.* Timothy Graf and James O. Malley. October 2004.

PEER 2004/02 *Analytical Investigations of New Methods for Reducing Residual Displacements of Reinforced Concrete Bridge Columns.* Junichi Sakai and Stephen A. Mahin. August 2004.

PEER 2004/01 *Seismic Performance of Masonry Buildings and Design Implications.* Kerri Anne Taeko Tokoro, James C. Anderson, and Vitelmo V. Bertero. February 2004.

PEER 2003/18 *Performance Models for Flexural Damage in Reinforced Concrete Columns.* Michael Berry and Marc Eberhard. August 2003.

PEER 2003/17 *Predicting Earthquake Damage in Older Reinforced Concrete Beam-Column Joints.* Catherine Pagni and Laura Lowes. October 2004.

PEER 2003/16 *Seismic Demands for Performance-Based Design of Bridges.* Kevin Mackie and Božidar Stojadinović. August 2003.

PEER 2003/15 *Seismic Demands for Nondeteriorating Frame Structures and Their Dependence on Ground Motions.* Ricardo Antonio Medina and Helmut Krawinkler. May 2004.

PEER 2003/14 *Finite Element Reliability and Sensitivity Methods for Performance-Based Earthquake Engineering*. Terje Haukaas and Armen Der Kiureghian. April 2004.

PEER 2003/13 *Effects of Connection Hysteretic Degradation on the Seismic Behavior of Steel Moment-Resisting Frames.* Janise E. Rodgers and Stephen A. Mahin. March 2004.

PEER 2003/12 *Implementation Manual for the Seismic Protection of Laboratory Contents: Format and Case Studies*. William T. Holmes and Mary C. Comerio. October 2003.

PEER 2003/11 *Fifth U.S.-Japan Workshop on Performance-Based Earthquake Engineering Methodology for Reinforced Concrete Building Structures*. February 2004.

PEER 2003/10 *A Beam-Column Joint Model for Simulating the Earthquake Response of Reinforced Concrete Frames.* Laura N. Lowes, Nilanjan Mitra, and Arash Altoontash. February 2004.

PEER 2003/09 *Sequencing Repairs after an Earthquake: An Economic Approach.* Marco Casari and Simon J. Wilkie. April 2004.

PEER 2003/08 *A Technical Framework for Probability-Based Demand and Capacity Factor Design (DCFD) Seismic Formats*. Fatemeh Jalayer and C. Allin Cornell. November 2003.

PEER 2003/07 *Uncertainty Specification and Propagation for Loss Estimation Using FOSM Methods.* Jack W. Baker and C. Allin Cornell. September 2003.

PEER 2003/06 *Performance of Circular Reinforced Concrete Bridge Columns under Bidirectional Earthquake Loading*. Mahmoud M. Hachem, Stephen A. Mahin, and Jack P. Moehle. February 2003.

PEER 2003/05 *Response Assessment for Building-Specific Loss Estimation.* Eduardo Miranda and Shahram Taghavi. September 2003.

PEER 2003/04 *Experimental Assessment of Columns with Short Lap Splices Subjected to Cyclic Loads*. Murat Melek, John W. Wallace, and Joel Conte. April 2003.

PEER 2003/03 *Probabilistic Response Assessment for Building-Specific Loss Estimation*. Eduardo Miranda and Hesameddin Aslani. September 2003.

PEER 2003/02 *Software Framework for Collaborative Development of Nonlinear Dynamic Analysis Program*. Jun Peng and Kincho H. Law. September 2003.

PEER 2003/01 *Shake Table Tests and Analytical Studies on the Gravity Load Collapse of Reinforced Concrete Frames.* Kenneth John Elwood and Jack P. Moehle. November 2003.

PEER 2002/24 *Performance of Beam to Column Bridge Joints Subjected to a Large Velocity Pulse.* Natalie Gibson, André Filiatrault, and Scott A. Ashford. April 2002.

PEER 2002/23 *Effects of Large Velocity Pulses on Reinforced Concrete Bridge Columns.* Greg L. Orozco and Scott A. Ashford. April 2002.

PEER 2002/22 *Characterization of Large Velocity Pulses for Laboratory Testing.* Kenneth E. Cox and Scott A. Ashford. April 2002.

PEER 2002/21 *Fourth U.S.-Japan Workshop on Performance-Based Earthquake Engineering Methodology for Reinforced Concrete Building Structures*. December 2002.

PEER 2002/20 *Barriers to Adoption and Implementation of PBEE Innovations.* Peter J. May. August 2002.

PEER 2002/19 *Economic-Engineered Integrated Models for Earthquakes: Socioeconomic Impacts.* Peter Gordon, James E. Moore II, and Harry W. Richardson. July 2002.

PEER 2002/18 *Assessment of Reinforced Concrete Building Exterior Joints with Substandard Details.* Chris P. Pantelides, Jon Hansen, Justin Nadauld, and Lawrence D. Reaveley. May 2002.

PEER 2002/17 *Structural Characterization and Seismic Response Analysis of a Highway Overcrossing Equipped with Elastomeric Bearings and Fluid Dampers: A Case Study*. Nicos Makris and Jian Zhang. November 2002.

PEER 2002/16 *Estimation of Uncertainty in Geotechnical Properties for Performance-Based Earthquake Engineering*. Allen L. Jones, Steven L. Kramer, and Pedro Arduino. December 2002.

PEER 2002/15 *Seismic Behavior of Bridge Columns Subjected to Various Loading Patterns*. Asadollah Esmaeily-Gh. and Yan Xiao. December 2002.

PEER 2002/14 *Inelastic Seismic Response of Extended Pile Shaft Supported Bridge Structures.* T.C. Hutchinson, R.W. Boulanger, Y.H. Chai, and I.M. Idriss. December 2002.

PEER 2002/13 *Probabilistic Models and Fragility Estimates for Bridge Components and Systems.* Paolo Gardoni, Armen Der Kiureghian, and Khalid M. Mosalam. June 2002.

PEER 2002/12 *Effects of Fault Dip and Slip Rake on Near-Source Ground Motions: Why Chi-Chi Was a Relatively Mild M7.6 Earthquake*. Brad T. Aagaard, John F. Hall, and Thomas H. Heaton. December 2002.

PEER 2002/11 *Analytical and Experimental Study of Fiber-Reinforced Strip Isolators*. James M. Kelly and Shakhzod M. Takhirov. September 2002.

PEER 2002/10 *Centrifuge Modeling of Settlement and Lateral Spreading with Comparisons to Numerical Analyses***.** Sivapalan Gajan and Bruce L. Kutter. January 2003.

PEER 2002/09 *Documentation and Analysis of Field Case Histories of Seismic Compression during the 1994 Northridge, California, Earthquake*. Jonathan P. Stewart, Patrick M. Smith, Daniel H. Whang, and Jonathan D. Bray. October 2002.

PEER 2002/08 *Component Testing, Stability Analysis and Characterization of Buckling-Restrained Unbonded Braces™*. Cameron Black, Nicos Makris, and Ian Aiken. September 2002.

PEER 2002/07 *Seismic Performance of Pile-Wharf Connections.* Charles W. Roeder, Robert Graff, Jennifer Soderstrom, and Jun Han Yoo. December 2001.

PEER 2002/06 *The Use of Benefit-Cost Analysis for Evaluation of Performance-Based Earthquake Engineering Decisions*. Richard O. Zerbe and Anthony Falit-Baiamonte. September 2001.

PEER 2002/05 *Guidelines, Specifications, and Seismic Performance Characterization of Nonstructural Building Components and Equipment*. André Filiatrault, Constantin Christopoulos, and Christopher Stearns. September 2001.

PEER 2002/04 *Consortium of Organizations for Strong-Motion Observation Systems and the Pacific Earthquake Engineering Research Center Lifelines Program: Invited Workshop on Archiving and Web Dissemination of Geotechnical Data, 4–5 October 2001*. September 2002.

PEER 2002/03 *Investigation of Sensitivity of Building Loss Estimates to Major Uncertain Variables for the Van Nuys Testbed*. Keith A. Porter, James L. Beck, and Rustem V. Shaikhutdinov. August 2002.

PEER 2002/02 *The Third U.S.-Japan Workshop on Performance-Based Earthquake Engineering Methodology for Reinforced Concrete Building Structures*. July 2002.

PEER 2002/01 *Nonstructural Loss Estimation: The UC Berkeley Case Study.* Mary C. Comerio and John C. Stallmeyer. December 2001.

PEER 2001/16 *Statistics of SDF-System Estimate of Roof Displacement for Pushover Analysis of Buildings.* Anil K. Chopra, Rakesh K. Goel, and Chatpan Chintanapakdee. December 2001.

PEER 2001/15 *Damage to Bridges during the 2001 Nisqually Earthquake.* R. Tyler Ranf, Marc O. Eberhard, and Michael P. Berry. November 2001.

PEER 2001/14 *Rocking Response of Equipment Anchored to a Base Foundation.* Nicos Makris and Cameron J. Black. September 2001.

PEER 2001/13 *Modeling Soil Liquefaction Hazards for Performance-Based Earthquake Engineering*. Steven L. Kramer and Ahmed-W. Elgamal. February 2001.

PEER 2001/12 *Development of Geotechnical Capabilities in OpenSees*. Boris Jeremić. September 2001.

PEER 2001/11 *Analytical and Experimental Study of Fiber-Reinforced Elastomeric Isolators*. James M. Kelly and Shakhzod M. Takhirov. September 2001.

PEER 2001/10 *Amplification Factors for Spectral Acceleration in Active Regions.* Jonathan P. Stewart, Andrew H. Liu, Yoojoong Choi, and Mehmet B. Baturay. December 2001.

PEER 2001/09 *Ground Motion Evaluation Procedures for Performance-Based Design.* Jonathan P. Stewart, Shyh-Jeng Chiou, Jonathan D. Bray, Robert W. Graves, Paul G. Somerville, and Norman A. Abrahamson. September 2001.

PEER 2001/08 *Experimental and Computational Evaluation of Reinforced Concrete Bridge Beam-Column Connections for Seismic Performance*. Clay J. Naito, Jack P. Moehle, and Khalid M. Mosalam. November 2001.

PEER 2001/07 *The Rocking Spectrum and the Shortcomings of Design Guidelines.* Nicos Makris and Dimitrios Konstantinidis. August 2001.

PEER 2001/06 *Development of an Electrical Substation Equipment Performance Database for Evaluation of Equipment Fragilities*. Thalia Agnanos. April 1999.

PEER 2001/05 *Stiffness Analysis of Fiber-Reinforced Elastomeric Isolators.* Hsiang-Chuan Tsai and James M. Kelly. May 2001.

PEER 2001/04 *Organizational and Societal Considerations for Performance-Based Earthquake Engineering*. Peter J. May. April 2001.

PEER 2001/03 *A Modal Pushover Analysis Procedure to Estimate Seismic Demands for Buildings: Theory and Preliminary Evaluation*. Anil K. Chopra and Rakesh K. Goel. January 2001.

PEER 2001/02 *Seismic Response Analysis of Highway Overcrossings Including Soil-Structure Interaction*. Jian Zhang and Nicos Makris. March 2001.

PEER 2001/01 *Experimental Study of Large Seismic Steel Beam-to-Column Connections.* Egor P. Popov and Shakhzod M. Takhirov. November 2000.

PEER 2000/10 *The Second U.S.-Japan Workshop on Performance-Based Earthquake Engineering Methodology for Reinforced Concrete Building Structures*. March 2000.

PEER 2000/09 *Structural Engineering Reconnaissance of the August 17, 1999 Earthquake: Kocaeli (Izmit), Turkey.* Halil Sezen, Kenneth J. Elwood, Andrew S. Whittaker, Khalid Mosalam, John J. Wallace, and John F. Stanton. December 2000.

PEER 2000/08 *Behavior of Reinforced Concrete Bridge Columns Having Varying Aspect Ratios and Varying Lengths of Confinement*. Anthony J. Calderone, Dawn E. Lehman, and Jack P. Moehle. January 2001.

PEER 2000/07 *Cover-Plate and Flange-Plate Reinforced Steel Moment-Resisting Connections.* Taejin Kim, Andrew S. Whittaker, Amir S. Gilani, Vitelmo V. Bertero, and Shakhzod M. Takhirov. September 2000.

PEER 2000/06 *Seismic Evaluation and Analysis of 230-kV Disconnect Switches.* Amir S. J. Gilani, Andrew S. Whittaker, Gregory L. Fenves, Chun-Hao Chen, Henry Ho, and Eric Fujisaki. July 2000.

PEER 2000/05 *Performance-Based Evaluation of Exterior Reinforced Concrete Building Joints for Seismic Excitation*. Chandra Clyde, Chris P. Pantelides, and Lawrence D. Reaveley. July 2000.

PEER 2000/04 *An Evaluation of Seismic Energy Demand: An Attenuation Approach*. Chung-Che Chou and Chia-Ming Uang. July 1999.

PEER 2000/03 *Framing Earthquake Retrofitting Decisions: The Case of Hillside Homes in Los Angeles.* Detlof von Winterfeldt, Nels Roselund, and Alicia Kitsuse. March 2000.

PEER 2000/02 *U.S.-Japan Workshop on the Effects of Near-Field Earthquake Shaking*. Andrew Whittaker, Editor. July 2000.

PEER 2000/01 *Further Studies on Seismic Interaction in Interconnected Electrical Substation Equipment.* Armen Der Kiureghian, Kee-Jeung Hong, and Jerome L. Sackman. November 1999.

PEER 1999/14 *Seismic Evaluation and Retrofit of 230-kV Porcelain Transformer Bushings*. Amir S. Gilani, Andrew S. Whittaker, Gregory L. Fenves, and Eric Fujisaki. December 1999.

PEER 1999/13 *Building Vulnerability Studies: Modeling and Evaluation of Tilt-up and Steel Reinforced Concrete Buildings*. John W. Wallace, Jonathan P. Stewart, and Andrew S. Whittaker, Editors. December 1999.

PEER 1999/12 *Rehabilitation of Nonductile RC Frame Building Using Encasement Plates and Energy-Dissipating Devices*. Mehrdad Sasani, Vitelmo V. Bertero, James C. Anderson. December 1999.

PEER 1999/11 *Performance Evaluation Database for Concrete Bridge Components and Systems under Simulated Seismic Loads*. Yael D. Hose and Frieder Seible. November 1999.

PEER 1999/10 *U.S.-Japan Workshop on Performance-Based Earthquake Engineering Methodology for Reinforced Concrete Building Structures*. December 1999.

PEER 1999/09 *Performance Improvement of Long Period Building Structures Subjected to Severe Pulse-Type Ground Motions*. James C. Anderson, Vitelmo V. Bertero, and Raul Bertero. October 1999.

PEER 1999/08 *Envelopes for Seismic Response Vectors.* Charles Menun and Armen Der Kiureghian. July 1999.

PEER 1999/07 *Documentation of Strengths and Weaknesses of Current Computer Analysis Methods for Seismic Performance of Reinforced Concrete Members*. William F. Cofer. November 1999.

PEER 1999/06 *Rocking Response and Overturning of Anchored Equipment under Seismic Excitations*. Nicos Makris and Jian Zhang. November 1999.

PEER 1999/05 *Seismic Evaluation of 550 kV Porcelain Transformer Bushings.* Amir S. Gilani, Andrew S. Whittaker, Gregory L. Fenves, and Eric Fujisaki. October 1999.

PEER 1999/04 *Adoption and Enforcement of Earthquake Risk-Reduction Measures.* Peter J. May, Raymond J. Burby, T. Jens Feeley, and Robert Wood. August 1999.

PEER 1999/03 *Task 3 Characterization of Site Response General Site Categories*. Adrian Rodriguez-Marek, Jonathan D. Bray and Norman Abrahamson. February 1999.

PEER 1999/02 *Capacity-Demand-Diagram Methods for Estimating Seismic Deformation of Inelastic Structures: SDF Systems*. Anil K. Chopra and Rakesh Goel. April 1999.

PEER 1999/01 *Interaction in Interconnected Electrical Substation Equipment Subjected to Earthquake Ground Motions*. Armen Der Kiureghian, Jerome L. Sackman, and Kee-Jeung Hong. February 1999.

PEER 1998/08 *Behavior and Failure Analysis of a Multiple-Frame Highway Bridge in the 1994 Northridge Earthquake*. Gregory L. Fenves and Michael Ellery. December 1998.

PEER 1998/07 *Empirical Evaluation of Inertial Soil-Structure Interaction Effects.* Jonathan P. Stewart, Raymond B. Seed, and Gregory L. Fenves. November 1998.

PEER 1998/06 *Effect of Damping Mechanisms on the Response of Seismic Isolated Structures*. Nicos Makris and Shih-Po Chang. November 1998.

PEER 1998/05 *Rocking Response and Overturning of Equipment under Horizontal Pulse-Type Motions*. Nicos Makris and Yiannis Roussos. October 1998.

PEER 1998/04 *Pacific Earthquake Engineering Research Invitational Workshop Proceedings, May 14–15, 1998: Defining the Links between Planning, Policy Analysis, Economics and Earthquake Engineering*. Mary Comerio and Peter Gordon. September 1998.

PEER 1998/03 *Repair/Upgrade Procedures for Welded Beam to Column Connections*. James C. Anderson and Xiaojing Duan. May 1998.

PEER 1998/02 *Seismic Evaluation of 196 kV Porcelain Transformer Bushings.* Amir S. Gilani, Juan W. Chavez, Gregory L. Fenves, and Andrew S. Whittaker. May 1998.

PEER 1998/01 *Seismic Performance of Well-Confined Concrete Bridge Columns.* Dawn E. Lehman and Jack P. Moehle. December 2000.

PEER REPORTS: ONE HUNDRED SERIES

The following PEER reports are available by Internet only at http://peer.berkeley.edu/publications/peer_reports_complete.html.

PEER 2012/103 *Performance-Based Seismic Demand Assessment of Concentrically Braced Steel Frame Buildings.* Chui-Hsin Chen and Stephen A. Mahin. December 2012.

PEER 2012/102 *Procedure to Restart an Interrupted Hybrid Simulation: Addendum to PEER Report 2010/103.* Vesna Terzic and Bozidar Stojadinovic. October 2012.

PEER 2012/101 *Mechanics of Fiber Reinforced Bearings.* James M. Kelly and Andrea Calabrese. February 2012.

PEER 2011/107 *Nonlinear Site Response and Seismic Compression at Vertical Array Strongly Shaken by 2007 Niigata-ken Chuetsu-oki Earthquake.* Eric Yee, Jonathan P. Stewart, and Kohji Tokimatsu. December 2011.

PEER 2011/106 *Self Compacting Hybrid Fiber Reinforced Concrete Composites for Bridge Columns.* Pardeep Kumar, Gabriel Jen, William Trono, Marios Panagiotou, and Claudia Ostertag. September 2011.

PEER 2011/105 *Stochastic Dynamic Analysis of Bridges Subjected to Spacially Varying Ground Motions.* Katerina Konakli and Armen Der Kiureghian. August 2011.

PEER 2011/104 *Design and Instrumentation of the 2010 E-Defense Four-Story Reinforced Concrete and Post-Tensioned Concrete Buildings.* Takuya Nagae, Kenichi Tahara, Taizo Matsumori, Hitoshi Shiohara, Toshimi Kabeyasawa, Susumu Kono, Minehiro Nishiyama (Japanese Research Team) and John Wallace, Wassim Ghannoum, Jack Moehle, Richard Sause, Wesley Keller, Zeynep Tuna (U.S. Research Team). June 2011.

PEER 2011/103 *In-Situ Monitoring of the Force Output of Fluid Dampers: Experimental Investigation.* Dimitrios Konstantinidis, James M. Kelly, and Nicos Makris. April 2011.

PEER 2011/102 *Ground-Motion Prediction Equations 1964–2010.* John Douglas. April 2011.

PEER 2011/101 *Report of the Eighth Planning Meeting of NEES/E-Defense Collaborative Research on Earthquake Engineering.* Convened by the Hyogo Earthquake Engineering Research Center (NIED), NEES Consortium, Inc. February 2011.

PEER 2010/111 *Modeling and Acceptance Criteria for Seismic Design and Analysis of Tall Buildings.* Task 7 Report for the Tall Buildings Initiative - Published jointly by the Applied Technology Council. October 2010.

PEER 2010/110 *Seismic Performance Assessment and Probabilistic Repair Cost Analysis of Precast Concrete Cladding Systems for Multistory Buildlings.* Jeffrey P. Hunt and Božidar Stojadinovic. November 2010.

PEER 2010/109 *Report of the Seventh Joint Planning Meeting of NEES/E-Defense Collaboration on Earthquake Engineering. Held at the E-Defense, Miki, and Shin-Kobe, Japan, September 18–19, 2009.* August 2010.

PEER 2010/108 *Probabilistic Tsunami Hazard in California.* Hong Kie Thio, Paul Somerville, and Jascha Polet, preparers. October 2010.

PEER 2010/107 *Performance and Reliability of Exposed Column Base Plate Connections for Steel Moment-Resisting Frames.* Ady Aviram, Božidar Stojadinovic, and Armen Der Kiureghian. August 2010.

PEER 2010/106 *Verification of Probabilistic Seismic Hazard Analysis Computer Programs.* Patricia Thomas, Ivan Wong, and Norman Abrahamson. May 2010.

PEER 2010/105 *Structural Engineering Reconnaissance of the April 6, 2009, Abruzzo, Italy, Earthquake, and Lessons Learned.* M. Selim Günay and Khalid M. Mosalam. April 2010.

PEER 2010/104 *Simulating the Inelastic Seismic Behavior of Steel Braced Frames, Including the Effects of Low-Cycle Fatigue.* Yuli Huang and Stephen A. Mahin. April 2010.

PEER 2010/103 *Post-Earthquake Traffic Capacity of Modern Bridges in California.* Vesna Terzic and Božidar Stojadinović. March 2010.

PEER 2010/102 *Analysis of Cumulative Absolute Velocity (CAV) and JMA Instrumental Seismic Intensity (I_{JMA}) Using the PEER–NGA Strong Motion Database.* Kenneth W. Campbell and Yousef Bozorgnia. February 2010.

PEER 2010/101 *Rocking Response of Bridges on Shallow Foundations.* Jose A. Ugalde, Bruce L. Kutter, and Boris Jeremic. April 2010.

PEER 2009/109 *Simulation and Performance-Based Earthquake Engineering Assessment of Self-Centering Post-Tensioned Concrete Bridge Systems.* Won K. Lee and Sarah L. Billington. December 2009.

PEER 2009/108 *PEER Lifelines Geotechnical Virtual Data Center.* J. Carl Stepp, Daniel J. Ponti, Loren L. Turner, Jennifer N. Swift, Sean Devlin, Yang Zhu, Jean Benoit, and John Bobbitt. September 2009.

PEER 2009/107 *Experimental and Computational Evaluation of Current and Innovative In-Span Hinge Details in Reinforced Concrete Box-Girder Bridges: Part 2: Post-Test Analysis and Design Recommendations.* Matias A. Hube and Khalid M. Mosalam. December 2009.

PEER 2009/106 *Shear Strength Models of Exterior Beam-Column Joints without Transverse Reinforcement.* Sangjoon Park and Khalid M. Mosalam. November 2009.

PEER 2009/105 *Reduced Uncertainty of Ground Motion Prediction Equations through Bayesian Variance Analysis.* Robb Eric S. Moss. November 2009.

PEER 2009/104 *Advanced Implementation of Hybrid Simulation.* Andreas H. Schellenberg, Stephen A. Mahin, Gregory L. Fenves. November 2009.

PEER 2009/103 *Performance Evaluation of Innovative Steel Braced Frames.* T. Y. Yang, Jack P. Moehle, and Božidar Stojadinovic. August 2009.

PEER 2009/102 *Reinvestigation of Liquefaction and Nonliquefaction Case Histories from the 1976 Tangshan Earthquake.* Robb Eric Moss, Robert E. Kayen, Liyuan Tong, Songyu Liu, Guojun Cai, and Jiaer Wu. August 2009.

PEER 2009/101 *Report of the First Joint Planning Meeting for the Second Phase of NEES/E-Defense Collaborative Research on Earthquake Engineering.* Stephen A. Mahin et al. July 2009.

PEER 2008/104 *Experimental and Analytical Study of the Seismic Performance of Retaining Structures.* Linda Al Atik and Nicholas Sitar. January 2009.

PEER 2008/103 *Experimental and Computational Evaluation of Current and Innovative In-Span Hinge Details in Reinforced Concrete Box-Girder Bridges. Part 1: Experimental Findings and Pre-Test Analysis.* Matias A. Hube and Khalid M. Mosalam. January 2009.

PEER 2008/102 *Modeling of Unreinforced Masonry Infill Walls Considering In-Plane and Out-of-Plane Interaction.* Stephen Kadysiewski and Khalid M. Mosalam. January 2009.

PEER 2008/101 *Seismic Performance Objectives for Tall Buildings.* William T. Holmes, Charles Kircher, William Petak, and Nabih Youssef. August 2008.

PEER 2007/101 *Generalized Hybrid Simulation Framework for Structural Systems Subjected to Seismic Loading*. Tarek Elkhoraibi and Khalid M. Mosalam. July 2007.

PEER 2007/100 *Seismic Evaluation of Reinforced Concrete Buildings Including Effects of Masonry Infill Walls.* Alidad Hashemi and Khalid M. Mosalam. July 2007.

The Pacifi c Earthquake Engineering Research Center (PEER) is a multi-institutional research and education center with headquarters at the University of California, Berkeley. Investigators from over 20 universities, several consulting companies, and researchers at various state and federal government agencies contribute to research programs focused on performance-based earthquake engineering.

These research programs aim to identify and reduce the risks from major earthquakes to life safety and to the economy by including research in a wide variety of disciplines including structural and geotechnical engineering, geology/ seismology, lifelines, transportation, architecture, economics, risk management, and public policy.

PEER is supported by federal, state, local, and regional agencies, together with industry partners.

PEER Core Institutions

University of California, Berkeley (Lead Institution)
California Institute of Technology
Oregon State University
Stanford University
University of California, Davis
University of California, Irvine
University of California, Los Angeles
University of California, San Diego
University of Nevada, Reno
University of Southern California
University of Washington

PEER reports can be ordered at https://peer.berkeley.edu/peer-reports or by contacting

Pacific Earthquake Engineering Research Center
University of California, Berkeley
325 Davis Hall, Mail Code 1792
Berkeley, CA 94720-1792
Tel: 510-642-3437
Email: peer_center@berkeley.edu

ISSN 2770-8314
https://doi.org/10.55461/CFHS8430